

國立交通大學

機械工程學系

博士論文

雙互質分解干擾觀測器



**Doubly Coprime Factorization  
Disturbance Observer**

研究生：潘怡仁

指導教授：李安謙

中華民國九十九年七月

# 雙互質分解干擾觀測器

## Doubly Coprime Factorization Disturbance Observer

研究生：潘怡仁

Student :Yi-Ren Pan

指導教授：李安謙

Advisor :An-Chen Lee

國立交通大學

機械工程學系

博士論文

Submitted to Department of Mechanical Engineering

College of Engineering

National Chiao Tung University

in partial Fulfillment of the Requirements

for the Degree of

Doctor of Philosophy

in

Mechanical Engineering

July 2010

Hsinchu, Taiwan, Republic of China

中華民國九十九年七月

# 雙互質分解干擾觀測器

研究生：潘怡仁

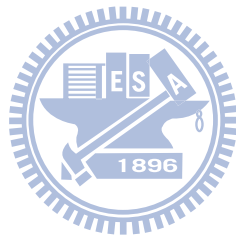
指導教授：李安謙

國立交通大學機械工程學系

## 摘要

本論文旨在提出一個採用雙互質分解之干擾觀測器，此干擾觀測器乃基於雙互質分解 (Doubly coprime) 及 Bezout Identity 加以延伸演變而來。以往干擾觀測器方面之研究多數採用 Ohnishi 於 1987 年所提出之概念加以延伸，不過該種干擾觀測器架構無法應用於非極小相位系統。本論文所提出之雙互質分解干擾觀測器則可應用於穩定、非穩定、極小相位及非極小相位等線性系統，文中對於不同系統狀況之內部穩定及穩健性皆加有詳細分析，並對於非極小相位系統不穩定零點之影響有較深入之探討。當應用於非穩定系統，除了採用外迴路控制器穩定外，本文亦結合此干擾觀測器與 Vidyasagar's structure 發展一新穎獨立雙參數架構，除保證系統穩定外，亦可獨立設計干擾抑制參數與追跡響應參數。當系統為多輸入多輸出時，方陣系統可同時抑制輸入與輸出干擾，倘若系統為非方陣型態時，干擾抑制能力則受限於輸入與輸出頻道相對個數。

對於探討系統非確定性與穩健干擾觀測器的發展上，本文則採用 Small gain theorem 設計觀測器參數以滿足系統穩健性。對於穩健雙互質分解干擾觀測器，吾人亦利用 McFarlane 及 Glover 發展之迴路整形法設計觀測器參數，藉此滿足系統穩健性與響應規格。在最後一章節中，本文提供數個數值模擬來驗證各章節之論點與推導正確性並以交流馬達定位控制實驗來抑制鈍齒力干擾用以驗證穩定性與系統響應。



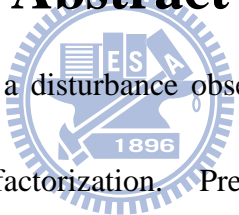
# Doubly Coprime Factorization Disturbance Observer

Student : Yi-Ren Pan

Advisor : An-Chen Lee

Department of Mechanical Engineering  
National Chiao-Tung University

## Abstract



In this thesis, one provides a disturbance observer which is based on “Bezout Identity” and doubly coprime factorization. Previous studies about disturbance observer were extended from the concept that provided by Ohnishi in 1987. Unfortunately, that structure cannot be applied to the non-minimum phase systems. The disturbance observer we proposed is quite in general, which can be applied to stable, unstable, minimum-phase and non-minimum-phase linear systems. Besides, this thesis also discusses the internal stability and robust stability for different plant cases, and studies about the influences and limitations caused by non-minimum-phase zeros. For unstable systems, in this thesis, we combine the proposed disturbance observer and Vidyasagar’s structure to develop a novel two degrees of freedom

structure containing two independent parameters which can not only stabilize the system but eliminate the disturbances and improve the tracking performance. When multi-input-multi-output systems are applied, the rejection capability is restricted by the relative numbers of input / output channels. Roughly speaking, the capability of the input and output disturbances rejections is good when the plant is square and is deteriorated when the plant is non-square.

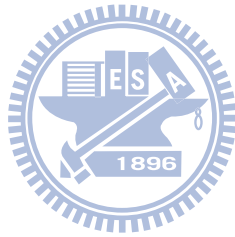
A robust disturbance observer is developed to treat plant uncertainty. We applied the small gain theorem to design the disturbance observer that satisfies the robust stability criteria. Also, to guarantee the robust stability and robust performance, we used  $H_\infty$  - loop shaping method developed by McFarlane and Glover to design the observer parameter. In the final chapter, we provided some numerical examples and an experimental result of positioning control and cogging force rejection of an AC servomotor to verify the correctness of the theoretical developments.

# 致謝

感謝所有過去、現在以及未來生命旅途中遇見的人

-潘怡仁

2010年7月



# Contents

摘要.....	i
Abstract.....	iii
致謝.....	v
Contents.....	vi
List of Figures.....	x
List of Tables.....	xvii
<b>Chapter 1 Introduction.....</b>	<b>1</b>
1.1 Classical Disturbance Observer.....	1
1.2 Coprime Factorization.....	5
1.2.1 Why coprime.....	6
1.2.2 State-space model for general coprime factorization.....	8
1.2.3 Normalized coprime factorization.....	9
1.3 Organization.....	12
<b>Chapter 2 Development of Doubly Coprime Factorization</b>	
<b>Disturbance Observer.....</b>	<b>16</b>
2.1 Doubly Coprime Disturbance Observer and Bezout Identity.....	16
2.2 Applications to Stable Systems.....	20
2.2.1 Design method for minimum-phase systems.....	23

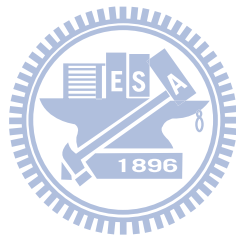


2.2.2 Design method for non-minimum-phase systems.....	25
2.2.2.1 Model matching method in non-minimum plants.....	25
2.2.2.2 Nehari problem.....	27
2.2.2.3 Weighting function design.....	30
2.3 Applications to Unstable systems.....	33
2.4 Combination of the DCFDOB and Vidyasagar's structure.....	38
2.4.1 Vidyasagar's structure.....	38
2.4.2 The DCFDOB co-structure with Vidyasagar's structure.....	40
2.4.2.1 $H(s)$ on tracking control using the inverse dynamic.....	45
2.4.2.2 $Q_Y(s)$ on disturbance elimination design.....	46
<b>Chapter 3 Extension to General Plant Cases and Input/Output</b>	
<b>Disturbances.....</b>	<b>55</b>
3.1 Input/Output Sensitivity Functions of the DCFDOB.....	56
3.2 Model Matching Method of MIMO square System.....	58
3.3 Input/Output Sensitivity Functions with Feedback Controller.....	60
3.4 The DCFDOB for Non-square Plant.....	62
3.4.1 The thin plant case.....	62
3.4.2 The wide plant case.....	63
<b>Chapter 4 Uncertainty and Robustness.....</b>	<b>71</b>

4.1 Coprime Factor Uncertainty.....	71
4.1.1 Small gain theorem.....	72
4.2 Robust Stability Analysis.....	73
4.2.1 Robust stability analysis of DCFDOB.....	73
4.2.2 Robust stability analysis of DCFDOB-VS.....	76
4.3 Robust DCFDOB .....	81
4.4 Robust DCFDOB Using the $H_\infty$ - Loop Shaping Design.....	84
4.4.1 The $H_\infty$ -loop shaping design procedure of the robust DCFDOB....	87
4.4.2 On the achieved loop shape.....	89
4.4.3 Bounds of the robust DCFDOB.....	92
<b>Chapter 5 Numerical Examples and Experimental Results.....</b>	<b>98</b>
5.1 Numerical Example Part 1: minimum-phase plants.....	98
5.2 Numerical Example Part 2: non-minimum phase plants.....	107
5.3 Numerical Example Part 3: non-square, minimum phase plants.....	113
5.4 Numerical Example Part 4: the loop-shaping design method.....	129
5.5 Part 5: experimental results of an AC servo motor.....	140
<b>Conclusion and Future Work.....</b>	<b>145</b>
<b>References.....</b>	<b>148</b>
<b>Appendix A.....</b>	<b>156</b>

**Appendix B**.....158

**Appendix C**.....161



# List of Figures

## Chapter 1

Fig.1.1 Classical disturbance observer.....1

## Chapter 2

Fig. 2.1 Basic Structure based on Bezout identity.....17

Fig. 2.2 Internal states estimation with input disturbance.....17

Fig. 2.3 Extended structure with virtual disturbance entry point.....18

Fig. 2.4 Extended structure with actual disturbance entry point.....18

Fig. 2.5 Virtual structure for ideal DOB.....19

Fig. 2.6 Block diagram of the DCFDOB.....20

Fig. 2.7 The DCFDOB for stable systems.....21

Fig. 2.8 Model matching problem.....26

Fig. 2.9 (a) Different weighting functions and (b) corresponding input sensitivity  
functions.....33

Fig. 2.10 The DCFDOB with outer-loop controller.....34

Fig. 2.11 Classic control feedback loop.....35

Fig. 2.12 Control scheme for the Youla-Kucera parameterization.....36

Fig. 2.13 The DCFDOB with Youla-Kucera parameterization controller.....36

Fig. 2.14 Vidyasagar's structure: (a) observer-controller compensator and

	(b) equivalent compensator.....	39
Fig. 2.15 (a)	Internal states estimation with input disturbance	
	(b) The DCFDOB structure	
	(c) Vidyasagar's structure: observer-controller compensator.....	41
Fig. 2.16	The DCFDOB co-structure with Vidyasagar's structure.....	42
Fig. 2.17	The DCFDOB-VS scheme.....	42
Fig. 2.18	Simulation result of an unstable system with DCFDOB-VS for case 1.....	50
Fig. 2.19	Frequency responses from (a) $d_{i,1} \rightarrow e_{d,1}$ (b) $d_{i,2} \rightarrow e_{d,1}$ (c) $d_{i,1} \rightarrow e_{d,2}$	
	(d) $d_{i,2} \rightarrow e_{d,2}$ of DCFDOB-VS for case 1.....	51
Fig. 2.20	Frequency response from (a) $r_1 \rightarrow y_1$ (b) $r_2 \rightarrow y_1$ (c) $r_1 \rightarrow y_2$ (d) $r_2 \rightarrow y_2$	
	of DCFDOB-VS for case 1.....	52
Fig. 2.21	Simulation results of an unstable system with DCFDOB-VS for case 2.....	53
Fig. 2.22	Frequency response from (a) $r_1 \rightarrow y_1$ (b) $r_2 \rightarrow y_1$ (c) $r_1 \rightarrow y_2$ (d) $r_2 \rightarrow y_2$	
	of DCFDOB-VS case 2.....	53

### Chapter 3

Fig. 3.1	DCFDOB with input and output disturbances.....	55
----------	--	----

### Chapter 4

Fig. 4.1	Block diagram of DCFDOB with system uncertainties.....	72
Fig. 4.2	$M_\Delta - \Delta$ loop stability analysis.....	73

Fig. 4.3 $M_{\Delta} - \Delta$ loop stability analysis of Fig. 4.1.....	73
Fig. 4.4 The complete feasible form of DCFDOB.....	76
Fig. 4.5 $M_{\Delta} - \Delta$ loop of DCFDOB-VS.....	77
Fig. 4.6 The modification of DCFDOB-VS.....	78
Fig. 4.7 (a) The modification of DCFDOB-VS (b) the equivalent block diagram of with two independent parameters $H(s)$ and $Q_Y(s)$ .....	78
Fig. 4.8 Right coprime factor perturbed system with the reduced DCFDOB.....	82
Fig. 4.9 Open - loop singular value shaping.....	86
Fig. 4.10 Two cases of the transfer functions from $(\tilde{d}_i \ \tilde{d}_o)$ to $(\tilde{y}_1 \ \tilde{y}_2)$ and $(\bar{y}_1 \ \bar{y}_2)$ .....	89
Fig. 4.11 Specified and achieved loop shapes.....	90

## Chapter 5

Fig. 5.1 Frequency responses of input sensitivity of part 1 - example 1.....	100
Fig. 5.2 Frequency responses from noise to system output of part 1 – example 1....	100
Fig. 5.3 Simulation results of part 1 – example 1.....	101
Fig. 5.4 (a) Simulation results when considered both input and output disturbances of part 1 – example 1.  (b) Detailed response from 4 sec to 6 sec of Fig. 5.4(a)  (c) Detailed response from 6 sec to 8 sec of Fig. 5.4(a).....	102

Fig. 5.5 (a) Frequency responses (b) phase plots of nominal plant and the ones  
 from I/O points of DCFDOB with  $Q_1(s)$  and  $Q_2(s)$  .....103

Fig. 5.6 Frequency responses from (a)  $\begin{bmatrix} d_{i,1} \\ d_{o,1} \end{bmatrix} \rightarrow y_1$  (b)  $\begin{bmatrix} d_{i,2} \\ d_{o,2} \end{bmatrix} \rightarrow y_1$  (c)  $\begin{bmatrix} d_{i,1} \\ d_{o,1} \end{bmatrix} \rightarrow y_2$   
 (d)  $\begin{bmatrix} d_{i,2} \\ d_{o,2} \end{bmatrix} \rightarrow y_2$  and (e) simulation results of part 1 - example 2.....106

Fig. 5.7 Frequency responses of part 2 – example 1.....109

Fig. 5.8 (a) System outputs of simulation results of part 2 – example 1.

(b) System output  $y_{w_1}$  of DCFDOB with parameter  $Q_{w_1}(s)$ .

(c) System output  $y_{w_2}$  of DCFDOB with parameter  $Q_{w_2}(s)$  .....110

Fig. 5.9 Frequency responses from (a)  $\begin{bmatrix} d_{i,1} \\ d_{o,1} \end{bmatrix} \rightarrow y_1$  (b)  $\begin{bmatrix} d_{i,2} \\ d_{o,2} \end{bmatrix} \rightarrow y_1$

(c)  $\begin{bmatrix} d_{i,1} \\ d_{o,1} \end{bmatrix} \rightarrow y_2$  (d)  $\begin{bmatrix} d_{i,2} \\ d_{o,2} \end{bmatrix} \rightarrow y_2$  and

(e) simulation results of part 2 – example 2.....112

Fig. 5.10 Simulation block of numerical example part 3 – example 1.....115

Fig. 5.11 (a) Simulation results of non-square thin plant with DCFDOB and input  
 disturbance.

(b) Detailed responses from 1.5 sec to 3.5 sec of Fig. 5.1(a)

(c) Detailed responses from 6.5 sec to 8.5 sec of Fig. 5.1(a)

(d) Simulation results of non-square thin plant without DCFDOB.....116

Fig. 5.12 Frequency responses of input sensitivity functions of part 3 – example 1.....	117
Fig. 5.13 Simulation results of output disturbances on non-square thin plant - design 1.....	118
Fig. 5.14 Frequency responses of output sensitivity functions (design 1) of part 3 - example 1.....	118
Fig. 5.15 Simulation results of output disturbances on non-square thin plant - design 2.....	120
Fig.5.16 Frequency responses of output sensitivity functions (design 2) of part 3 - example 1.....	121
Fig. 5.17 Simulation results of example 5.3 part 1 – design 3.....	122
Fig. 5.18 Frequency responses of output sensitivity functions (design 3) of part 3 - example 1.....	123
Fig.5.19 Simulation results of output disturbances for non-square wide plant.....	126
Fig. 5.20 Frequency responses of output sensitivity functions of part 3 - example 2.....	127
Fig. 5.21 Singular values: (a) the nominal plant (b) the shaped plant $W_2P_nW_1$ .....	130
Fig 5.22 Singular values of (a) $K_{DOB}P_n$ (b) $P_nK_{DOB}$ .....	131
Fig. 5.23 Singular values of (a) input sensitivity function and	

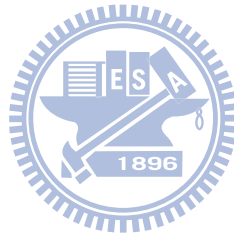


	(b) output sensitivity function.....	131
Fig. 5.24	Frequency responses of (a) the origin parameter matrix $Q_{2 \times 2}$ and (b) the reduced order parameter matrix.....	132
Fig 5.25	The Singular values of (a) the original parameter matrix (solid line) and (b) the reduced parameter matrix (dashed line).....	133
Fig. 5.26	Time domain simulation results with various uncertainty norms of example.....	134
Fig. 5.27	The $\bar{\sigma}(S_i(j\omega))$ and its corresponding upper boundaries plots of Eq.(4.45).....	135
Fig. 5.28	The $\bar{\sigma}(P_n S_i(j\omega))$ and its corresponding upper boundaries plots of Eq. (4.46).....	136
Fig. 5.29	The $\bar{\sigma}(S_i K_{DOB}(j\omega))$ and its corresponding upper boundaries plots of Eq. (4.47).....	136
Fig. 5.30	The $\bar{\sigma}(P_n S_i K_{DOB}(j\omega))$ and its corresponding upper boundaries plots of Eq. (4.48).....	137
Fig. 5.31	The $\bar{\sigma}(K_{DOB} S_o P_n(j\omega))$ and its corresponding upper boundaries plots of Eq. (4.49).....	137
Fig. 5.32	The $\bar{\sigma}(K_{DOB} S_o(j\omega))$ and its corresponding upper boundaries plots of Eq. (4.50).....	138

Fig. 5.33 The $\bar{\sigma}(S_o P_n(j\omega))$ and its corresponding upper boundaries plots of Eq. (4.51).....	138
Fig. 5.34 The $\bar{\sigma}(S_o(j\omega))$ and its corresponding upper boundaries plots of Eq. (4.52).....	139
Fig. 5.35 (a)Tracking responses of 4000 counts position command (b) Tracking errors of 4000 counts position command.....	142
Fig. 5.36 (a) Tracking errors without DCFDOB from 1 sec to 4 sec. (b) Tracking errors with DCFDOB from 1 sec to 4 sec. (c) Frequency analysis of Fig. 5.36(a). (d) Frequency analysis of Fig. 5.36(b).....	143
Fig. 5.37 (a)Tracking responses of 400 counts ( $18^\circ$ ) position command (b)Tracking error of 400 counts ( $18^\circ$ ) position command with DCFDOB....	144
Fig. 5.38 (a)Tracking responses of 200 counts ( $9^\circ$ ) position command (b)Tracking error of 200 counts ( $9^\circ$ ) position command with DCFDOB.....	144

# List of Tables

Table 3.1 Solutions of parameter $Q(s)$ and corresponding sensitivity functions.....	57
Table 3.2 Design properties of the DCFDOB for non-square plant cases.....	66
Table 4.1 Plots of $ M_{\Delta}(j\omega) $ with different bandwidth of $J(s)$ , $\alpha(s)$ and corresponding $\ M_{\Delta}\ _{\infty}$ .....	80
Table 5.1 Physical parameters of AC servomotor of experiment.....	141



# CHAPTER 1

## INTRODUCTION

### 1.1 Classical Disturbance Observer

When a mechanical plant is controlled, the performance is primarily affected by friction, disturbance, sensor noises and unknown uncertainties. The control structure and design methodologies which consider the effect of disturbance is called “disturbance observer (DOB)”. The DOB shown below was first proposed by Ohnishi [1] and using the inverse dynamic control methods.

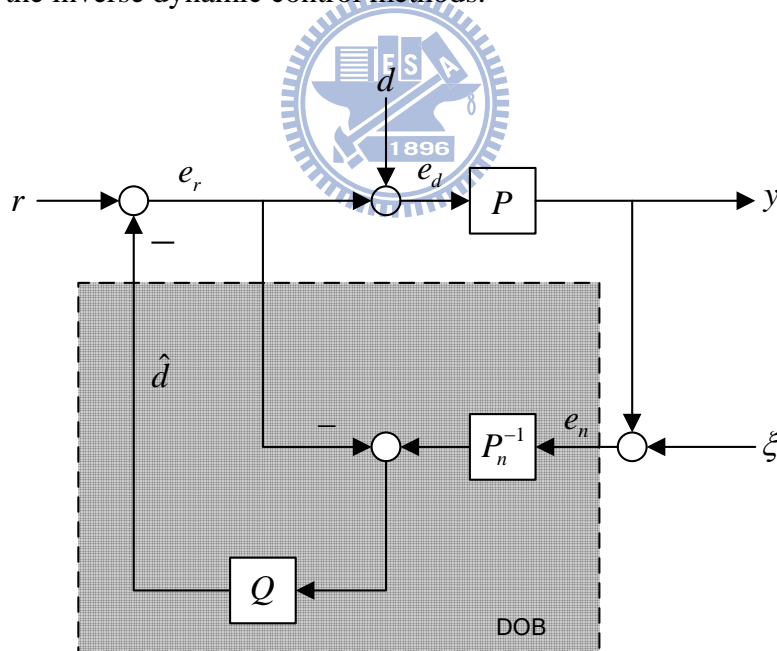


Fig. 1.1 Classical disturbance observer

The symbols are defined as follows.

$P(s)$ : the actual plant

$P_n(s)$ : the nominal plant

$Q(s)$ : the design parameter and usually designed as a low-pass filter

$r(s)$ : the control input

$d(s)$ : the input disturbance

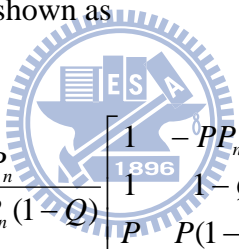
$\hat{d}(s)$ : the value of estimated disturbance with a low-pass filter

$\xi(s)$ : the measurement noise

$y(s)$ : system output

Moreover, the nine transfer function from external inputs  $[r \ d \ \xi]^T$  to internal states

$[e_r \ e_d \ e_n]^T$  of Fig. 1.1 can be shown as


$$\begin{bmatrix} e_r \\ e_d \\ e_n \end{bmatrix} = \frac{P_n}{PQ + P_n(1-Q)} \begin{bmatrix} 1 & -PP_n^{-1}Q & -P_n^{-1}Q \\ 1 & 1-Q & -P_n^{-1}Q \\ P & P(1-Q) & 1-Q \end{bmatrix} \begin{bmatrix} r \\ d \\ \xi \end{bmatrix}. \quad (1.1)$$

Since the nine transfer functions of Eq. (1.1) should be stable to achieve the internally stable, therefore, the internally stabilizing conditions can be represented as

1.  $P(s)$ ,  $P_n(s)$  and  $Q(s)$  must be stable and
2.  $(PQ + P_n(1-Q))^{-1}$  should be stable.

If the real plant  $P(s)$  is unstable, the system with disturbance observer can not be internally stable. The second condition says that the real plant should be of minimum phase.

In recent years, the DOB has been introduced into motion control systems to eliminate as much of the “equivalent disturbance” as possible, and to force the actual system to become a nominal model. The equivalent disturbance consists of external disturbance signals which include friction and signals associated with model uncertainties and nonlinearity. If these uncertainties are eliminated by disturbance observer, the linear feedback controller can be applied to construct an asymptotically stable system. Lee and Tomizuka [2] and other researchers [3]—[10] demonstrated the effectiveness of the disturbance observer by performing experiments with various uncertainties and external disturbances, to improve performance in tracking or point-to-point control. Umeno *et al.* [11] studied the disturbance observer using the concept of two degrees of freedom control [12]—[13] in theoretical respect. Yamada *et al.* [14] used this inverse dynamic concept and realized a nominal system which can control acceleration for fast and precise servo system using high order DOB. In 1996, Choi *et al.* [15] proposed a novel DOB structure which was derived from the concept of partial plant inversion to estimate the input disturbance and performed in  $H_\infty$  frameworks but did not deeply discuss the DOB properties of non-minimum phase system and approximated minimum phase to non-minimum phase system using model reduction. In 1998, Yamada *et al.* [16] used the same concept of inverse dynamic and extended to a MIMO DOB for robust control of robot manipulator. In 2000, Komada *et al.* [17] discussed the relationship between robust stability and selection of coefficients of DOB for redundant manipulator control. Also, White *et al.* [18] used the DOB structure shown in Fig. 1.1 to improve track following in Magnetic Disk Drives. K. Ohishi *et al.* [19] proposed a new high speed robust tracking control system based on both “zero phase error tracking” (ZPET) and disturbance observer for an optical disk recording system in 2000. Yang *et al.* [20] continued researching the

DOB structure that proposed by [15] and used only position error to construct a DOB (error-based disturbance observer, EDOB) for robust tracking control of optical disk drive in 2005. In 2003, Choi *et al.* [21] proposed a criterion to design a robust DOB system and suggested its design guidelines especially for second-order systems.

However, the disturbance observer which proposed by [1] cannot be applied to general plants, in other words, especially the non-minimum phase plants are impossible to use it because the internal stability cannot be attained. Although [15] proposed a novel DOB scheme and claimed that the proposed scheme can be applied to non-minimum phase systems, but that study used model reduction only, and as we know, there may exist a large reduction error. Although there exist some research works on DOB for non-minimum phase systems [22]—[26], they seem to have difficulties in handling general cases. Chen *et al.* [22] proposed a complex methodology to approximate inverse systems for non-minimum phase and provided its application to disturbance observer based on the least-square approximation without considering the stability of the closed-loop system. The application of [23] is limited to those disturbances that come from a known external system, and the approach of [24] is limited to the case where the plant model does not have uncertainty. Yang and Shiu [25] dealt with non-minimum phase systems simply by inverting only the invertible (stable minimum phase) part and [26] is limited to the case where the plant is single input / single output (SISO) strictly proper rational transfer functions. In this thesis, an internally stabilizing disturbance observer based on doubly coprime factorization and suitable for general linear systems is provided to make up these deficiencies.

## 1.2 Coprime Factorization

This section studies the properties of the coprime factorization which is a useful mathematical tool and will be applied in the later chapters. Coprime factorization can be characterized as a series connection of a stable system and the inverse of a stable system with no unstable pole-zero cancellations between factors. As an example consider the system with transfer function  $G(s)$  where

$$G(s) = \frac{(s+1)(s-2)}{(s+3)(s-4)(s+5)} \quad (1.2)$$

Then a coprime factorization of this system is indicated as follows:

$$G(s) = N_1(s)M_1^{-1}(s) \quad (1.3)$$

where


$$N_1(s) = \frac{(s-2)(s+1)}{(s+3)\alpha(s)}, \quad M_1(s) = \frac{(s-4)(s+5)}{\alpha(s)}$$

with  $\alpha(s)$  being any polynomial of degree 2 having no zeros in the closed right half plane.

Notice that this choice of degree for  $\alpha(s)$  ensures that  $M_1(s)$  is invertible whereas the restriction on the location of the zeros of  $\alpha(s)$  ensures that  $\alpha(s)$  is not involved in any unstable pole-zero cancellations between  $N_1(s)$  and  $M_1^{-1}(s)$ . Thus even if  $\alpha(s)$  has zeros at  $s = -1$  and/or  $-5$  the resulting pole-zero cancellations in  $N_1(s)$  and  $M_1^{-1}(s)$  are allowed. Stable systems which do not share any system zeros in the closed right-half plane are said to be “coprime”.



### 1.2.1 Why coprime [28]

In the foregoing example the numerator  $N_1(s)$  and denominator  $M_1(s)$  are coprime. In order to better appreciate this fact we give a second factorization of  $G(s)$  in which the factors are not coprime.

Suppose we re-express  $G(s)$  of Eq. (1.2) as

$$G(s) = N_2(s)M_2^{-1}(s) \quad (1.4)$$

where

$$N_2(s) = \frac{(s-6)(s-2)(s+1)}{(s+3)\beta(s)}, \quad M_2(s) = \frac{(s-6)(s-4)(s+5)}{\beta(s)}$$

with  $\beta(s)$  restricted to be any degree 3 polynomial with no zeros in the closed right-half plane. Although this factorization has the desired property that  $N_2(s), M_2(s) \in RH_\infty$  with  $M_2(s)$  being invertible, it does not satisfy the requirement that  $N_2(s)$  and  $M_2(s)$  be coprime since they share a right-half plane zero at  $s=6$ . Thus Eq. (1.4) is not a coprime factorization of  $G(s)$ . We can demonstrate the importance of not having unstable pole-zero cancellations between factors as follows.

Suppose that we have a strictly proper scalar transfer function  $G(s)$  having one of its  $n$  poles,  $n > 2$ , at  $s = s_0$  on the positive real axis with the remaining  $n-1$  poles being in the open left-half plane. These specifications imply that  $G(s)$  can be written as

$$G(s) = \frac{q(s)[s - (s_0 + \varepsilon)]}{(s - s_0)p(s)} \quad 0 \leq \varepsilon < \infty, \quad s_0 > 0 \quad (1.5)$$

where the degree of  $q(s)$  is less than  $p(s)$  with  $q(s_0) \neq 0$  and  $p(s)$  having no zeros in the closed right half plane, Now the system having this transfer function is stable only if  $\varepsilon = 0$  so that there is an unstable pole-zero cancellation. However, closer inspection of the consequences of such a pole-zero cancellation reveals that we cannot rely, in practice, on unstable pole-zero cancellations to make an unstable system stable. This becomes immediately evident when we consider the system's impulse response,  $L^{-1}[G(s)] = g(t)$

$$g(t) = -\varepsilon \frac{q(s_0)}{p(s_0)} e^{s_0 t} + r(t) \quad (1.6)$$

with  $r(t)$  bounded for  $0 \leq t < \infty$ .

Notice that if  $\varepsilon = 0$ ,  $-\varepsilon \frac{q(s_0)}{p(s_0)} e^{s_0 t}$  is missing from  $g(t)$ . Then the system's impulse response is bounded and the system is stable. However, if  $\varepsilon \neq 0$ , then  $-\varepsilon \frac{q(s_0)}{p(s_0)} e^{s_0 t}$  is present in  $g(t)$  and the system's impulse response tends to infinity with time and the system is unstable. Thus the system's stability is sensitive to  $\varepsilon$ . If  $s_0$  is in the open-left plane then  $-\varepsilon \frac{q(s_0)}{p(s_0)} e^{s_0 t}$  tends to zero with time and the system is stable for all  $\varepsilon$ .

Comparing the two types of pole-zero cancellation, stable and unstable, we understand that unstable pole-zero cancellation is not a reliable way in designing control system. We will see that the coprime factorization can not only make a feedback control system input-output stable but prevent unstable pole-zero cancellations between

the controller and the plant so that the closed loop system is internally stable.

### 1.2.2 State-space model for general coprime factorization

In this paragraph, a method is presented for obtaining left and right coprime factorizations of a system transfer matrix from its state-space description.

Consider a system described by the equations

$$\begin{cases} \dot{x}(t) = Ax(t) + Bu(t) \\ y(t) = Cx(t) + Du(t) \end{cases} \quad (1.7)$$

where  $A \in \mathbb{R}^{n \times n}$ ,  $B \in \mathbb{R}^{n \times m}$ ,  $C \in \mathbb{R}^{p \times n}$  and  $D \in \mathbb{R}^{p \times m}$  are real constant matrices.  $\mathbb{R}^{m \times n}$

represents the set of  $m \times n$  real constant matrices. The transfer matrix of this system

is

$$G(s) = C(sI - A)^{-1}B + D. \quad (1.8)$$

The objective is to derive a doubly coprime factorization of  $G(s)$ . One such factorization is given in theorem 1.1 below.

**Theorem 1.1** [36]: Given the system Eq. (1.7), suppose the pair  $(A, B)$ ,  $(A, C)$  are stabilizable and detectable, respectively. Select constant matrices  $F \in \mathbb{R}^{m \times n}$  and  $L \in \mathbb{R}^{n \times p}$  such that all eigenvalues of matrices  $A + BF$  and  $A + LC$  have negative real parts, i.e. Hurwitz, then  $G(s) = N(s)M^{-1}(s) = \tilde{M}^{-1}(s)\tilde{N}(s)$ . In addition both factorization pairs  $\{N(s), M(s)\}$ , and  $\{\tilde{N}(s), \tilde{M}(s)\}$  are called as right and left coprime factorizations since the denominator is on the right in  $G(s) = N(s)M^{-1}(s)$

and on the left in  $G(s) = \tilde{M}^{-1}(s)\tilde{N}(s)$ .

In addition, if  $N(s), M(s), (\tilde{N}(s), \tilde{M}(s))$  is right (left) coprime factor, we also have theorem 1.2 and Eq. (1.9) below [27].

$$\begin{bmatrix} X_r & Y_r \\ -\tilde{N} & \tilde{M} \end{bmatrix} \begin{bmatrix} M & -Y_l \\ N & X_l \end{bmatrix} = \begin{bmatrix} M & -Y_l \\ N & X_l \end{bmatrix} \begin{bmatrix} X_r & Y_r \\ -\tilde{N} & \tilde{M} \end{bmatrix} = I \quad (1.9)$$

where

$$\left[ \begin{array}{c|c} M & -Y_l \\ \hline N & X_l \end{array} \right] = \left[ \begin{array}{cc|c} A+BF & B & -L \\ \hline F & I & 0 \\ \hline C+DF & D & I \end{array} \right] \quad (1.10)$$

$$\left[ \begin{array}{c|c} X_r & Y_r \\ \hline -\tilde{N} & \tilde{M} \end{array} \right] = \left[ \begin{array}{cc|c} A+LC & -(B+LD) & L \\ \hline F & I & 0 \\ \hline C & -D & I \end{array} \right] \quad (1.11)$$

**Theorem 1.2** [28]: The factors  $M(s), N(s) \in RH_\infty$  ( $\tilde{M}(s), \tilde{N}(s) \in RH_\infty$ ) are right (left) coprime factors if and only if there exist  $X_r(s), Y_r(s) \in RH_\infty$  ( $X_l(s), Y_l(s) \in RH_\infty$ ) which satisfy the following Bezout identity:

$$X_r M + Y_r N = I \quad (1.12)$$

$$\tilde{M} X_l + \tilde{N} Y_l = I \quad (1.13)$$

**Proof:** Please refer to Chapter 8 of Ref. [28] for more details in the proof. □

### 1.2.3 Normalized coprime factorization

According to foregoing paragraph, we can obtain the right/left coprime factors of a given plant and its corresponding factors which satisfy Bezout identity by selecting any

compatible dimensions  $F$  and  $L$  matrices such that all eigenvalues of matrices  $A + BF$  and  $A + LC$  have negative real parts. This also implies that the coprime factorizations of Eqs. (1.10) and (1.11) are not unique ones. In the following paragraph, a unique coprime factorizations obtained in terms of solution to the generalized control (respectively, filter) algebraic Riccati equation are introduced.

**Theorem 1.3** [42]: A right coprime factorization of  $G(s) = N(s)M^{-1}(s)$  with  $N(s), M(s) \in RH_\infty$  is called *normalized right coprime factorization* if  $M^*M + N^*N = I$ ; that is, if  $\begin{bmatrix} M \\ N \end{bmatrix}$  is an **inner** function. The superscript  $(\bullet)^*$  denotes the shorthand of  $(\bullet)^T(-s)$ . Similarly, a left coprime factorization  $G(s) = \tilde{M}^{-1}(s)\tilde{N}(s)$  is called a *normalized left coprime factorization* if  $[\tilde{M} \ \tilde{N}]$  is a **co-inner**. Let a realization of  $G(s)$  be given by  $G(s) = \begin{bmatrix} A & B \\ C & D \end{bmatrix}$  and define  $R_\infty = I + D^*D > 0$  and  $\tilde{R}_\infty = I + DD^* > 0$ .

(a) Suppose  $(A, B)$  is stabilizable and  $(C, A)$  has no unobservable modes on the imaginary axis, there is a normalized right coprime factorization  $G = NM^{-1}$ , where

$$\begin{bmatrix} M \\ N \end{bmatrix} := \begin{bmatrix} A + BF & | & BR_\infty^{-1/2} \\ F & | & R_\infty^{-1/2} \\ C + DF & | & DR_\infty^{-1/2} \end{bmatrix} \in RH_\infty \quad (1.14)$$

and

$$F = -R_\infty^{-1}(B^*X_\infty + D^*C), \quad (1.15)$$

and the unique parameter  $X_\infty$  is the solution of the following generalized control algebraic Riccati equation (GCARE):

$$(A - BR_\infty^{-1}D^*C)^* X_\infty + X_\infty (A - BR_\infty^{-1}D^*C) - X_\infty BR_\infty^{-1}B^* X_\infty + C^* \tilde{R}_\infty^{-1}C = 0 \quad (1.16)$$

(b) Suppose  $(C, A)$  is detectable and  $(A, B)$  has no uncontrollable modes on the imaginary axis, there is a normalized left coprime factorization  $G = \tilde{M}^{-1} \tilde{N}$

$$\begin{bmatrix} \tilde{M} & \tilde{N} \end{bmatrix} := \left[ \begin{array}{c|cc} A + LC & L & B + LD \\ \hline \tilde{R}_\infty^{-1/2}C & \tilde{R}_\infty^{-1/2} & \tilde{R}_\infty^{-1/2}D \end{array} \right] \in RH_\infty \quad (1.17)$$

where

$$L = -(BD^* + Y_\infty C^*) \tilde{R}_\infty^{-1} \quad (1.18)$$

and the unique parameter  $Y_\infty$  is solved from the generalized filter algebraic Riccati equation (GFARE) as below:

$$(A - BR_\infty^{-1}D^*C)Y_\infty + Y_\infty (A - BR_\infty^{-1}D^*C)^* - Y_\infty C^* \tilde{R}_\infty^{-1}C Y_\infty + BR_\infty^{-1}B^* = 0. \quad (1.19)$$

□

**Remark 1.4** [36]: A transfer function  $N(s)$  is called *inner* if  $N(s) \in RH_\infty$  and  $N^{\sim}N = I$  and *co-inner* if  $N(s) \in RH_\infty$  and  $NN^{\sim} = I$ . Note that  $N(s)$  need not be square. Inner and co-inner are dual notions (i.e.  $N(s)$  is an inner iff  $N^T(s)$  is a co-inner).

**Theorem 1.5** [36]: Let  $N(s), M(s) (\tilde{N}(s), \tilde{M}(s))$  be a normalized right/left coprime factorization of  $G(s)$ , then we have

$$\|[\tilde{M} \quad \tilde{N}]\|_{\infty} = \left\| \begin{bmatrix} M \\ N \end{bmatrix} \right\|_{\infty} = 1 \quad (1.20) \square$$

Equation (1.20) is an important property of normalized right/left coprime factorization and will be frequently used in the later chapters.

### 1.3 Organization

This thesis is divided into five chapters, and a summary of these will now be given.

## **Chapter 2: DEVELOPMENT OF DOUBLY COPRIME FACTORIZATION DISTURBANCE OBSERVER**

In this chapter, we introduce how the Bezout identity motivated us to develop this novel doubly coprime factorization disturbance observer (DCFDOB) and its properties and stability. For minimum phase plants, the parameter  $Q(s)$  is designed as  $J \cdot (Y_l \tilde{N}_n)^{-1}$ . In non-minimum phase plant case, the  $Q(s)$  parameter is solved from the Nehari problem formed from model matching method. Furthermore, we also discuss the properties, parameter design method and stability of DCFDOB for unstable plants. Two control schemes, outer-loop controller and Vidyasagar's structure (VS) are provided when a plant is unstable. Furthermore, we co-structure the DCFDOB with VS to form a new 2 degree of freedom (2DOF) scheme (DCFDOB-VS). This novel control scheme provides two independent parameters,  $Q_Y(s)$  and  $H(s)$ , to not only stabilize the system but reject the disturbance.

## Chapter 3: Extension to General Plant Cases and Input/Output

### Disturbance

In classic control point of view, in general, good input disturbance rejection does not necessarily imply good output disturbance rejection unless feedback controller and plant are square and diagonal. In this chapter, we apply the proposed DCFDOB to general plant cases and consider both input and output disturbances and prove that the DCFDOB can eliminate both disturbances simultaneously. Also, four plant cases, minimum phase, non-minimum phase, stable and unstable plants are all discussed. In the previous chapter, we only consider the input sensitivity function, but in this chapter, the performances of both input and output sensitivity function are considered. When a plant is non-square, the rejection capability will be restricted, and we will discuss the design properties of non-square plant in this chapter. Moreover, the model matching method for MIMO systems is represented as well as for SISO systems in chapter 2.

## Chapter 4: Plant Uncertainty and System Robustness

In this chapter, we investigate the robust stability of DCFDOB and DCFDOB-VS under left coprime factorization plant uncertainties,  $P = (N_n + \Delta_N) \cdot (M_n + \Delta_M)^{-1}$ .

The small gain theorem is used here to derive robust stability tests and the modeling

error  $\Delta = \begin{bmatrix} \Delta_N \\ \Delta_M \end{bmatrix}$  will be assumed to be stable. In order to incorporate performance

objectives into the robust DCFDOB design, we propose a four-stage design procedure



which uses a loop shaping approach to deal performance / robustness trade-offs, and uses the normalized coprime factor robust stabilization method to guarantee closed-loop stability and a certain level of robust stability. The procedure is then as follows:

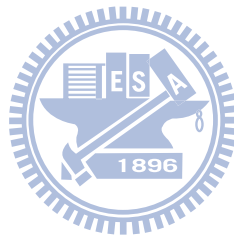
- (1) Reduce the original DCFDOB structure to an output feedback type structure.
- (2) Using pre- and / or post- weighting matrix to shape the singular values of the nominal plant as a desired open-loop shape, and then calculate  $\varepsilon_{s,\max}$ , the maximum stability margin.
- (3) An output feedback type of the DCFDOB which satisfies the robust condition is synthesized, then the output feedback type of the DCFDOB and shaping weighting matrix are combined to form the final output feedback type of the DCFDOB.
- (4) The  $Q(s)$  parameter of original DCFDOB can be obtained according to the relations between the original DCFDOB and the reduced one.

We give theoretical justification of this technique, and show that it is a simple and systematic approach to design.

## **Chapter 5: Numerical Examples and Experimental Results**

This chapter demonstrates those design methods introduced in each chapter. In part 1, minimum phase plant cases are shown. In the first example of part 2, an unstable and non-minimum phase SISO plant is used and in the second example of part 2, a stable and non-minimum phase MIMO plant is considered. These results show

that the DCFDOB structure is flexible in designing. In part 3, one shows the design properties of DCFDOB for both thin and wide plant cases. In part 4, one demonstrates the steps of  $H_\infty$ -loop shaping design method of Robust DCFDOB developed in chapter 4. Finally, an experimental result of a positioning control for an AC brushless servomotor system and cogging force suppressing will be illustrated. Final chapter will draw the conclusions.



## CHAPTER 2

### DEVELOPMENT OF DOUBLY COPRIME FACTORIZATION

#### DISTURBANCE OBSERVER

##### 2.1 Doubly coprime disturbance observer and Bezout identity

This section introduces how the *Bezout Identity* motivated us to develop this novel DCFDOB. According to Eqs. (1.10) and (1.11), one can obtain the right (left) coprime factorizations of plant  $P(s)$ ,  $P(s) = NM^{-1}$  ( $P(s) = \tilde{M}^{-1}\tilde{N}$ ) and its corresponding left (right) coprime factorization  $X_r(s), Y_r(s) \in RH_\infty$  ( $X_l(s), Y_l(s) \in RH_\infty$ ) such that satisfy “Bezout Identity” and doubly coprime factorization shown in Eq. (1.9).

If one construct the block diagram as Fig.2.1, according to Eq. (1.12), the following equation can be obtained.

$$\begin{aligned}\hat{Z} &= X_r \cdot u + Y_r \cdot N \cdot M^{-1} \cdot u \\ &= (X_r M + Y_r N) M^{-1} \cdot u \\ &= I \cdot (M^{-1} \cdot u) \\ &= Z\end{aligned}\tag{2.1}$$

From Eq. (2.1), the internal states  $Z$  of the system can be estimated and this basic structure can be extended to develop a disturbance observer.

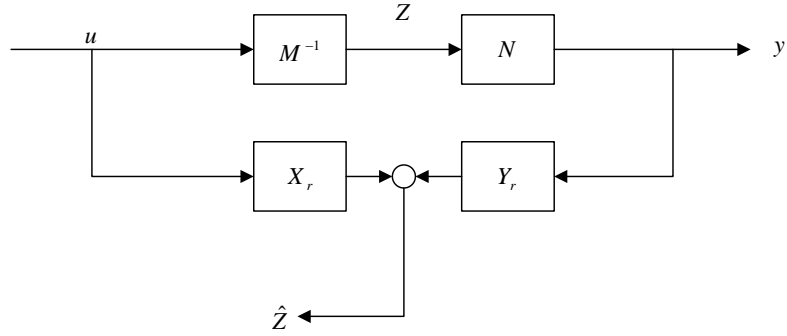


Fig. 2.1 Basic Structure based on Bezout identity

Assume that the plant ( $P(s) = NM^{-1}$ ) contains no uncertainty i.e.  $M = M_n, N = N_n$  and noise free ( $\xi = 0$ ). If the system suffers only input disturbance, one can plot the block diagram as follows.

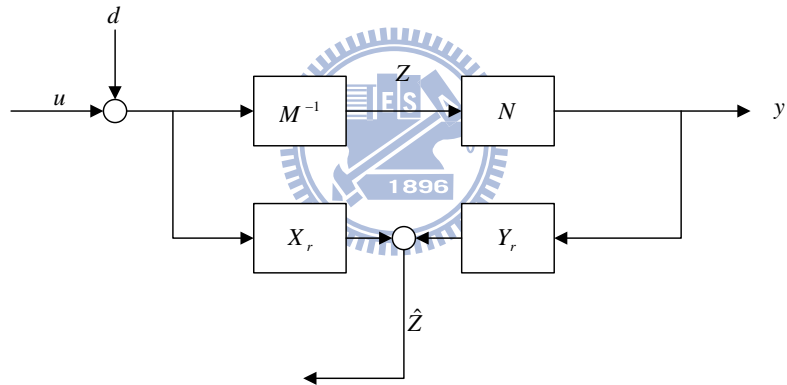


Fig. 2.2 Internal states estimation with input disturbance

and the estimated disturbance can be derived from the block diagram as follow:

$$\begin{aligned}
 \hat{Z} &= X_r(u+d) + Y_r N M^{-1}(u+d) \\
 \Rightarrow M\hat{Z} &= (X_r M + Y_r N) \cdot (u+d) \\
 \Rightarrow d &= M\hat{Z} - u
 \end{aligned}
 \tag{2.2}$$

One can extend the basic structure as following figures to eliminate the input disturbance ( $\hat{d} = d$ ) from such a derivation.

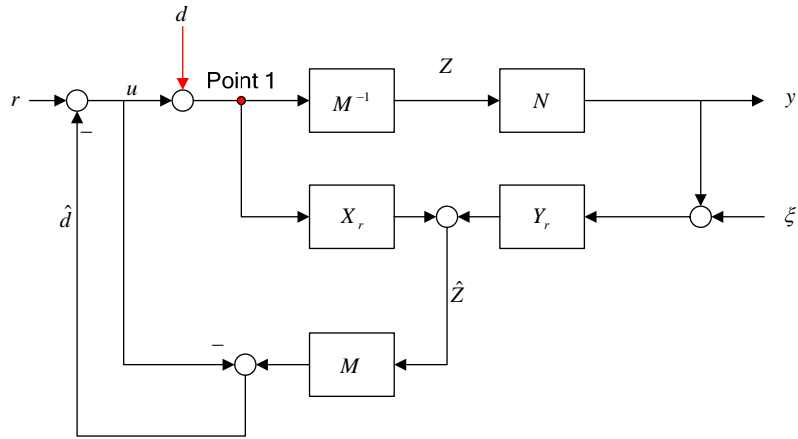


Fig. 2.3 Extended structure with virtual disturbance entry point

Actually, it is impossible (very difficult) to acquire the signals of point 1, that is, the real disturbance can not be reconstructed precisely, only input signal  $u(t)$  can be obtained, and the structure should be modified as follows.

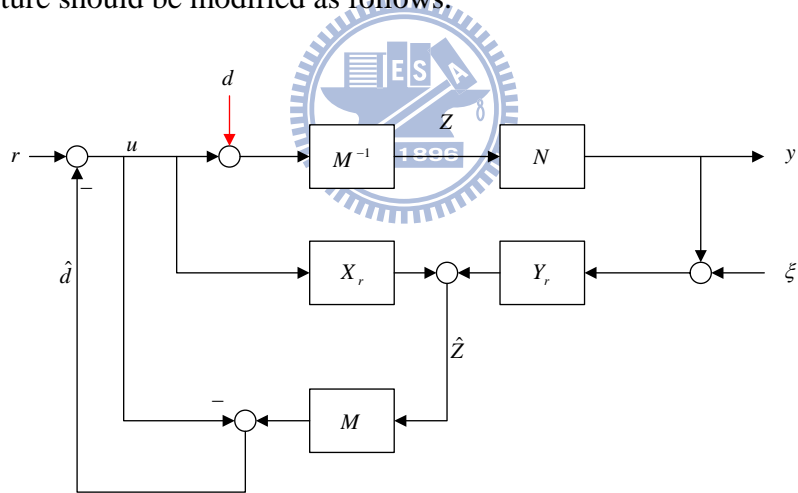


Fig. 2.4 Extended structure with actual disturbance entry point

And then one can obtain the estimated disturbance from the following derivation shown in Eq. (2.3).

$$\begin{aligned}
&\Rightarrow \hat{Z} = X_r \cdot u + Y_r N M^{-1} (u + d) \\
&\Rightarrow M \hat{Z} = M (X_r M + Y_r N) M^{-1} \cdot u + M Y_r N M^{-1} \cdot d \\
&\Rightarrow M \hat{Z} - u = M (I - X_r M) M^{-1} \cdot d \\
&\Rightarrow M \hat{Z} - u = (I - M X_r) \cdot d \\
&\Rightarrow M \hat{Z} - u = Y_l \tilde{N} \cdot d \\
&\Rightarrow \tilde{N}^{-1} Y_l^{-1} (M \hat{Z} - u) = d = \hat{d}
\end{aligned} \tag{2.3}$$

and modify the block diagram as Fig.2.5 to eliminate the input disturbance completely.

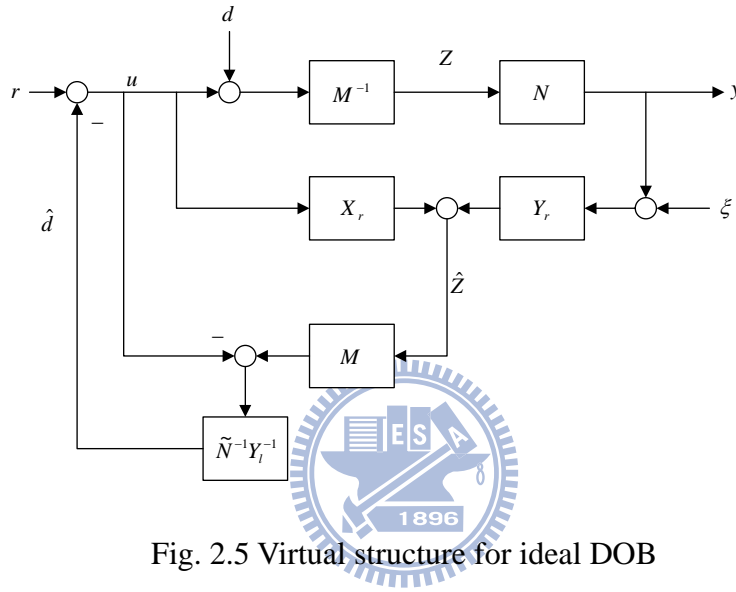


Fig. 2.5 Virtual structure for ideal DOB

After the modification, here arises a general problem that  $\tilde{N}^{-1} Y_l^{-1}$  are not guarantee to be stable or proper transfer functions. So, above structure must be modified again. In this thesis, one replaces  $\tilde{N}^{-1} Y_l^{-1}$  with a stable and proper parameter  $Q(s)$  such that  $Q(M \hat{Z} - u) = \hat{d} \approx d$  to estimate the real disturbance and suppress the influence of input disturbance. The novel structure is shown in Fig. 2.6 and called the “Doubly coprime factorization disturbance observer (DCFDOB)”.

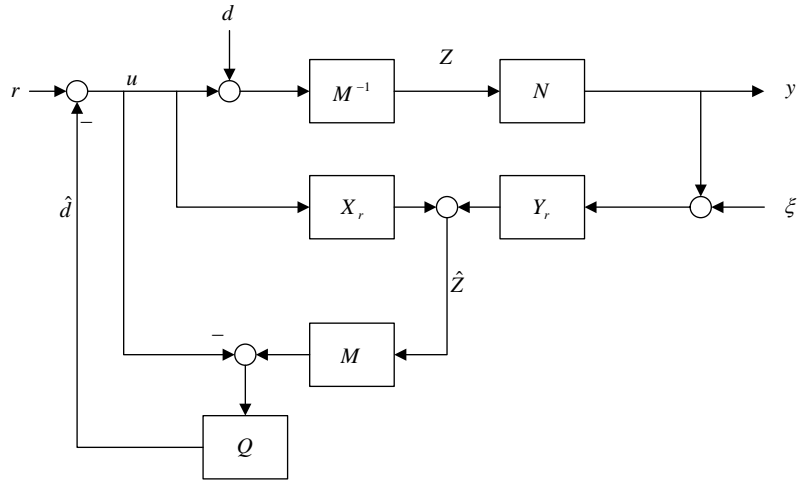


Fig. 2.6 Block diagram of the DCFDOB

After introducing the DCFDOB scheme, the following sections will investigate and discuss the properties about this scheme and apply it to general plant cases, such as stable, unstable, minimum-phase, non-minimum-phase systems, square and non-square plants.



## 2.2 Applications to Stable systems

In this paragraph, we look into the properties of DCFDOB and design methods of parameter  $Q(s)$  when the DCFDOB be used in stable system. Suppose that the plant is stable and without plant uncertainties, i.e.  $N_n M_n^{-1} = P_n = P \in RH_\infty$  and  $M_n, N_n, X_r, Y_r, Q \in RH_\infty$ .

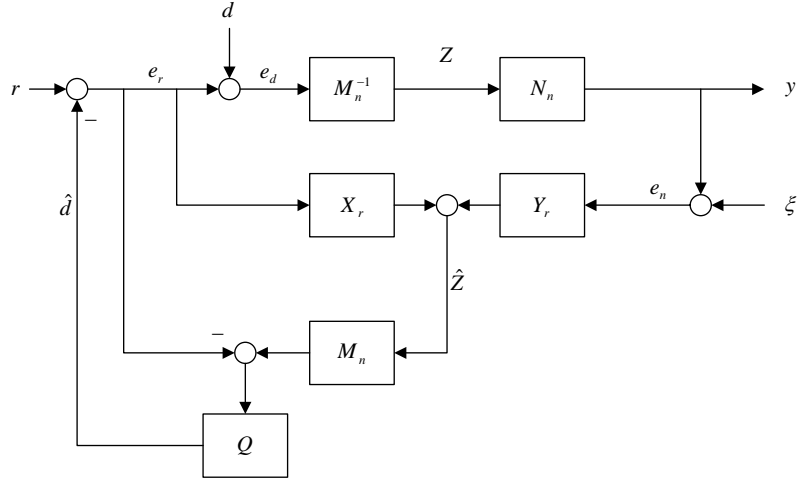


Fig. 2.7 The DCFDOB for stable system

The nine transfer functions from external input signals  $[r \ d \ \xi]^T$  to internal signals  $[e_r \ e_d \ e_n]^T$  is shown below.

$$\begin{bmatrix} e_r \\ e_d \\ e_n \end{bmatrix} = \begin{bmatrix} I & -Q(I - M_n X_r) & -QM_n Y_r \\ I & I - Q(I - M_n X_r) & -QM_n Y_r \\ N_n M_n^{-1} & N_n M_n^{-1}(I - Q(I - M_n X_r)) & I - N_n M_n^{-1} QM_n Y_r \end{bmatrix} \begin{bmatrix} r \\ d \\ \xi \end{bmatrix} \quad (2.4)$$

From the  $3 \times 3$  transfer function matrix, one can obtain all elements are stable and then the system will be internally stable. One of the main objects of this study is designing  $Q(s) \in RH_\infty$  such that  $I - Q(I - M_n X_r) \approx 0$  to suppress the influence from input disturbance  $d$  to compensated input signals  $e_d$ . That is, the transfer function from real disturbance  $d$  to estimated disturbance  $\hat{d}$  is one. It seems that one can design  $Q = (I - M_n X_r)^{-1} = \tilde{N}_n^{-1} \cdot Y_l^{-1}$  directly to achieve this aim, but at least two basic criteria must be satisfied.

- 1).  $(I - M_n X_r) = (Y_l \tilde{N}_n)$  must be proper but not strictly proper, that is,  $(I - M_n X_r)^{-1}$  is realizable.



2). The zeros of  $(I - M_n X_r)$  must lie in left half plane, i.e.  $(I - M_n X_r)^{-1} = (Y_l \tilde{N}_n)^{-1}$

is stable.

For the first criterion, according to [27] one can obtain the doubly coprime

factorization of a system transfer matrix from its state-space description as follows.

$$\left[ \begin{array}{c|c} M & Y_l \\ \hline N & X_l \end{array} \right] = \left[ \begin{array}{c|c|c} A+BF & B & -L \\ \hline F & I & 0 \\ \hline C+DF & D & I \end{array} \right] \quad (2.5)$$

$$\left[ \begin{array}{c|c} X_r & -Y_r \\ \hline -\tilde{N} & \tilde{M} \end{array} \right] = \left[ \begin{array}{c|c|c} A+LC & -(B+LD) & L \\ \hline F & I & 0 \\ \hline C & -D & I \end{array} \right] \quad (2.6)$$

where  $A \in \mathbb{R}^{n \times n}$ ,  $B \in \mathbb{R}^{n \times m}$ ,  $C \in \mathbb{R}^{p \times n}$  and  $D \in \mathbb{R}^{p \times m}$  are real constant matrices.  $\mathbb{R}^{m \times n}$

represents the set of  $m \times n$  real constant matrices.  $F \in \mathbb{R}^{m \times n}$  is a control gain matrix

and  $L \in \mathbb{R}^{n \times p}$  is an observer gain matrix such that the real parts of eigenvalues of

$A+BF$  and  $A+LC$  are negative. One obtains

$$\begin{aligned} M_n X_r &= \left[ \begin{array}{c|c} A+BF & B \\ \hline F & I \end{array} \right] \cdot \left[ \begin{array}{c|c} A+LC & -(B+LD) \\ \hline F & I \end{array} \right] \\ &= \left[ \begin{array}{c|c|c} A+BF & BF & B \\ \hline 0 & A+LC & -(B+LD) \\ \hline F & F & I \end{array} \right] \\ &= \left[ \begin{array}{c|c} \hat{A} & \hat{B} \\ \hline \hat{C} & I \end{array} \right] \end{aligned} \quad (2.7)$$

$I - M_n X_r = I - (I + \hat{C}(sI - \hat{A})^{-1} \hat{B}) = \left[ \begin{array}{c|c} \hat{A} & \hat{B} \\ \hline -\hat{C} & 0 \end{array} \right]$ , since  $\hat{D} = 0$ , i.e.  $I - M_n X_r$  is strictly

proper,  $(I - M_n X_r)^{-1}$  must be improper and unrealizable.

For the second criterion and Eq. (1.9), the Eq. (2.8) is obtained,

$$I - M_n X_r = Y_l \tilde{N}_n. \quad (2.8)$$

The transfer function  $Y_l(s)\tilde{N}_n(s)$  contains non-minimum phase zeros while the plant contains non-minimum phase zeros (non-minimum phase zeros exist in  $\tilde{N}_n(s)$ ), that is, the unstable poles exist in  $(I - M_n X_r)^{-1}$ .

The following paragraphs will show how to design  $Q(s) \in RH_\infty$  to reject input disturbance for minimum phase and non-minimum phase systems in stable systems.

### 2.2.1 Design method for minimum-phase systems

As one stated above, for a stable plant, the DCFDOB will be internally stable. Suppose that the plant is single-input, single-output and then  $1 - Q(1 - M_n X_r) = 1 - QY_l \tilde{N}_n$ . For a minimum phase plant,  $\tilde{N}_n(s)$  does not contain right half plane-zeros (RHP-zeros), i.e.  $\tilde{N}_n^{-1}(s)$  is stable; In addition, Eq. (2.5) indicates that  $Y_l(s)$  of a minimum phase plant can be obtained by the control gain matrix  $F$  and the observer gain matrix  $L$  for the plant, that is,  $Y_l^{-1}(s)$  is stable, too. So that the simplest way in designing  $Q(s)$  can be done as follows.

$$Q(s) = J \cdot (Y_l \tilde{N}_n)^{-1} \in RH_\infty \quad (2.9)$$

where  $J(s)$  is a low-pass filter and the transfer function from  $d$  to  $e_d$  will become  $1 - J(s)$ . Clearly, the capacity of disturbance rejection increases with the bandwidth of  $J(s)$ ; Furthermore, the transfer function from measurement noise  $\xi$  to system output

$y$  is  $-J(s)$ . Although one can enlarge the bandwidth of  $J(s)$  to increase the rejecting capacity, the measurement noise will affect system performance more seriously and the tradeoff must be considered. Besides, substituting the particular solution  $Q(s) = J \cdot (Y_l \tilde{N}_n)^{-1}$  into Eq. (2.4) yields Eq. (2.10).

$$\begin{bmatrix} e_r \\ e_d \\ e_n \end{bmatrix} = \begin{bmatrix} 1 & -J & -P_n^{-1}J \\ 1 & (1-J) & -P_n^{-1}J \\ P_n & P_n(1-J) & (1-J) \end{bmatrix} \begin{bmatrix} r \\ d \\ \xi \end{bmatrix} \quad (2.10)$$

Recalling Eq. (1.1) and a low-pass filter  $J(s)$  is substituted for  $Q(s)$ , one also can obtain the same result as Eq. (2.10) when assumption  $P(s) = P_n(s)$  is made. That is, the DCFDOB can be reduced to the one which proposed by [1], hence the designing guideline of low pass filter and stability analysis that provided by previous literatures can be used. With these points in mind, one may look into MIMO plant for generality.

Suppose a MIMO, stable, and minimum phase plant,  $P_{n \times m}$  with  $n \times m$  ( $n \geq m$ ) dimension i.e. the input channel number is greater than the output channel number, and  $(I_{m \times m} - M_{n, m \times m} X_{r, m \times m})$  is also minimum phase, the elements of  $Q(s)$  can be solved from

$$Q_{m \times m} = J_{m \times m} \cdot (I_{m \times m} - M_{n, m \times m} X_{r, m \times m})^{-1} = J_{m \times m} \cdot (Y_{l, m \times n} \cdot \tilde{N}_{n \times m})^{-1} \quad (2.11)$$

and  $J_{m \times m}$  is a diagonal matrix which is composed of low-pass filters,

$J_{m \times m} = \text{diag}\{j_{11} \cdots j_{mm}\}_{m \times m}$ . Equation (2.11) implies that the DCFDOB can be

applied to not only square plant but also non-square thin plant and this advantaged

property cannot be done in the scheme of [1] because the non-square plant cannot be inverted.

### 2.2.2 Design method for non-minimum-phase systems

For non-minimum-phase systems, one can **NOT** design  $Q(s)$  as  $J \cdot (Y_l \tilde{N}_n)^{-1}$ , since  $(Y_l \tilde{N}_n)$  term contains RHP-zeros, i.e.  $(Y_l \tilde{N}_n)^{-1}$  is unstable. For internally stability purpose, this thesis applies model matching method to design parameter  $Q(s) \in RH_\infty$ .



#### 2.2.2.1 Model matching method in non-minimum plants

The main object of the DCFDOB is to suppress the influence from  $d$  to  $e_d$  as small as possible and can be described as

$$\min_{Q \in RH_\infty} \|I - Q(I - M_n X_r)\|_\infty < \gamma \leq 1 \quad (2.12)$$

According to Eq. (1.9), one can rewrite Eq. (2.12) in following equations.

$$\begin{aligned} & \min_{Q \in RH_\infty} \|I - Q(I - M_n X_r)\|_\infty \\ &= \min_{Q \in RH_\infty} \|M_n X_r + \hat{Q} Y_l \tilde{N}_n\|_\infty \\ &= \min_{Q \in RH_\infty} \|T_1 + T_2 \hat{Q} T_3\|_\infty \end{aligned} \quad (2.13)$$

where  $T_1 = M_n X_r \in RH_\infty$ ,  $T_2 = I$ ,  $T_3 = Y_l \tilde{N}_n \in RH_\infty$ ,  $\hat{Q} = (I - Q) \in RH_\infty$ . The main design object of model matching problem is to find the whole sets of  $\hat{Q}(s) \in RH_\infty$  that satisfy  $\|T_1 + T_2 \hat{Q} T_3\|_\infty < \gamma \leq 1$ . That is,  $\|I - Q(I - M_n X_r)\|_\infty < \gamma \leq 1$ .

**Model matching problem:**

Finding the whole satisfied sets of  $\hat{Q}(s)$  such that the distance between model  $T_2\hat{Q}T_3$  and reference model  $T_1$  shorter than a constant  $\gamma$  can be described as:

$$\|T_1 + T_2\hat{Q}T_3\|_{\alpha} < \gamma, \quad \alpha = 2, \infty, \mu, \quad (2.14)$$

and Fig. 2.8 illustrates the meaning of model matching problem. The distance between two models can be measured by  $H_2$ - norm,  $H_{\infty}$ - norm or  $\mu$ - norm. Equation (2.14) is called ‘‘Nevanlinna-Pick Problem’’ and its main objective is described as Eq. (2.15)

[29]:

$$\varepsilon_{\gamma} = \{\Phi = T_1 + T_2\hat{Q}T_3 \mid \hat{Q} \in RH_{\infty}, \|\Phi\|_{\infty} < \gamma\} \quad (2.15)$$

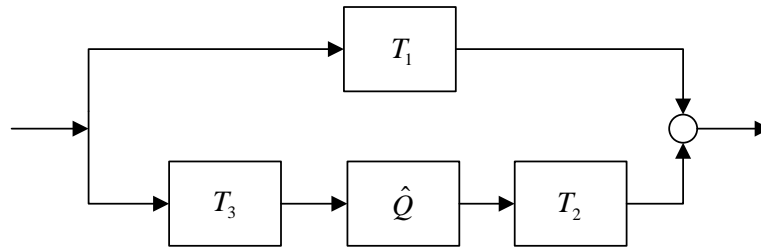


Fig. 2.8 Model matching problem

Since  $T_2$  of Eq. (2.13) is a unit matrix then  $\|T_1 + T_2\hat{Q}T_3\|_{\infty} = \|T_1 + \hat{Q}T_3\|_{\infty}$  and

$$\begin{aligned} \|T_1 + \hat{Q}T_3\|_{\infty} &= \|T_1 + \hat{Q}T_{3o}T_{3i}\|_{\infty} \\ &= \|T_1T_{3i} + \hat{Q}T_{3o}\|_{\infty} \end{aligned} \quad (2.16)$$

where  $T_{3i}$  is an inner function, and  $T_{3o}$  is an outer function that satisfy the following properties:

$$\begin{cases} T_{3i}^{\sim} \cdot T_{3i} = I, & T_{3i}^{\sim} = T_{3i}^T(-s) \\ T_{3o}^{-1} \in RH_{\infty} \end{cases} \quad (2.17)$$

Here  $T_{3i}$  is an inner function, from lemma 2.1 we know that a function multiplied by an inner function will not influence the  $H_{\infty}$  - norm of a function.

**Lemma 2.1** [29]: If  $U$  is an inner function, then  $\|AU\|_{\infty} = \|UA\|_{\infty} = \|A\|_{\infty}$ .  $\square$

According to lemma 2.1 and then Eq. (2.16) can be rewritten as follows.

$$\begin{aligned} \|T_1 + \hat{Q}T_3\|_{\infty} &= \|T_1 + \hat{Q}T_{3o}T_{3i}\|_{\infty} \\ &= \|T_1T_{3i}^{\sim} + \hat{Q}T_{3o}\|_{\infty} \\ &= \|R - \tilde{Q}\|_{\infty} \quad (R \in RL_{\infty}, \tilde{Q} \in RH_{\infty}) \end{aligned} \quad (2.18)$$

where  $R = T_1T_{3i}^{\sim} \in RL_{\infty}$ ,  $\tilde{Q} = -\hat{Q}T_{3o}$ ,  $\hat{Q} = -\tilde{Q}T_{3o}^{-1} \in RH_{\infty}$  and  $RL_{\infty}$  denotes the space of all real rational transfer function matrices which have no poles on the imaginary axis.

Through these operations, the model matching problem becomes a well-known

Nehari Problem [30].

### 2.2.2.2 Nehari problem

#### **Nehari problem:**

For a function  $R(s) \in RL_{\infty}$ , finding a set  $\tilde{Q}(s) \in RH_{\infty}$  such that the distance between  $R(s)$  and  $\tilde{Q}(s)$  ( $H_{\infty}$  - norm) smaller than a constant  $\gamma$  is expressed as

$$\|R - \tilde{Q}\|_{\infty} < \gamma \quad (2.19)$$

According to [31], the minimum value of  $\gamma$  is equal to the Hankel operator norm., i.e.

the shortest distance from  $R(s)$  to the  $RH_\infty$  set.

$$\min_{\tilde{Q}_{opt} \in RH_\infty} \|R - \tilde{Q}_{opt}\|_\infty = \|H_R\| \quad (2.20)$$

**Recall** [29]: (1)  $RL_n^2$  denotes an  $n \times 1$  vector with strictly proper rational functions

contains no poles on the imaginary axis, that is, it belongs to Hilbert space and the inner

product for the Hilbert space is defined as

$$\langle u, v \rangle = \frac{1}{2\pi} \int_{-\infty}^{\infty} u^{\sim}(j\omega) \cdot v(j\omega) d\omega \quad (2.21)$$

where  $u^{\sim}(j\omega) = u^T(-j\omega)$

(2)  $RH_n^2$ : The subspace of  $RL_n^2$  and analytic in RHP

(3)  $RH_n^{2\perp}$ : The orthogonal complement space of  $RH_n^2$

$$RH_n^{2\perp} = \{u \in RL_n^2 \mid \langle u, v \rangle = 0 \forall v \in RH_n^2\} \quad (2.22)$$

**Definition 2.2** [29]: If  $R \in RL_{m \times n}^\infty$ , we define the relation between  $RH_n^2$  and  $RH_m^{2\perp}$

as Hankel operator  $H_R$

$$H_R : RH_n^2 \rightarrow RH_m^{2\perp}, \quad \square (2.23)$$

and its norm is Hankel norm of  $R$ .

$$\|H_R\| = \|R\|_H \quad (2.24)$$

[29] showed that

$$\min_{\tilde{Q}_{opt} \in RH_\infty} \|R - \tilde{Q}_{opt}\|_\infty = \|H_R\| = \rho(L_o L_c)^{1/2} \quad (2.25)$$

where  $L_c, L_o$  denotes controllability matrix and observability matrix respectively and

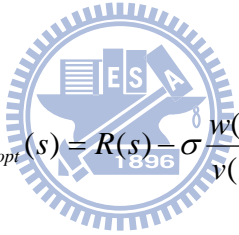
satisfy the Lyapunov equation.

$$\begin{aligned} A_{R_-} L_c + L_c A_{R_-}^T &= B_{R_-} B_{R_-}^T \\ A_{R_-}^T L_o + L_o A_{R_-} &= C_{R_-}^T C_{R_-} \end{aligned} \quad (2.26)$$

where  $A_{R_-}$ ,  $B_{R_-}$ , and  $C_{R_-}$  denote the state space minimum realization of  $R_-(s)$ , the unstable parts of  $R(s)$ , and  $R(s) = R_+(s) + R_-(s)$ . If one define  $\rho(L_o L_c) = \max |\lambda_i(L_o L_c)|$ , i.e. the spectral radius of  $(L_o L_c)$ , then the Hankel operator norm is

$$\|H_R\| = \|R\|_H = \rho(L_o L_c)^{1/2} \quad (2.27)$$

As one mentioned earlier, the minimum value of  $\|R - \tilde{Q}_{opt}\|_\infty$  is equal to the Hankel operator norm. According to [29], one can find the optimum solution of  $\tilde{Q}_{opt}(s)$  as follows.



$$\tilde{Q}_{opt}(s) = R(s) - \sigma \frac{w(s)}{v(s)} \quad (2.28)$$

where

$$w(s) = \left[ \begin{array}{c|c} A_{R_-} & \sigma^{-1} L_c B_v \\ \hline C_{R_-} & 0 \end{array} \right], \quad (2.29)$$

$$v(s) = \left[ \begin{array}{c|c} -A_{R_-}^T & B_v \\ \hline B_{R_-}^T & 0 \end{array} \right], \quad (2.30)$$

and

$$L_o L_c B_v = \sigma^2 B_v \quad (2.31)$$

The notations  $\sigma$  and  $B_v$  of Eq. (2.31) denotes the maximum eigenvalue of  $L_c L_o$  and its corresponding eigenvector, respectively. The above steps to find the optimum solution are only suitable for SISO plant. For MIMO plant, one shows the solving



steps in Chapter 3.

### 2.2.2.3 Weighting function design

From previous statements, the optimum  $\tilde{Q}_{opt}(s)$  can be obtained via solving Nehari problem such that  $\min_{Q \in RH_\infty} \|I - Q(I - M_n X_r)\|_\infty = \|R\|_H$ . But for rejecting the specific frequency range disturbance purpose, particularly in the low-frequency in most cases, adding a weighting function  $W(s)$  is needed. Then the main objective becomes

$$\min_{Q \in RH_\infty} \|W - Q(I - M_n X_r)W\|_\infty < \gamma \leq 1 \quad (2.32)$$

If one define input sensitivity function as  $S_i = (I - Q(I - M_n X_r))$  then Eq. (2.32) can be rewritten as

$$\begin{aligned} \|W - Q(I - M_n X_r)W\|_\infty &= \|S_i \cdot W\|_\infty < \gamma \leq 1 \\ \Leftrightarrow |S_i(j\omega)| &\leq |W^{-1}(j\omega)| \end{aligned} \quad (2.33)$$

Equation (2.33) indicates that the frequency response of input sensitivity function will less than the inversion of a specific weighting function one, i.e. the design specification can be given clearly via giving a specific weighting function. However, the sensitivity function must satisfy the integral function as follows.

$$\int_0^z \ln |S_i(j\omega)| d\omega = \int_0^z \ln |I - Q(j\omega)(I - M_n X_r(j\omega))| d\omega \approx 0 \quad (\text{for } |S_i| \approx 1 \text{ at } \omega > z)$$

(2.34)

From Eq. (2.34), it is easy to understand that a tradeoff between  $S_i(j\omega)$  less than 1 and  $S_i(j\omega)$  larger than 1, is done over a limited frequency range. Thus, a large peak  $|S_i(j\omega)|$  is unavoidable if one tries to reduce  $|S_i(j\omega)|$  at low frequencies and the lower level of sensitivity function one pushes down in low frequency region the large peak greater than 1 of sensitivity one obtain somewhere. This phenomenon is called “waterbed effect” and unavoidable, particularly when plant contains RHP-zeros. This benefit and harmful influence must be tradeoff; furthermore, the crossover frequency of sensitivity function is also limited by RHP-zeros. For example, when plant contains a dominant real RHP-zero  $z$  the approximate crossover frequency  $\omega_c$  of sensitivity function encounters the limitation :  $\omega_c < \frac{z}{2}$ . In other words, the disturbance rejecting frequency region is smaller than  $\frac{z}{2}$  and the location of system zeros will affect the capacity of disturbance rejection significantly. About this topic, please refer [32] for more detail derivation. Basing on above previous discussion, it is known that RHP-zeros will not only limit the disturbance rejecting performance but also rejecting bandwidth. Moreover, the crossover frequency of weighting function  $W(s)$  must be constrained to satisfy the bandwidth limitation and Eq. (2.33). To specify the capacity of disturbance rejection, here, one provides a design method which can specify not only the DC-gain but also the crossover frequency  $\omega_c$  for weighting function. The weighting function is exhibited as below.

$$W(s) = \frac{M_w}{C_1 s + a} \quad (2.35)$$

And one gives  $a > 0$  arbitrarily, and the DC-gain of the weighting function is  $\frac{M_w}{a}$ .

Since the weighting function must cross 0dB at specific frequency,  $\omega_c$  and the satisfies the limitation  $\omega_c < \frac{z}{2}$ , one can write a equation as Eq. (2.36).

$$\left| \frac{M_w}{C_1(j\omega_c) + a} \right|_{\omega_c < \frac{z}{2}} = 1 \quad (2.36)$$

For giving a specific DC-gain  $\frac{M_w}{a}$  and crossover frequency,  $\omega_c < \frac{z}{2}$ , then the parameter  $C_1$  can be solved. Suppose a non-minimum phase nominal plant

$P_n(s) = \frac{0.2s - 20}{s + 20}$  with single real zero at 100rad/sec, one designs a weighting

function with different DC-gains as 20dB, 60dB and 100dB, and gives  $\omega_c = 40$ rad/sec,

$a = 10$  and  $M_w = 10^2, 10^4, 10^6$ , then the corresponding parameters can be solved as

$C_1 = \frac{1985}{798}, 250, 25000$ . The frequency responses of weighting functions and

corresponding input sensitivity functions are plotted in Fig. 2.9(a)-(b). Clearly, the

frequency responses of input sensitivity function below the one of inversion weighting

function indeed. Moreover, the crossover frequency of input sensitivity function and

its limitation is 41.7rad/sec and 50rad/sec respectively. The maximum peak value

of input sensitivity function is 1.7873, 1.8293, and 1.8297 respectively.

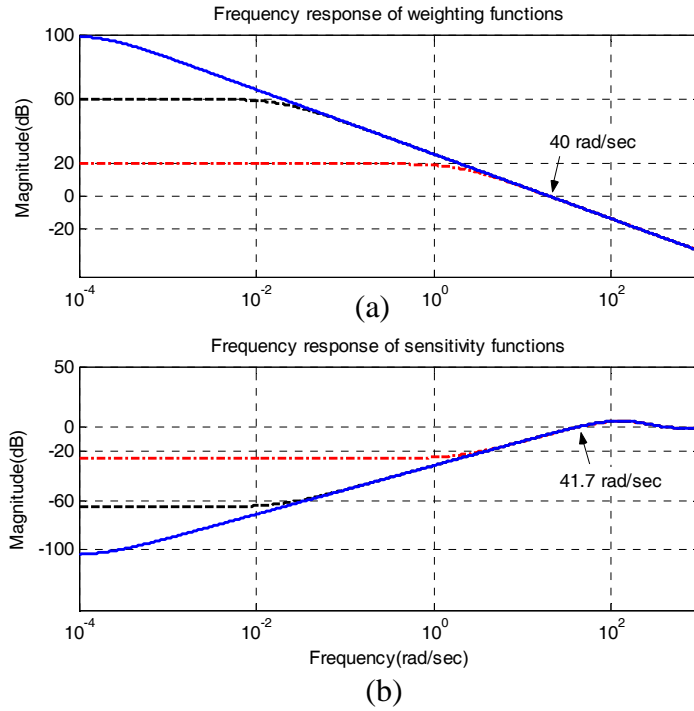
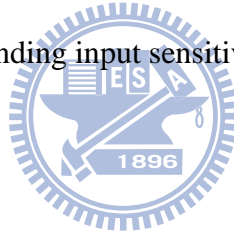


Fig. 2.9 (a) Different weighting functions and

(b) corresponding input sensitivity functions



### 2.3 The Application to Unstable Systems

One applies DCFDOB structure to unstable plant in the following section. If a plant is unstable, from the transfer functions matrix in Eq. (2.4), the transfer function from reference command  $r$  to system output  $y$  is  $N_n M_n^{-1}$ , i.e. the DCFDOB could not change the tracking property and the system is unstable without controller. To solve this problem, one can add an outer-loop controller  $K(s)$  to stabilize the system. The block diagram and nine transfer functions from  $[r \ d \ \xi]^T$  to  $[e_r \ e_d \ e_n]^T$  are shown in Fig. 2.10 and Eq. (2.37).

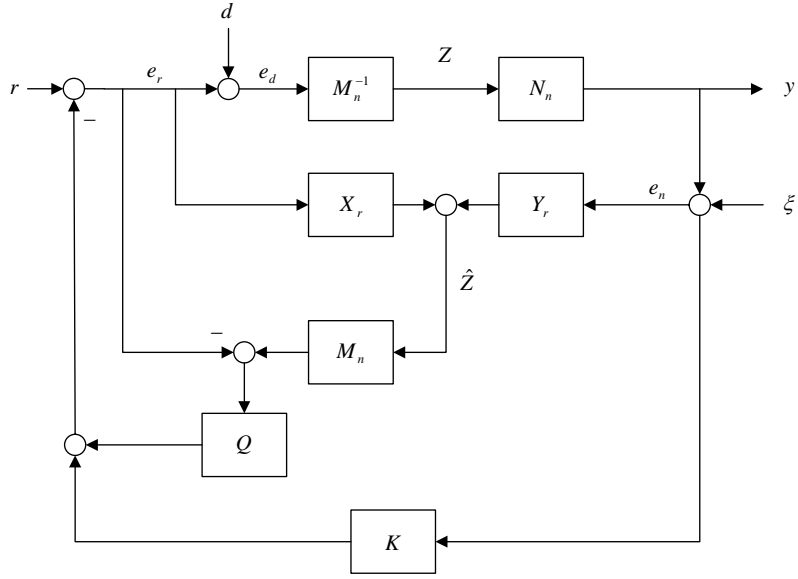


Fig. 2.10 The DCFDOB with outer-loop controller

$$\begin{bmatrix} e_r \\ e_d \\ e_n \end{bmatrix} = \begin{bmatrix} \Lambda^{-1} & -\Lambda^{-1}[(K + QM_n Y_r)N_n M_n^{-1}] & -\Lambda^{-1}(K + QM_n Y_r) \\ \Lambda^{-1} & \Lambda^{-1}[I - Q(I - M_n X_r)] & -\Lambda^{-1}(K + QM_n Y_r) \\ N_n M_n^{-1} \Lambda^{-1} & N_n M_n^{-1} \Lambda^{-1}[I - Q(I - M_n X_r)] & I - N_n M_n^{-1} \Lambda^{-1}(K + QM_n Y_r) \end{bmatrix} \begin{bmatrix} r \\ d \\ \xi \end{bmatrix} \quad (2.37)$$

where  $\Lambda = (I + KN_n M_n^{-1})$ . From Eq. (2.37), because the unstable poles exist in  $M_n^{-1}(s)$ , one designs a controller  $K(s) \in RH_\infty$  to stabilize the system such that

$$(I + KN_n M_n^{-1})^{-1} \in RH_\infty \quad (2.38)$$

and

$$\begin{cases} (I + KN_n M_n^{-1})^{-1} N_n M_n^{-1} \in RH_\infty \\ N_n M_n^{-1} (I + KN_n M_n^{-1})^{-1} \in RH_\infty \end{cases} \quad (2.39)$$

Furthermore, the coprime factors,  $M_n(s)$ ,  $N_n(s)$ ,  $X_r(s)$ ,  $Y_r(s) \in RH_\infty$  and

$Q(s) \in RH_\infty$ , one can derive that each element of the transfer function matrix is stable

and the DCFDOB structure with an outer-loop controller is internally stable. That is, the outer loop controller can not only stabilizes the system but also changes the system dynamics from input command to system output. These stable criteria (2.38) and (2.39) can be modified as a simple classic control negative feedback loop shown below.

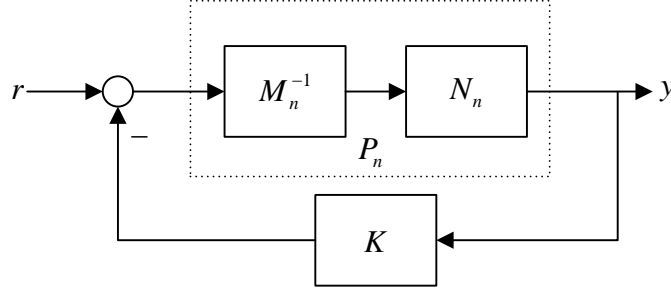


Fig. 2.11 Classic control feedback loop

Various kinds of control theorems such as Proportional-Integral-Derivative (PID), pole placement and  $H_\infty$  controllers can achieve stable conditions. In this thesis, the Youla-Kucera parameterization, all stabilizing compensators, is introduced.

**Theorem 2.1** [36]: Let  $P_n = N_n M_n^{-1} = \tilde{M}_n^{-1} \tilde{N}_n$  be the right coprime factorization (rcf) and left coprime factorization (lcf) of nominal plant  $P_n$  over  $RH_\infty$ , respectively. Then the set of all proper controller achieving internal stability is parameterized either by

$$K_Y = (X_r + Q_{YK} \tilde{N}_n)^{-1} (Y_r - Q_{YK} \tilde{M}_n), \quad \det(I + Q_{YK} \tilde{N}_n X_r^{-1})(\infty) \neq 0 \quad (2.40)$$

or by

$$K_Y = (Y_l - M_n Q_{YK})(X_l + N_n Q_{YK})^{-1}, \quad \det(I + X_l^{-1} N_n Q_{YK})(\infty) \neq 0 \quad (2.41)$$

for  $Q_{YK} \in RH_\infty$ , where  $X_r, Y_r, X_l, Y_l \in RH_\infty$  satisfy the Bezout identities.  $\square$

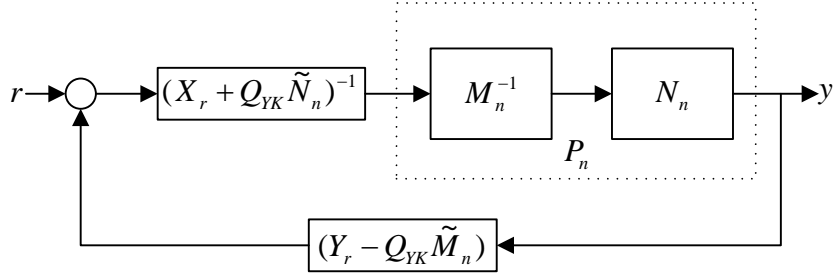


Fig. 2.12 Control scheme for the Youla-Kucera parameterization

Substituting  $K_Y(s)$  of Eq.(2.42), for  $K$  in Eq.(2.37) , one can build the following block diagram and yields Eq. (2.42).

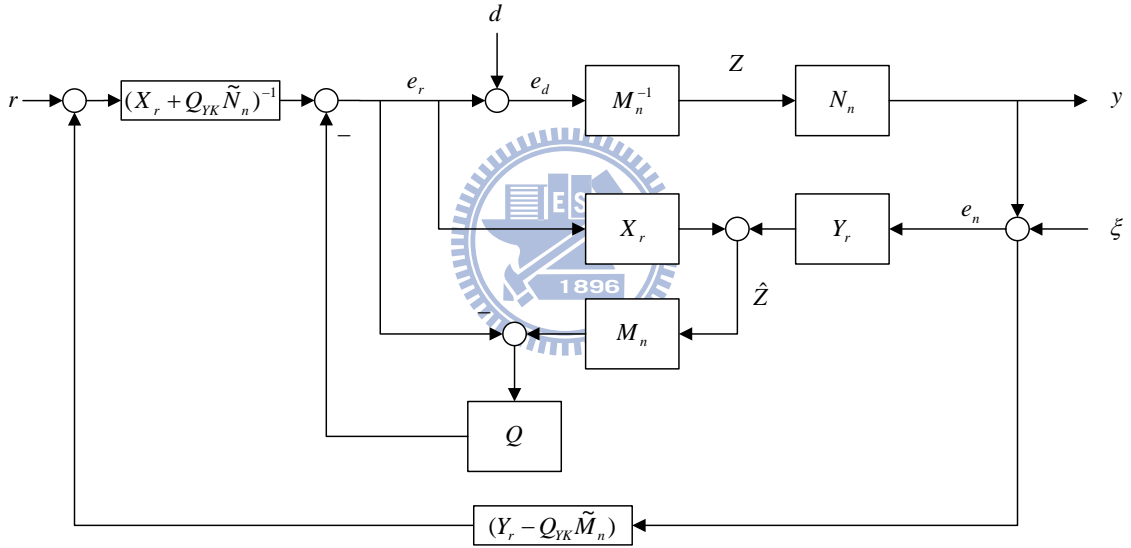


Fig. 2.13 The DCFDOB with Youla-Kucera parameterization controller

$$\begin{bmatrix} e_r \\ e_d \\ e_n \end{bmatrix} = \begin{bmatrix} M_n & (I - QY_l \tilde{N}_n)M_n(X_r + Q_{YK} \tilde{N}_n) - I \\ M_n & M_n(X_r + Q_{YK} \tilde{N}_n)(I - QY_l \tilde{N}_n) \\ N_n & N_n(X_r + Q_{YK} \tilde{N}_n)(I - QY_l \tilde{N}_n) \end{bmatrix} \begin{bmatrix} r \\ d \\ \xi \end{bmatrix}$$

$$\begin{bmatrix} -M_n(Y_r - Q_{YK} \tilde{M}_n) - M_n(X_r + Q_{YK} \tilde{N}_n)QM_n Y_r \\ -M_n(Y_r - Q_{YK} \tilde{M}_n) - M_n(X_r + Q_{YK} \tilde{N}_n)QM_n Y_r \\ I - N_n(Y_r - Q_{YK} \tilde{M}_n) - N_n(X_r + Q_{YK} \tilde{N}_n)QM_n Y_r \end{bmatrix} \begin{bmatrix} r \\ d \\ \xi \end{bmatrix}$$

$$(2.42)$$

Again, one can derive each element of the transfer function matrix of Eq. (2.42) is stable,

i.e. the system is internally stable. Moreover, if  $Q_{YK}(s) = 0$ , i.e. the central controller,

$X_r^{-1}Y_r$ , Eq. (2.42) can be rewritten as below:

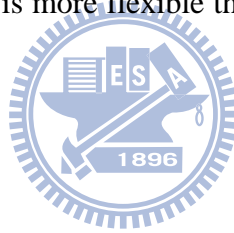
$$\begin{bmatrix} e_r \\ e_d \\ e_n \end{bmatrix} = \begin{bmatrix} M_n & (I - QY_l\tilde{N}_n)M_nX_r - I & -(I + M_nX_rQ)M_nY_r \\ M_n & M_nX_r(I - QY_l\tilde{N}_n) & -(I + M_nX_rQ)M_nY_r \\ N_n & N_nX_r(I - QY_l\tilde{N}_n) & I - N_nY_r(I + QM_nY_r) \end{bmatrix} \begin{bmatrix} r \\ d \\ \xi \end{bmatrix} \quad (2.43)$$

After discussing the properties and design methods, one showed that the DCFDOB can be applied to stable, minimum-phase and non-minimum phase systems and eliminates the input disturbance. If the plant is unstable, an output feedback controller can not only stabilize the system but change the tracking properties. Moreover, the Youla-Kucera parameterization is used for obtaining all stabilizing controller and the stability of the overall system is guaranteed. In the following section, one will combine DCFDOB structure with Vidyasagar's structure, the observer-controller compensator, and discuss the internally stable condition.



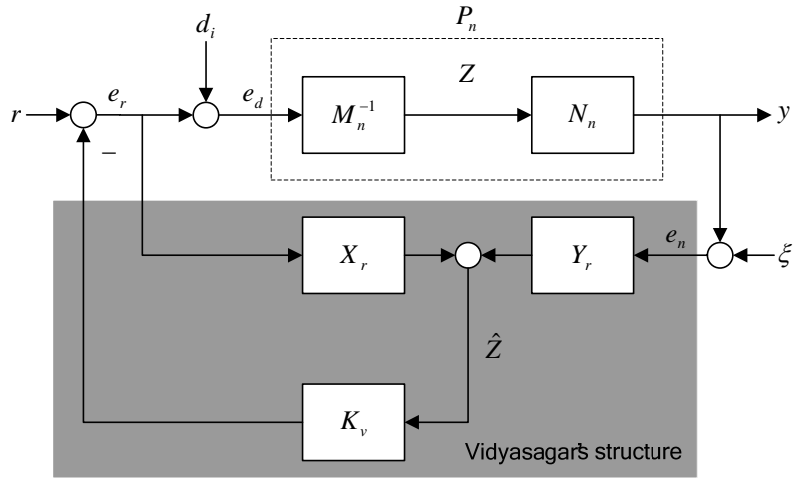
## 2.4 Combination of the DCFDOB and Vidyasagar's structure

As mentioned in section 2.3, an outer-loop controller  $K(s)$  was applied to stabilize the system and various kinds of control theorems can be applied to design the controller  $K(s)$ . In this section, one will study Vidyasagar's structure and combine it with our DCFDOB. [33] showed that Vidyasagar's structure has the subset stabilizing solutions of the Youla-Kucera parameterization, but Vidyasagar's structure has fewer dimensions than Youla-Kucera's structure in the form of the Youla-Kucera parameterization. Hence, the feedback system made by Vidyasagar's structure, which simplifies the controller structure, is more flexible than the one by the central controller of Youla-Kucera parameterization.

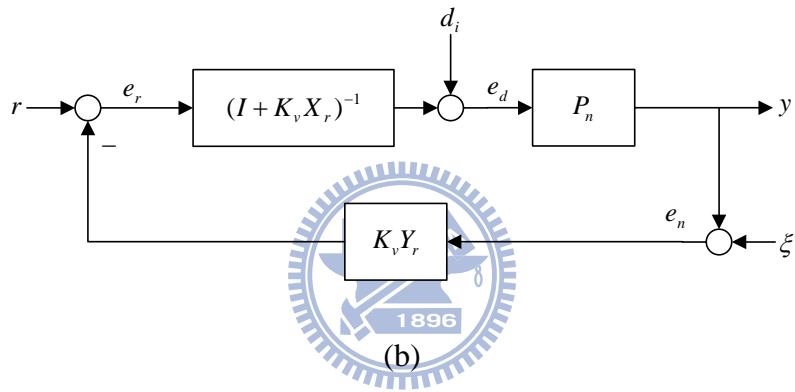


### 2.4.1 Vidyasagar's structure

[34] and [35] proposed Vidyasagar's structure, the observer-controller compensator of Fig. 2.14(a), where the nominal plant  $P_n$  has a right coprime factorization, i.e.  $P_n = N_n M_n^{-1}$ , the observer composed of  $X_r$  and  $Y_r$  observes the "internal state"  $z$  to be  $\hat{z}$ , and the controller  $K_v$  feeds  $\hat{z}$  back. Moreover,  $r$  is the command reference,  $d_i$  is the input disturbance and  $\xi$  is the measurement noise;  $e_r$ ,  $e_d$  and  $e_n$  are the internal signals, and  $y$  is the system output.



(a)



(b)

Fig. 2.14 Vidyasagar's structure: (a) observer-controller compensator and  
(b) equivalent compensator

The system of Fig. 2.14(a) is internally stable [34, 35] if and only if

$$\begin{aligned} M_n(s) + K_v(s) &= H(s) \in \mathcal{U}(RH_\infty) \\ \Leftrightarrow K_v(s) &= H(s) - M_n(s) \end{aligned} \quad (2.44)$$

The system of Fig. 2.14(a) also can be transformed to the system of Fig. 2.14(b) in terms of input-output equivalence. The notation  $\mathcal{U}(RH_\infty)$  denotes a unit over  $RH_\infty$ .

When a square matrix and its inverse are stable, the matrix belongs to  $\mathcal{U}(RH_\infty)$ . [33]

pointed out that Vidyasagar's structure equals the Youla-Kucera parameterization by

replacing  $Q_{YK}$  with  $H^{-1}Y_l$  where  $H^{-1}Y_l \subset Q_{YK}$ . Replacing  $K_v$  of Fig. 2.14(a) with  $H - M_n$ , the nine transfer functions from  $[r \ d_i \ \xi]^T$  to  $[e_r \ e_d \ e_n]^T$  is

$$\begin{bmatrix} e_r \\ e_d \\ e_n \end{bmatrix} = \begin{bmatrix} M_n H^{-1} & M_n(X_r + H^{-1}Y_l \tilde{N}_n) - I & -M_n(Y_r - H^{-1}Y_l \tilde{M}_n) \\ M_n H^{-1} & M_n(X_r + H^{-1}Y_l \tilde{N}_n) & -M_n(Y_r - H^{-1}Y_l \tilde{M}_n) \\ N_n H^{-1} & N_n(X_r + H^{-1}Y_l \tilde{N}_n) & I - N_n(Y_r - H^{-1}Y_l \tilde{M}_n) \end{bmatrix} \begin{bmatrix} r \\ d_i \\ \xi \end{bmatrix}. \quad (2.45)$$

Replacing Vidyasagar's structure in Fig. 2.14(b) with the Youla-Kucera parameterization (2.40) and the nine transfer functions from  $[r \ d_i \ \xi]^T$  to  $[e_r \ e_d \ e_n]^T$  of Fig 2.12(b) is obtained as follows.

$$\begin{bmatrix} e_r \\ e_d \\ e_n \end{bmatrix} = \begin{bmatrix} M_n & M_n(X_r + Q_{YK} \tilde{N}_n) - I & -M_n(Y_r - Q_{YK} \tilde{M}_n) \\ M_n & M_n(X_r + Q_{YK} \tilde{N}_n) & -M_n(Y_r - Q_{YK} \tilde{M}_n) \\ N_n & N_n(X_r + Q_{YK} \tilde{N}_n) & I - N_n(Y_r - Q_{YK} \tilde{M}_n) \end{bmatrix} \begin{bmatrix} r \\ d_i \\ \xi \end{bmatrix} \quad (2.46)$$

Even if  $Q_{YK}$  of (2.46) is replaced with  $H^{-1}Y_l$ , Eq. (2.46) is still not equivalent to (2.45) with respect to  $r$ . This shows that  $H(s)$  has the unique tracking property and the feedback one [33].

#### 2.4.2 The DCFDOB co-structure with Vidyasagar's structure

According to the previous citation, one knows that the proposed DCFDOB and Vidyasagar's structure, the observer-controller compensator, are all extended from the basic structure shown in Fig. 2.15(a). We know the DCFDOB shown in Fig. 2.15 (b) provides good disturbance attenuation but lacks the tracking and stabilizing properties without the outer-loop controller. Moreover, Vidyasagar's structure shown in Fig

2.15(c) can be equivalent to the well-known Youla-Kucera parameterization, the set of all proper controllers, and provides the tracking property when  $K_v = H - M_n$  is applied. However, Vidyasagar's structure shown in Fig. 2.14(a) provides only one parameter  $H$  to trade-off tracking performance or feedback performance. In this paragraph, these two structures will be merged into a new two degree of freedom (2DOF) structure (DCFDOB-VS) that provides design parameters  $H(s) \in \mathbb{U}(RH_\infty)$  and  $Q(s) \in RH_\infty$  for the tracking performance and disturbance attenuation, respectively, and achieve the internal stability.

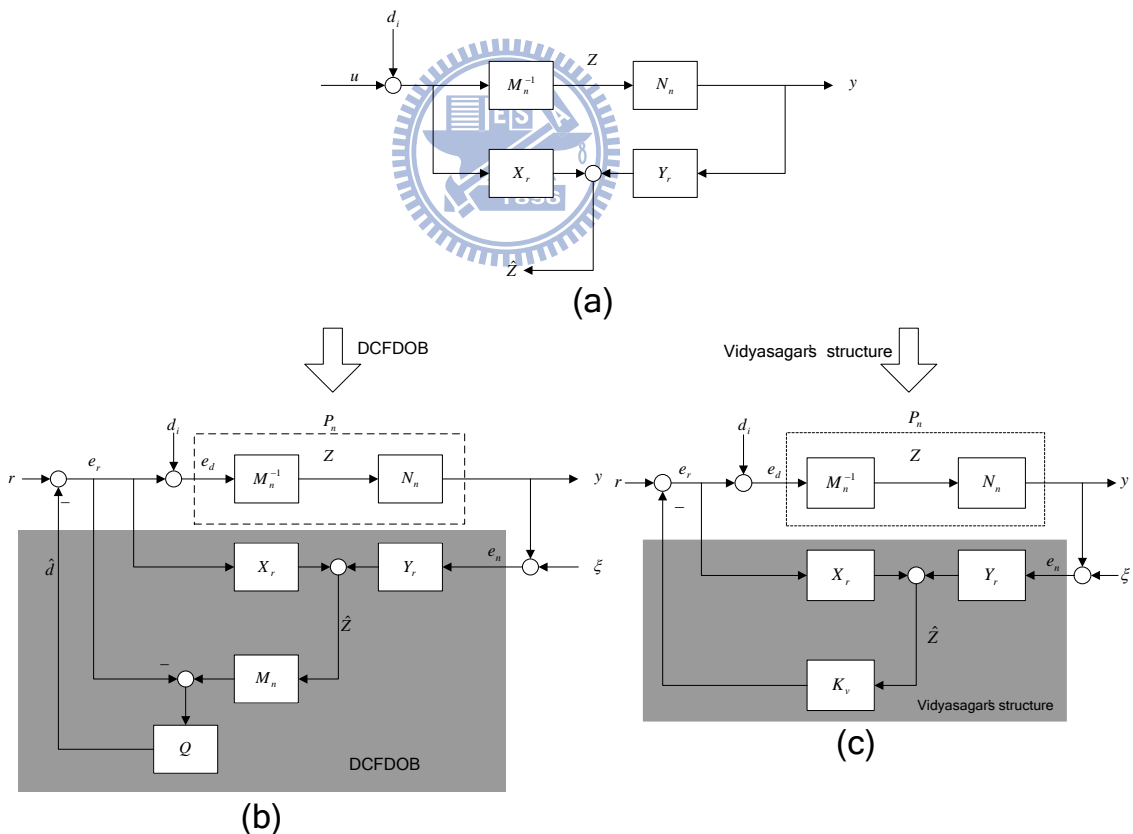


Fig. 2.15 (a) Internal states estimation with input disturbance

(b) The DCFDOB structure

(c) Vidyasagar's structure: observer-controller compensator

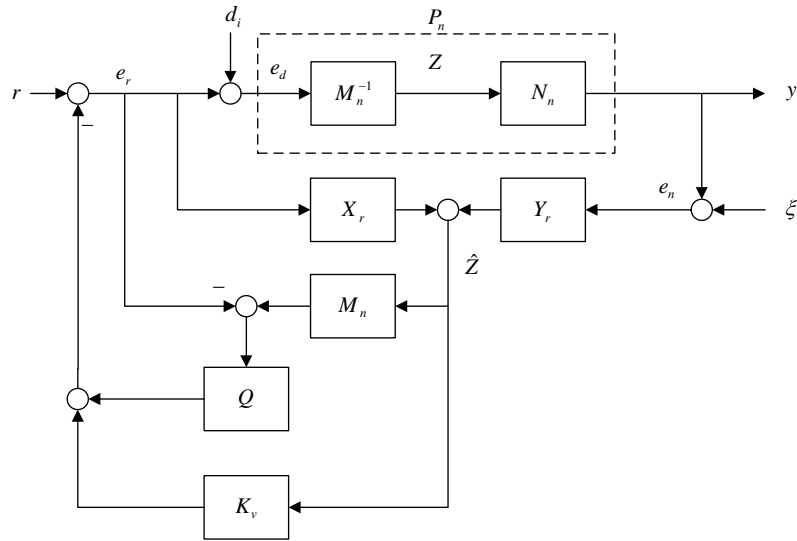


Fig. 2.16 The DCFDOB co-structure with Vidyasagar's structure

Furthermore, Fig. 2.16 can be transformed into Fig. 2.17 by replacing  $K_v$  with

$$H - M_n,$$

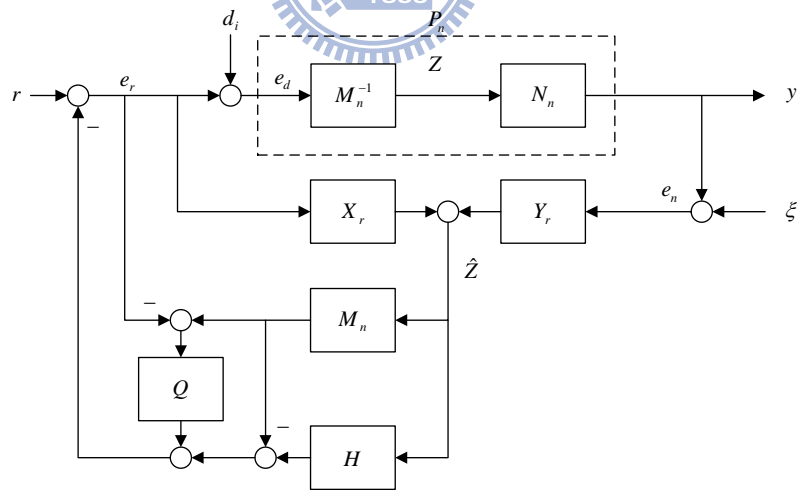


Fig. 2.17 The DCFDOB-VS

and the transfer functions matrix from  $[r \ d_i \ \xi]^T$  to  $[e_r \ e_d \ e_n]^T$  of Fig. 2.17 is

$$\begin{bmatrix} e_r \\ e_d \\ e_n \end{bmatrix} = \begin{bmatrix} M_n H^{-1} & M_n [X_r + H^{-1}(I-Q)Y_l \tilde{N}_n] - I & -M_n [Y_r - H^{-1}(I-Q)Y_l \tilde{M}_n] \\ M_n H^{-1} & M_n [X_r + H^{-1}(I-Q)Y_l \tilde{N}_n] & -M_n [Y_r - H^{-1}(I-Q)Y_l \tilde{M}_n] \\ N_n H^{-1} & N_n [X_r + H^{-1}(I-Q)Y_l \tilde{N}_n] & I - N_n [Y_r - H^{-1}(I-Q)Y_l \tilde{M}_n] \end{bmatrix} \begin{bmatrix} r \\ d_i \\ \xi \end{bmatrix} \quad (2.47)$$

If  $H^{-1}(I-Q)Y_l$  of the 2<sup>nd</sup> and the 3<sup>rd</sup> columns in Eq. (2.47) is replaced by  $Q_Y$ , i.e.

$Q(s) = I - HQ_Y Y_l^{-1}$ , one can obtain Eq. (2.48) as follows.

$$\begin{bmatrix} e_r \\ e_d \\ e_n \end{bmatrix} = \begin{bmatrix} M_n H^{-1} & M_n (X_r + Q_Y \tilde{N}_n) - I & -M_n (Y_r - Q_Y \tilde{M}_n) \\ M_n H^{-1} & M_n (X_r + Q_Y \tilde{N}_n) & -M_n (Y_r - Q_Y \tilde{M}_n) \\ N_n H^{-1} & N_n (X_r + Q_Y \tilde{N}_n) & I - N_n (Y_r - Q_Y \tilde{M}_n) \end{bmatrix} \begin{bmatrix} r \\ d_i \\ \xi \end{bmatrix} \quad (2.48)$$

Obviously, according to Eq. (2.48), one knows that DCFDOB-VS is internally stable

with these two independent  $Q_Y \in RH_\infty$  and  $H \in \mathcal{U}(RH_\infty)$ .

**Theorem 2.2:** If  $Q_Y \in RH_\infty$  and  $H \in \mathcal{U}(RH_\infty)$ , and let  $P_n = N_n M_n^{-1} = \tilde{M}_n^{-1} \tilde{N}_n$  be the right coprime factorization (*rcf*) and left coprime factorization (*lcf*) of nominal plant  $P_n$  over  $RH_\infty$ , respectively. DCFDOB-VS is internally stable.

**Proof:** For any  $H(s) \in \mathcal{U}(RH_\infty)$ , i.e.  $H^{-1}(s) \in RH_\infty$  and  $Q_Y(s) \in RH_\infty$ . The nine elements of Eq. (2.38) are all stable. The proofs of stable properties follow from simple manipulations of rational transfer functions. □

**Theorem 2.3:**  $Q_Y(s)$  in Eq. (2.48) must be strictly proper such that a realizable parameter  $Q(s)$  in DCFDOB-VS can be guaranteed.

**Proof:** Suppose  $H(s) \in \mathcal{U}(RH_\infty)$  with state-space representation:

$$H(s) = \left[ \begin{array}{c|c} A_H & B_H \\ \hline C_H & D_H \end{array} \right] \quad (2.49)$$

where  $D_H \neq \mathbf{0}$  and  $D_H^{-1}$  exists, one also has

$$\begin{aligned} H^{-1}(s) &= \left[ \begin{array}{c|c} A_H - B_H D_H^{-1} C_H & -B_H D_H^{-1} \\ \hline D_H^{-1} C_H & D_H^{-1} \end{array} \right] \\ &= \left[ \begin{array}{c|c} A_{H^{-1}} & B_{H^{-1}} \\ \hline C_{H^{-1}} & D_{H^{-1}} \end{array} \right]. \end{aligned} \quad (2.50)$$

Moreover, suppose

$$[I - Q(s)] = \left[ \begin{array}{c|c} A_Q & B_Q \\ \hline C_Q & D_Q \end{array} \right] \quad (2.51)$$

and

$$Y_l(s) = \left[ \begin{array}{c|c} A + BF & -L \\ \hline F & \mathbf{0} \end{array} \right], \quad (2.52)$$

one can obtain the state-space realization of  $Q_Y(s)$  in Eq. (2.53), where

$$Q_Y = H^{-1}(I - Q)Y_l.$$

$$\begin{aligned} Q_Y(s) &= \left[ \begin{array}{c|c} A_{Q_Y} & B_{Q_Y} \\ \hline C_{Q_Y} & D_{Q_Y} \end{array} \right] \\ &= \left[ \begin{array}{c|c} A_{H^{-1}} & B_{H^{-1}} \\ \hline C_{H^{-1}} & D_{H^{-1}} \end{array} \right] \cdot \left[ \begin{array}{c|c} A_Q & B_Q \\ \hline C_Q & D_Q \end{array} \right] \cdot \left[ \begin{array}{c|c} A + BF & -L \\ \hline F & \mathbf{0} \end{array} \right] \\ &= \left[ \begin{array}{ccc|c} A_{H^{-1}} & B_{H^{-1}} C_Q & B_{H^{-1}} D_Q F & \mathbf{0} \\ \hline \mathbf{0} & A_Q & B_Q F & \mathbf{0} \\ \hline \mathbf{0} & \mathbf{0} & A + BF & -L \\ \hline C_{H^{-1}} & D_{H^{-1}} C_Q & D_{H^{-1}} D_Q F & \mathbf{0} \end{array} \right] \end{aligned} \quad (2.53)$$

$Q_Y(s)$  must be a strictly proper rational function, since  $D_{Q_Y}$  is a zero matrix. In dual,

if  $Q_Y(s)$  is not strictly proper, i.e.  $D_{Q_Y} \neq \mathbf{0}$ ,  $D_Q$  does not exist and  $Q(s)$  must be

improper and unrealizable. □

In the future, we will continue on studying this novel structure and obtain more inherent properties. The follows shows a simple design methods of  $H(s)$  on tracking control and  $Q_Y(s)$  parameter for disturbance attenuation, respectively.

#### 2.4.2.1 $H(s)$ on tracking control using the inverse dynamic

In Fig. 2.17, the transfer function from  $r$  to  $y$  is

$$y(s) = N_n(s)H^{-1}(s)r. \quad (2.54)$$

Equation (2.54) represents that the tracking response can be improved by  $H(s)$ . For minimum-phase square plants, an inverse idea can be used to select the  $H(s)$  parameter as follows. If  $N_n(s)$  is a  $n \times n$  matrix,  $H(s)$  is selected to be  $\alpha(s)N_n(s)$ , where  $\alpha(s) = \text{diag}\{\alpha_1, \dots, \alpha_n\}$  in which  $\alpha_i(s)$  for  $i = 1 \sim n$  are polynomials:

$$\alpha_i(s) = \alpha_{i,n}s^n + \alpha_{i,n-1}s^{n-1} + \dots + \alpha_{i,1}s + 1 \quad (2.55)$$

and the roots are all in the left-half plane such that  $\alpha(s)N_n(s) \in \mathcal{U}(RH_\infty)$ . In the case,  $y \approx \alpha^{-1}(s)r$ , obviously, the system response is determined by the pole locations of  $\alpha^{-1}(s)$ . The degree of polynomial  $\alpha(s)$  depends on the relative degree of  $N_n(s)$ .

For example, if  $N_n(s)$  is given by

$$N_n(s) = \begin{bmatrix} \frac{s^2 + 7s + 2}{s^3 + 4s^2 + 5s + 1} & \frac{s + 2}{s^3 + 4s^2 + 5s + 1} \\ \frac{s + 3}{s^3 + 4s^2 + 5s + 1} & \frac{2s + 1}{s^3 + 4s^2 + 5s + 1} \end{bmatrix}, \quad (2.56)$$



$\alpha(s)$  can be selected as

$$\alpha(s) = \begin{bmatrix} \alpha_{1,1}s + 1 & 0 \\ 0 & \alpha_{2,2}s^2 + \alpha_{2,1}s + 1 \end{bmatrix} \quad (2.57)$$

and

$$\begin{aligned} \alpha(s)N_n(s) &= \begin{bmatrix} \alpha_{1,1}s + 1 & 0 \\ 0 & \alpha_{2,2}s^2 + \alpha_{2,1}s + 1 \end{bmatrix} \cdot \begin{bmatrix} \frac{s^2 + 7s + 2}{s^3 + 4s^2 + 5s + 1} & \frac{s + 2}{s^3 + 4s^2 + 5s + 1} \\ \frac{s + 3}{s^3 + 4s^2 + 5s + 1} & \frac{2s + 1}{s^3 + 4s^2 + 5s + 1} \end{bmatrix} \\ &= \begin{bmatrix} \frac{\alpha_{1,1}s^3 + (1 + 7\alpha_{1,1})s^2 + (7 + 2\alpha_{1,1})s + 2}{s^3 + 4s^2 + 5s + 1} & \frac{\alpha_{1,1}s^2 + (1 + 2\alpha_{1,1})s + 2}{s^3 + 4s^2 + 5s + 1} \\ \frac{\alpha_{2,2}s^3 + (3\alpha_{2,2} + \alpha_{2,1})s^2 + (1 + \alpha_{2,1})s + 3}{s^3 + 4s^2 + 5s + 1} & \frac{2\alpha_{2,2}s^3 + (\alpha_{2,2} + 2\alpha_{2,1})s^2 + (2 + \alpha_{2,1})s + 1}{s^3 + 4s^2 + 5s + 1} \end{bmatrix} \end{aligned} \quad (2.58)$$

so that  $\alpha(s)N_n(s) = H(s) \in \mathbb{U}(RH_\infty)$  and the tracking performance for each channel output can be determined by the roots of  $\alpha_i(s)$ , respectively. For non-minimum phase systems, the unstable zeros are retained in  $H(s)$ .

#### 2.4.2.2 $Q_Y(s)$ on disturbance elimination design

##### a. Minimum phase and square plant

In Fig. 2.17, the transfer function from  $d_i$  to  $e_d$  is

$$e_d(s) = M_n(X_r + Q_Y \tilde{N}_n) \cdot d_i \quad (2.59)$$

Suppose  $P_n(s)$  is a  $n \times n$  matrix, i.e. the corresponding coprime factors are all  $n \times n$  matrices. To reject the input disturbance  $d_i$ , the simplest way in designing  $Q_Y(s)$  can be done as follows.

$$Q_Y(s) = -X_r J \tilde{N}_n^{-1} \quad (2.60)$$

$$Q_Y(s) = -J X_r \tilde{N}_n^{-1} \quad (2.61)$$

where  $J_{n \times n}(s)$  is a diagonal matrix which is composed of low-pass filters,

$J_{n \times n}(s) = \text{diag}\{j_{11} \cdots j_{nn}\}_{n \times n}$ . If  $Q_Y(s)$  is defined as Eq. (2.60) or Eq. (2.61), then Eq.

(2.59) can be rewritten as Eqs. (2.62) or (2.63) as follows.

$$\begin{aligned} e_d(s) &= M_n(X_r - X_r J) \cdot d_i \\ &= M_n[X_r(I - J)] \cdot d_i \end{aligned} \quad (2.62)$$

$$\begin{aligned} e_d(s) &= M_n(X_r - J X_r) \cdot d_i \\ &= M_n[(I - J)X_r] \cdot d_i \end{aligned} \quad (2.63)$$

The transfer function from  $d_i$  to  $e_d$   $M_n[X_r(I - J)](j\omega)$  ( $M_n[(I - J)X_r](j\omega)$ ) is

near zero when  $J(j\omega) \approx I$  and parameter  $Q(s)$  of DCFDOB can be obtained as,

$$Q(s) = I + H X_r \tilde{N}_n^{-1} Y_l^{-1} \quad (2.64)$$

or

$$Q(s) = I + H J X_r \tilde{N}_n^{-1} Y_l^{-1}, \quad (2.65)$$

and the parameter  $H(s) \in \mathbb{U}(RH_\infty)$  is given in foregoing tracking control design.

Note that the relative degree of each element of the low-pass filter  $J(s)$  depends on

the relative degree of  $X_r(s)$ ,  $\tilde{N}_n(s)$ , and  $Y_l(s)$  so that  $J X_r \tilde{N}_n^{-1} Y_l^{-1}$  is proper or

strictly proper, i.e.  $Q(s)$  is realizable.

*b. Non-minimum phase and square plants*

For rejecting the input disturbance  $d_i$  in non-minimum phase plant, the objective function can be described as follows.

$$\min_{Q_Y \in RH_\infty} \|X_r + Q_Y \tilde{N}_n\|_\infty \quad (2.66)$$

Also, the model matching methods represented in paragraph 2.2.2.1 for SISO system or in section 3.2 for MIMO system can be applied to solve the parameter  $Q_Y(s)$  according to following steps.

**Step 1:** Compute inner-outer factorizations of  $T_2$ ,  $T_3$  and  $T_2 = T_{2i} T_{2o}$ ,  $T_3 = T_{3o} T_{3i}$ , respectively, where  $T_2 = I$ ,  $T_3 = \tilde{N}_n$  and  $T_1 = X_r$ .

**Step 2:** Form the Nehari problem  $\|R - \tilde{Q}\|_\infty < \gamma$ , where  $R = T_{2i}^{-1} T_1 T_{3i} \in RL_\infty$  and

$$\tilde{Q} = T_{2o} Q_Y T_{3o} \in RH_\infty.$$

**Step 3:** Compute the optimum solution  $\tilde{Q}_{opt}(s)$  of  $\tilde{Q}(s)$  in SISO system or take the central solution  $\hat{Q}_o(s)$  in MIMO system.

**Step 4:** Obtain the parameter  $Q_Y = T_{2o}^{-1} \tilde{Q}_{opt} T_{3o}^{-1} \in RH_\infty$  in SISO system or

$$Q_Y = T_{2o}^{-1} \hat{Q}_o T_{3o}^{-1} \in RH_\infty \text{ in MIMO system.}$$

**Step 5:** Obtain the parameter of DCFDOB,  $Q = I + H Q_Y Y_l^{-1}$ .

Note that  $H Q_Y Y_l^{-1}$  must be a proper rational function so that  $Q(s)$  is realizable. If

$H Q_Y Y_l^{-1}$  is improper, the simplest way is pre- / post-multiplying a low-pass filter

matrix  $\beta(s)$  with wide bandwidth so that  $\beta H Q_Y Y_l^{-1}$  ( $H Q_Y Y_l^{-1} \beta$ ) is proper and

$H Q_Y Y_l^{-1}(j\omega) \approx \beta H Q_Y Y_l^{-1}(j\omega)$  ( $H Q_Y Y_l^{-1}(j\omega) \approx H Q_Y Y_l^{-1} \beta(j\omega)$ ) in low frequency

range.

c. A numerical example of DCFDOB-VS:

In the following section, we show a numerical example to demonstrate the design

steps of DCFDOB-VS. Suppose a MIMO unstable plant is given as follows:

$$P_n = \begin{bmatrix} \frac{10}{s-5} & \frac{2}{s+6} \\ \frac{5}{s+7} & \frac{3}{s-8} \end{bmatrix} \quad (2.67)$$

and its corresponding normalized coprime factors can be obtained via Eqs. (1.14) and

(1.17). The Smith-McMillan poles locate at -7, -6, 5 and 8 and zeros locate at -24.225

and -1.775. Since this plant is of minimum phase, we can apply the inverse dynamic

method to obtain the parameter  $H(s) \in \mathcal{U}$  as follows in order to change the tracking

property from  $r(t)$  to  $y(t)$ .

$$H(s) = \alpha \cdot N_n = \begin{bmatrix} \frac{0.1s^4 + 12.17s^3 + 232.3s^2 + 1610s + 3494}{s^4 + 33.75s^3 + 413.7s^2 + 2200s + 4123} & \frac{0.02s^4 + 2.184s^3 + 18.04s^2 - 35.83s - 362.4}{s^4 + 33.75s^3 + 413.7s^2 + 2200s + 4123} \\ \frac{0.05s^4 + 5.475s^3 + 46.63s^2 - 99.23s - 1137}{s^4 + 33.75s^3 + 413.7s^2 + 2200s + 4123} & \frac{0.03s^4 + 3.732s^3 + 79.89s^2 + 675.7s + 1133}{s^4 + 33.75s^3 + 413.7s^2 + 2200s + 4123} \end{bmatrix} \quad (2.68)$$

where

$$\alpha = \begin{bmatrix} 0.01s + 1 & 0 \\ 0 & 0.01s + 1 \end{bmatrix} \quad (2.69)$$

$$N_n = \begin{bmatrix} \frac{10s^3 + 216.5s^2 + 1575s + 3494}{s^4 + 33.76s^3 + 413.7s^2 + 2200s + 4123} & \frac{2s^3 + 18.36s^2 - 32.2s - 362.4}{s^4 + 33.76s^3 + 413.7s^2 + 2200s + 4123} \\ \frac{5s^3 + 47.51s^2 - 87.85s - 1137}{s^4 + 33.76s^3 + 413.7s^2 + 2200s + 4123} & \frac{3s^3 + 73.24s^2 + 664.3s + 1133}{s^4 + 33.76s^3 + 413.7s^2 + 2200s + 4123} \end{bmatrix} \quad (2.70)$$

According to Eq. (2.64), the  $Q(s)$  parameter which contains four elements with eight orders transfer function is obtained and the reduced one is given as follows.

$$Q(s) = \begin{bmatrix} \frac{4.623(s^2 + 131.2s + 4396)}{(s^2 + 141s + 1 \times 10^4)} & \frac{0.147(s + 100)(s + 63.14)(s - 15.09)}{(s + 5.974)(s^2 + 141s + 1 \times 10^4)} \\ \frac{0.434(s + 100)(s + 54.17)(s - 12.63)}{(s + 6.939)(s^2 + 141s + 1 \times 10^4)} & \frac{2.068(s + 7.615)(s + 5.324)(s^2 + 133.5s + 6203)}{(s + 6.939)(s + 5.974)(s^2 + 141s + 1 \times 10^4)} \end{bmatrix} \quad (2.71)$$

The time domain simulation result is given in Fig. 2.18, where the reference command

$$\text{is } r = \begin{bmatrix} r_1 \\ r_2 \end{bmatrix} = \begin{bmatrix} 1, t \geq 1 \text{ sec} \\ 2, t \geq 2 \text{ sec} \end{bmatrix} \text{ and the input disturbance is } d_i = \begin{bmatrix} d_{i,1} \\ d_{i,2} \end{bmatrix} = \begin{bmatrix} 3, t \geq 3 \text{ sec} \\ 6, t \geq 6 \text{ sec} \end{bmatrix}.$$

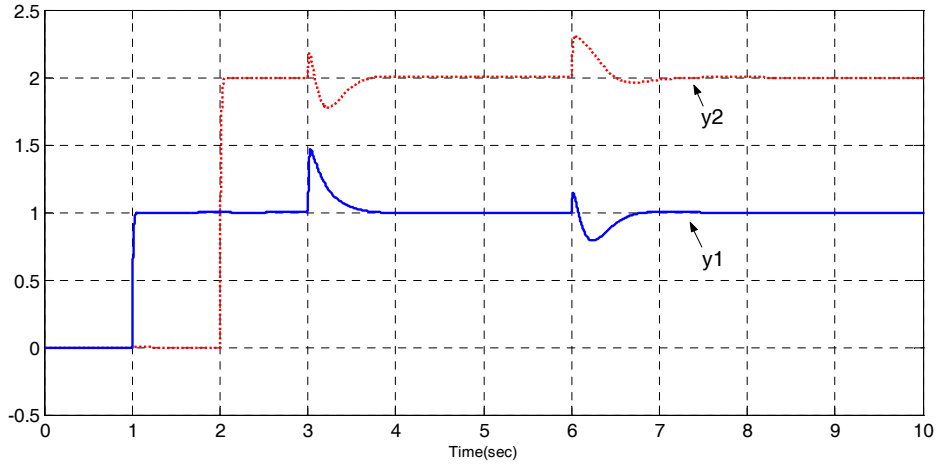


Fig. 2.18 Simulation result of an unstable system with DCFDOB-VS for case 1 where

$$\alpha = \begin{bmatrix} 0.01s + 1 & 0 \\ 0 & 0.01s + 1 \end{bmatrix}, \quad J = \begin{bmatrix} \frac{10000}{s^2 + 141s + 10000} & 0 \\ 0 & \frac{10000}{s^2 + 141s + 10000} \end{bmatrix}$$

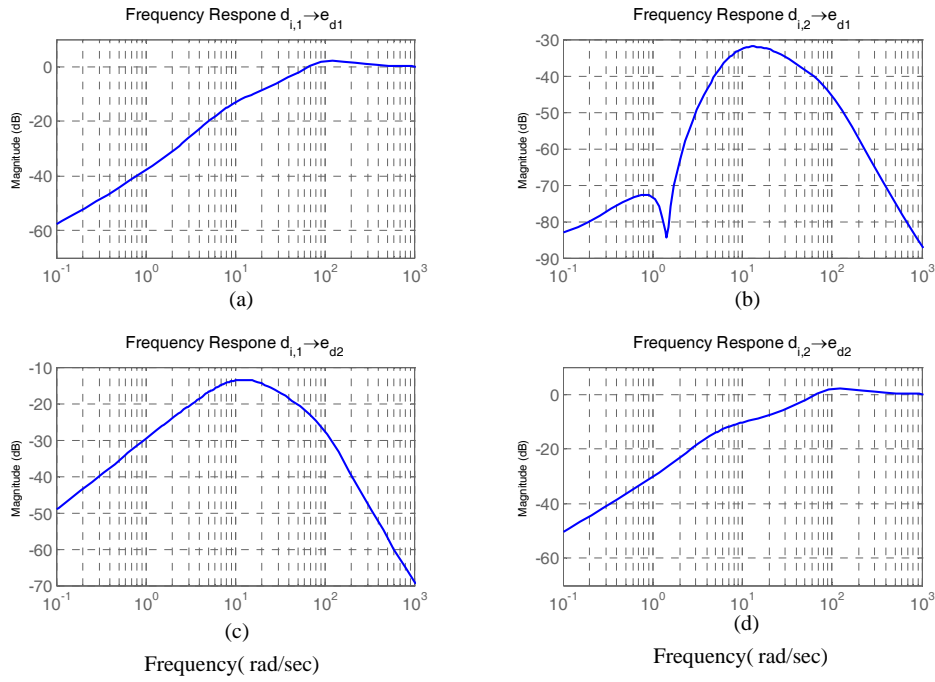


Fig. 2.19 Frequency responses from (a)  $d_{i,1} \rightarrow e_{d,1}$  (b)  $d_{i,2} \rightarrow e_{d,1}$

(c)  $d_{i,1} \rightarrow e_{d,2}$  (d)  $d_{i,2} \rightarrow e_{d,2}$  of DCFDOB-VS for case 1

Figures 2.19(a)-(d) show the frequency responses from  $\begin{bmatrix} d_{i,1} \\ d_{i,2} \end{bmatrix}$  to  $\begin{bmatrix} e_{d,1} \\ e_{d,2} \end{bmatrix}$  of Fig. 2.17,

i.e. input sensitivity functions. Moreover, Figures 2.20(a)-(d) show the frequency

responses from  $\begin{bmatrix} r_1 \\ r_2 \end{bmatrix}$  to  $\begin{bmatrix} y_1 \\ y_2 \end{bmatrix}$ .

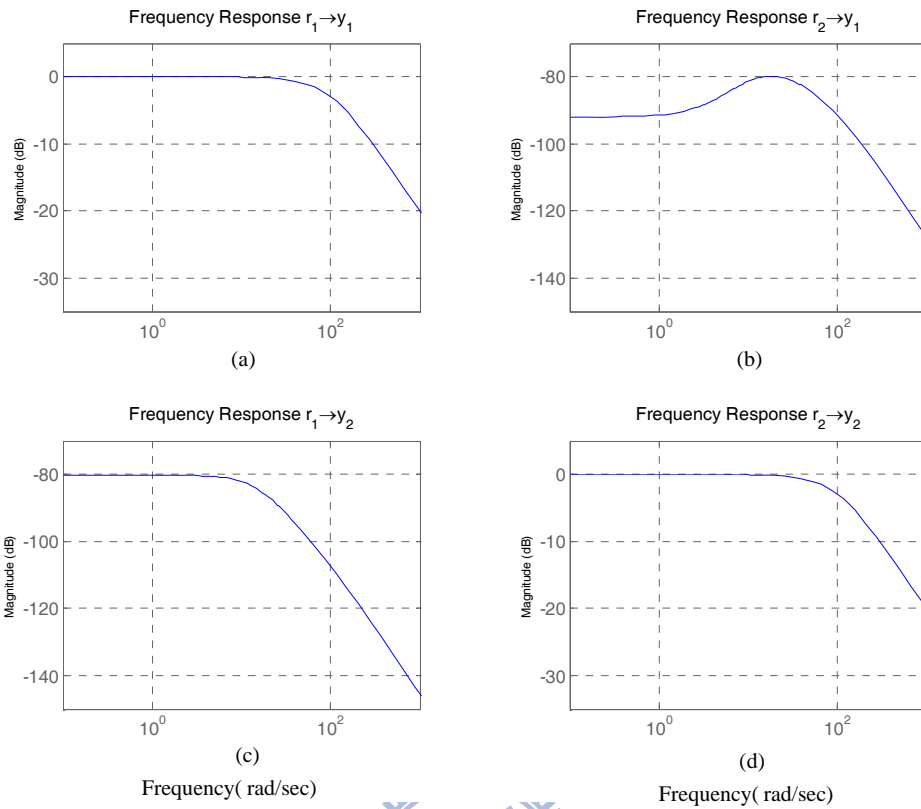


Fig. 2.20 Frequency response from (a)  $r_1 \rightarrow y_1$  (b)  $r_2 \rightarrow y_1$

(c)  $r_1 \rightarrow y_2$  (d)  $r_2 \rightarrow y_2$  of DCFDOB-VS for case 1

In case 2, we enlarge the coefficient of  $\alpha_{ii}(s)$  and remain the bandwidth of the low-pass filter  $J(s)$ . The simulation result is shown in Fig. 2.21 and Figs. 2.22(a)-(d)

plot the frequency responses from  $\begin{bmatrix} r_1 \\ r_2 \end{bmatrix}$  to  $\begin{bmatrix} y_1 \\ y_2 \end{bmatrix}$  of case 2. From these results, we

know that the roots of  $\alpha_{ii}(s)$  will influence the system response.

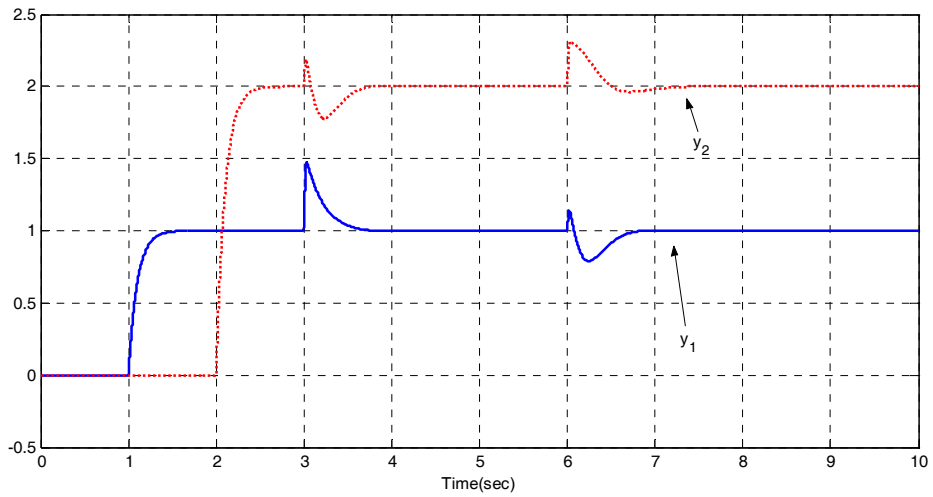


Fig. 2.21 Simulation result of an unstable system with DCFDOB-VS for case 2 where

$$\alpha = \begin{bmatrix} 0.1s + 1 & 0 \\ 0 & 0.1s + 1 \end{bmatrix}, \quad J = \begin{bmatrix} \frac{10000}{s^2 + 141s + 10000} & 0 \\ 0 & \frac{10000}{s^2 + 141s + 10000} \end{bmatrix}$$

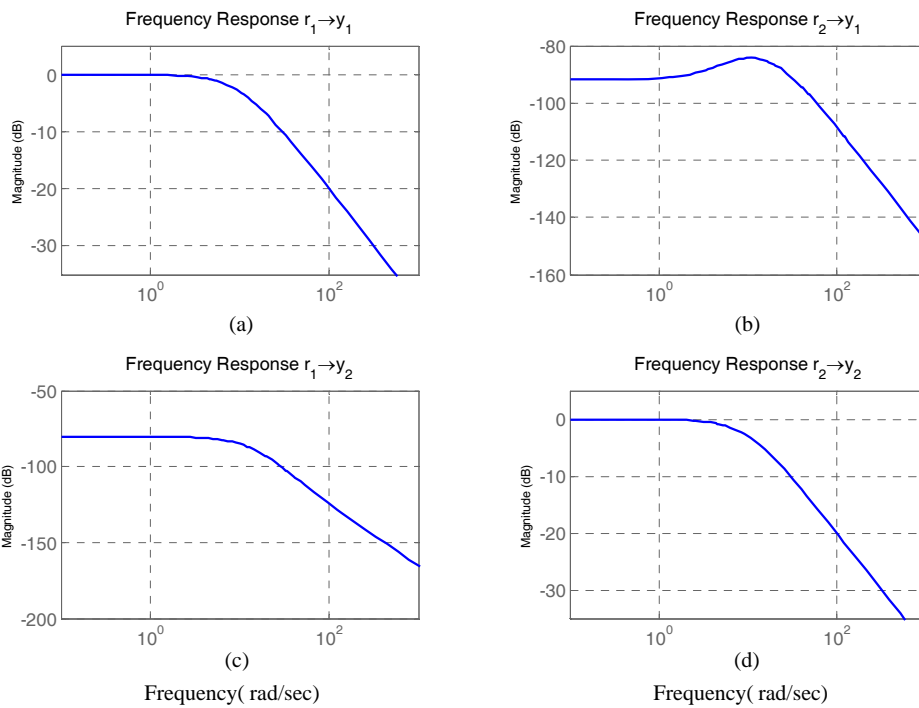


Fig. 2.22 Frequency response from (a)  $r_1 \rightarrow y_1$  (b)  $r_2 \rightarrow y_1$

(c)  $r_1 \rightarrow y_2$  (d)  $r_2 \rightarrow y_2$  of DCFDOB-VS case 2



Comparing the bandwidth from  $\begin{bmatrix} r_1 \\ r_2 \end{bmatrix}$  to  $\begin{bmatrix} y_1 \\ y_2 \end{bmatrix}$  of case 1 with the one of case 2, the tracking bandwidth can be enlarged arbitrarily since the tracking and disturbance attenuation are independent. However, actuator saturation and control power must be considered in real realization.

In this chapter, we introduced the DCFDOB and its properties, stability conditions and design methods for tracking objective and input disturbance attenuation. For minimum phase plants, the parameter  $Q(s)$  can be design as  $J \cdot (Y_l \tilde{N}_n)^{-1}$  to reject the input disturbance. For non-minimum phase plants, the model matching method and Nehari problem were applied to solve the optimum solution of  $Q(s)$  parameter. Moreover, the limitation of sensitivity function and waterbed phenomenon caused by the non-minimum phase zeros were also discussed. When a plant is unstable, an outer-loop controller  $K(s)$  is added not only to stabilize the system but change the tracking performance. After that, we co-structured DCFDOB with Vidyasagar's structure, the subset of stabilizing solutions of the Youla-Kucera parameterization, by sharing the common observer configuration to form the DCFDOB-VS which contains  $H(s)$  and  $Q(s)$  parameters to deal with tracking objective and feedback objective, respectively.

## CHAPTER 3

### EXTENSION TO GENERAL PLANT CASES AND INPUT/OUTPUT DISTURBANCES

This thesis only considered the influence of input disturbance, denoted as  $d_i$  in the above chapters. But in general, the system may also be influenced by output disturbance, denoted as  $d_o$ , meantime. In classic control point of view, in general, good input disturbance rejection does not necessarily imply good output disturbance rejection unless feedback controller and plant are square and diagonal [36, page 83].

In this Chapter, one will consider both input disturbance and output disturbance for system generality and prove that the DCFDOB can eliminate both disturbances simultaneously in square plant cases. Considering the whole exogenous input signals

and Fig. 3.1,

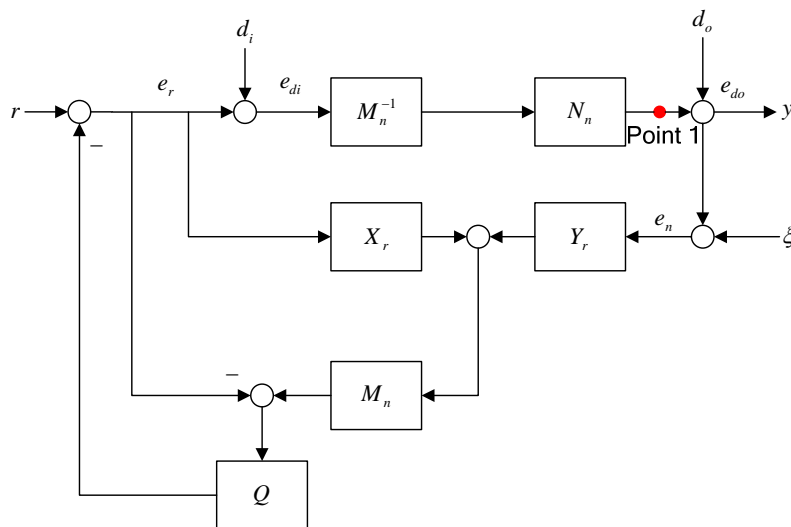


Fig. 3.1 DCFDOB with input and output disturbance

the transfer functions from  $[r \ d_i \ d_o \ \xi]^T$  to  $[e_r \ e_{di} \ e_{do} \ e_n]^T$  are shown as below.

$$\begin{bmatrix} e_r \\ e_{di} \\ e_{do} \\ e_n \end{bmatrix} = \begin{bmatrix} I & -Q(I - M_n X_r) & -QM_n Y_r & -QM_n Y_r \\ I & I - Q(I - M_n X_r) & -QM_n Y_r & -QM_n Y_r \\ N_n M_n^{-1} & N_n M_n^{-1}(I - Q(I - M_n X_r)) & I - N_n M_n^{-1} QM_n Y_r & -N_n M_n^{-1} QM_n Y_r \\ N_n M_n^{-1} & N_n M_n^{-1}(I - Q(I - M_n X_r)) & I - N_n M_n^{-1} QM_n Y_r & I - N_n M_n^{-1} QM_n Y_r \end{bmatrix} \begin{bmatrix} r \\ d_i \\ d_o \\ \xi \end{bmatrix} \quad (3.1)$$

### 3.1 Input/Output sensitivity functions of the DCFDOB

In a SISO plant, the input sensitivity function, denotes  $S_i$  is the same as the output sensitivity function, denotes  $S_o$  and given as follows.

$$\begin{aligned} S_i &= \frac{e_{di}}{d_i} = 1 - Q(1 - M_n X_r) \\ &= 1 - Q(1 - X_r M_n) \\ &= 1 - QY_r N_n \end{aligned} \quad (3.2)$$

$$\begin{aligned} S_o &= \frac{e_{do}}{d_o} = 1 - N_n M_n^{-1} QM_n Y_r \\ &= 1 - QY_r N_n \end{aligned} \quad (3.3)$$

Obviously, for SISO plant cases minimization of  $|S_i|$  will also reduce the influence of output disturbance to system output.

For MIMO plant,  $P_{n,n \times m}$ , with dimension  $n$  by  $m$ , the transfer functions of input/output sensitivity functions are represented as follows:

$$S_{i,d_i \rightarrow e_d}(s) = (I - QY_i \tilde{N}_n) \quad (3.4)$$

$$S_{o,d_o \rightarrow y}(s) = (I - N_n M_n^{-1} QM_n Y_r) \quad (3.5)$$

Equation (3.4) can be rewritten as follows when  $n \geq m$

$$S_{i,d_i \rightarrow e_d}(s) = \tilde{N}_n^{-1}(I - \tilde{N}_n Q Y_l) \tilde{N}_n \quad (3.6)$$

and Eq. (3.5) also can be rewritten as

$$S_{o,d_o \rightarrow y}(s) = \tilde{M}_n^{-1}(I - \tilde{N}_n Q Y_l) \tilde{M}_n \quad (3.7)$$

If one can design  $Q(s) \in RH_\infty$  such that  $\bar{\sigma}(I - \tilde{N}_n Q Y_l(j\omega))$  as small as possible, particularly in low frequency, that is, one can eliminate both input disturbance and output disturbance in low frequency ranges. For square, minimum phase plant cases, one can design  $Q = \tilde{N}_n^{-1} \cdot J \cdot Y_l^{-1}$  to achieve this aim and  $J(s)$  is a diagonal matrix which composes of low-pass filters. In comparison with Eq. (2.9), one suggests that the designer can apply solution (2.9) when considering input disturbance only, and applied solution  $Q = \tilde{N}_n^{-1} \cdot J \cdot Y_l^{-1}$  when considering both input/output disturbances.

These two solutions and corresponding sensitivity functions are shown in Table 3.1.

Table 3.1 Solutions of parameter  $Q(s)$  and corresponding sensitivity functions

	$Q = \tilde{N}_n^{-1} \cdot J \cdot Y_l^{-1}$	$Q = J \cdot \tilde{N}_n^{-1} \cdot Y_l^{-1}$
Input sensitivity, $S_i$	$\tilde{N}_n^{-1}(I - J)\tilde{N}_n$	$(I - J)$
Output sensitivity, $S_o$	$\tilde{M}_n^{-1}(I - J)\tilde{M}_n$	$\tilde{M}_n^{-1}(I - \tilde{N}_n \cdot J \cdot \tilde{N}_n^{-1})\tilde{M}_n$

For square, non-minimum phase plant cases, the model matching method also can

be applied to obtain the parameter  $Q(s) \in RH_\infty$  such that

$$\|I - \tilde{N}_n Q Y_l\|_\infty < \gamma \leq 1 \quad (3.8)$$

The following section will show the model matching method of MIMO system.

### 3.2 Model matching method of MIMO square system

For square MIMO, non-minimum phase plant cases, the main goal is finding

$Q(s) \in RH_\infty$  to satisfy Eq. (3.8) and

$$\begin{aligned} & \|I - \tilde{N}_n Q Y_l\|_\infty < 1 \\ \Leftrightarrow & \|I - \tilde{N}_i \tilde{N}_o \cdot Q \cdot Y_{l,o} Y_{l,i}\|_\infty < 1 \end{aligned} \quad (3.9)$$

where  $\tilde{N}_i$  and  $\tilde{N}_o$  is an inner function and an outer function of  $\tilde{N}_n$ , respectively.

$Y_{l,i}$  and  $Y_{l,o}$  is an inner function and an outer function of  $Y_l$ , respectively.

According to the norm preserving properties of inner function, Eq. (3.10) can be

obtained.

$$\|I - \tilde{N}_i \tilde{N}_o \cdot Q \cdot Y_{l,o} Y_{l,i}\|_\infty < 1 \quad (3.10)$$

$$\Leftrightarrow \|\tilde{N}_i \tilde{Y}_{l,i} - \tilde{N}_o \cdot Q \cdot Y_{l,o}\|_\infty < 1 \quad (3.11)$$

then Eq. (3.11) can be described as Nehari problem.

$$\begin{aligned} & \|\tilde{N}_i \tilde{Y}_{l,i} - \tilde{N}_o \cdot Q \cdot Y_{l,o}\|_\infty < 1 \\ & = \|R - \hat{Q}\|_\infty < 1 \end{aligned} \quad (3.12)$$

where  $\tilde{N}_i \tilde{Y}_{l,i} = R \in RL_\infty$  and  $\tilde{N}_o Q Y_{l,o} = \hat{Q} \in RH_\infty$ . Finally, the parameter  $\hat{Q}(s)$

which satisfies Eq. (3.12) can be found by solving Eq. (3.13) [29].

$$\begin{aligned}\hat{Q} &= R - \Phi_{\theta}(U) \\ &= R - (\theta_{11}U + \theta_{12}) \cdot (\theta_{21}U + \theta_{22})^{-1}, \forall U \in RH_{\infty}, \|U\|_{\infty} < 1\end{aligned}\quad (3.13)$$

where  $\Phi_{\theta}$  denotes the ‘‘Right Chain Scattering’’ Linear Fractional Transformation (LFT) of  $\theta$  which denotes the J-lossless function.

**Definition 3.1** [29]:

(1) If  $\theta \in RL_{(p+m) \times (p+m)}^{\infty}$  satisfied  $\theta^*(j\omega)\mathbf{J}_U\theta(j\omega) = \mathbf{J}_U$ ,  $\forall \omega \in R$ ,  $\theta$  is called

J-unitary, where  $\mathbf{J}_U = \begin{bmatrix} I_p & 0 \\ 0 & -I_m \end{bmatrix}$ .

(2) If a J-unitary  $\theta$  satisfied  $\theta^*(s)\mathbf{J}_U\theta(s) \leq \mathbf{J}_U$ ,  $\forall s$ ,  $\text{Re}(s) > 0$ ,  $\theta$  is called

J-lossless. □

Then the J-lossless function can be obtained as follows.

$$\theta = \begin{bmatrix} \theta_{11} & \theta_{12} \\ \theta_{21} & \theta_{22} \end{bmatrix}\quad (3.14)$$

$$[\theta_{11} \quad \theta_{12}] = \left[ \begin{array}{c|cc} A_R & -L_C N_{\theta} C_R^T & N_{\theta}^T B_R \\ \hline C_R & I & 0 \end{array} \right]\quad (3.15)$$

$$[\theta_{21} \quad \theta_{22}] = \left[ \begin{array}{c|cc} -A_R^T & -N_{\theta} C_R^T & N_{\theta} L_O B_R \\ \hline B_R^T & 0 & I \end{array} \right]\quad (3.16)$$

where  $N_{\theta} = (I - L_o L_c)^{-1}$  and  $[A_R, B_R, C_R, D_R]$  denote the minimum state-space realization of  $R$  and  $L_c, L_o$  satisfy Lyapunov equation of Eq. (2.26). If one takes

$U = 0$  then the central solution  $\hat{Q}_o$  can be obtained.

$$\begin{aligned}\hat{Q}_o &= R - \theta_{12}\theta_{22}^{-1} \\ &= \left[ \begin{array}{c|c} A_R & B_R \\ \hline C_R & D_R \end{array} \right] - \left[ \begin{array}{c|c} A_R & N_{\theta}^T B_R \\ \hline C_R & \mathbf{0} \end{array} \right] \left[ \begin{array}{c|c} -A_R^T & N_{\theta} L_O B_R \\ \hline B_R^T & I \end{array} \right]^{-1}\end{aligned}\quad (3.17)$$

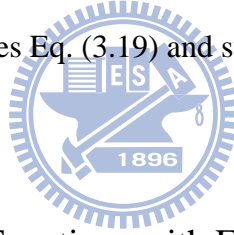
then the parameter  $Q(s)$  which satisfies Eq. (3.8) can be obtained.

$$Q(s) = \tilde{N}_o^{-1} \cdot \hat{Q}_o \cdot Y_{l,o}^{-1} \quad (3.18)$$

As one mentioned in section 3.1, our main goal is holding  $S_i$  and  $S_o$  as small as possible in low frequency ranges, that is, a good input/output disturbance rejecting capability. For this reason, a diagonal weighting function matrix  $W = \text{diag}\{w_1 \ \dots \ w_n\}_{n \times n}$  can be added to form the following objective.

$$\begin{aligned} & \|(I - \tilde{N}_n Q Y_l) W\|_\infty < 1 \\ \Leftrightarrow & \bar{\sigma}(I - \tilde{N}_n Q Y_l(j\omega)) < |W^{-1}(j\omega)| \end{aligned} \quad (3.19)$$

and the model matching method for square MIMO system also can be applied to obtain the parameter  $Q(s)$  which satisfies Eq. (3.19) and suppresses both  $S_i$  and  $S_o$ .



### 3.3 Input/Output Sensitivity Functions with Feedback Controller

If the outer-loop controller scheme that discussed in section 2.3 is applied, twelve transfer functions from  $[r \ d_i \ d_o \ \xi]^T$  to  $[e_r \ e_{di} \ e_{do} \ e_n]^T$  are shown below:

$$\begin{aligned} \begin{bmatrix} e_r \\ e_{di} \\ e_{do} \\ e_n \end{bmatrix} &= \begin{bmatrix} \Lambda^{-1} & -\Lambda^{-1}[(K + QM_n Y_r)N_n M_n^{-1}] \\ \Lambda^{-1} & \Lambda^{-1}[I - Q(I - M_n X_r)] \\ N_n M_n^{-1} \Lambda^{-1} & N_n M_n^{-1} \Lambda^{-1}[I - Q(I - QM_n X_r)] \\ N_n M_n^{-1} \Lambda^{-1} & N_n M_n^{-1} \Lambda^{-1}[I - Q(I - QM_n X_r)] \end{bmatrix} \times \begin{bmatrix} r \\ d_i \\ d_o \\ \xi \end{bmatrix} \\ & \quad \begin{bmatrix} -\Lambda^{-1}(K + QM_n Y_r) & -\Lambda^{-1}(K + QM_n Y_r) \\ -\Lambda^{-1}(K + QM_n Y_r) & -\Lambda^{-1}(K + QM_n Y_r) \\ I - N_n M_n^{-1} \Lambda^{-1}(K + QM_n Y_r) & -N_n M_n^{-1} \Lambda^{-1}(K + QM_n Y_r) \\ I - N_n M_n^{-1} \Lambda^{-1}(K + QM_n Y_r) & I - N_n M_n^{-1} \Lambda^{-1}(K + QM_n Y_r) \end{bmatrix} \end{aligned} \quad (3.20)$$

where  $\Lambda = (I + KN_n M_n^{-1})$  and the stable conditions are the same as Eqs. (2.38) and

(2.39). For DCFDOB-VS that discussed in section 2.4, the  $4 \times 4$  transfer functions

matrix from  $[r \ d_i \ d_o \ \xi]^T$  to  $[e_r \ e_{di} \ e_{do} \ e_n]^T$  is obtained as follows.

$$\begin{bmatrix} e_r \\ e_{di} \\ e_{do} \\ e_n \end{bmatrix} = \begin{bmatrix} M_n H^{-1} & M_n [X_r + H^{-1}(I-Q)Y_l \tilde{N}_n] - I \\ M_n H^{-1} & M_n [X_r + H^{-1}(I-Q)Y_l \tilde{N}_n] \\ N_n H^{-1} & N_n [X_r + H^{-1}(I-Q)Y_l \tilde{N}_n] \\ N_n H^{-1} & N_n [X_r + H^{-1}(I-Q)Y_l \tilde{N}_n] \end{bmatrix} \times \begin{bmatrix} r \\ d_i \\ d_o \\ \xi \end{bmatrix} + \begin{bmatrix} -M_n [Y_r - H^{-1}(I-Q)Y_l \tilde{M}_n] & -M_n [Y_r - H^{-1}(I-Q)Y_l \tilde{M}_n] \\ -M_n [Y_r - H^{-1}(I-Q)Y_l \tilde{M}_n] & -M_n [Y_r - H^{-1}(I-Q)Y_l \tilde{M}_n] \\ I - N_n [Y_r - H^{-1}(I-Q)Y_l \tilde{M}_n] & -N_n [Y_r - H^{-1}(I-Q)Y_l \tilde{M}_n] \\ I - N_n [Y_r - H^{-1}(I-Q)Y_l \tilde{M}_n] & I - N_n [Y_r - H^{-1}(I-Q)Y_l \tilde{M}_n] \end{bmatrix} \begin{bmatrix} r \\ d_i \\ d_o \\ \xi \end{bmatrix} \quad (3.21)$$

Also, we replace  $H^{-1}(I-Q)Y_l$  of the 2<sup>nd</sup>, 3<sup>rd</sup> and 4<sup>th</sup> columns in Eq. (3.21) with  $Q_Y$

and yield Eq. (3.22) and also form the 2DOF control scheme contains two independent parameters.

$$\begin{bmatrix} e_r \\ e_{di} \\ e_{do} \\ e_n \end{bmatrix} = \begin{bmatrix} M_n H^{-1} & M_n (X_r + Q_Y \tilde{N}_n) - I & -M_n (Y_r - Q_Y \tilde{M}_n) & -M_n (Y_r - Q_Y \tilde{M}_n) \\ M_n H^{-1} & M_n (X_r + Q_Y \tilde{N}_n) & -M_n (Y_r - Q_Y \tilde{M}_n) & -M_n (Y_r - Q_Y \tilde{M}_n) \\ N_n H^{-1} & N_n (X_r + Q_Y \tilde{N}_n) & I - N_n (Y_r - Q_Y \tilde{M}_n) & -N_n (Y_r - Q_Y \tilde{M}_n) \\ N_n H^{-1} & N_n (X_r + Q_Y \tilde{N}_n) & I - N_n (Y_r - Q_Y \tilde{M}_n) & I - N_n (Y_r - Q_Y \tilde{M}_n) \end{bmatrix} \begin{bmatrix} r \\ d_i \\ d_o \\ \xi \end{bmatrix} \quad (3.22)$$

The transfer functions of input/output sensitivity functions are represented as follows:

$$S_i = M_n (X_r + Q_Y \tilde{N}_n) \quad (3.23)$$

$$\begin{aligned} S_o &= I - N_n [Y_r - Q_Y \tilde{M}_n] \\ &= N_n (X_r + Q_Y \tilde{N}_n) \tilde{N}_n^{-1} \tilde{M}_n \end{aligned} \quad (3.24)$$

If one can design  $Q_Y(s)$  satisfying theorem 2.3 and make the common term

$\bar{\sigma}(X_r + Q_Y \tilde{N}_n(j\omega))$  as small as possible, particularly in low frequency, that is, one can



eliminate both input disturbance and output disturbance in low frequency ranges, simultaneously. The solving steps are provided in paragraphs 2.4.2.2 part a and part b for minimum phase and non-minimum phase systems, respectively.

### 3.4 The DCFDOB for non-square plant

#### 3.4.1 The thin plant case

For non-square plant, however, the non-square types of plant will restrict rejection capability. For a thin plant  $P_{n \times m}$  with  $n > m$  dimension, the output channel numbers are greater than input channel numbers. In section 3.1, we rewrote the input sensitivity

function as  $\tilde{N}_{n,m \times n}^{-1} (I_{n \times n} - \tilde{N}_{n,n \times m} \cdot Q_{m \times m} \cdot Y_{l,m \times n}) \tilde{N}_{n,n \times m}$  and output sensitivity function as

$\tilde{M}_{n,n \times n}^{-1} (I_{n \times n} - \tilde{N}_{n,n \times m} \cdot Q_{m \times m} \cdot Y_{l,m \times n}) \tilde{M}_{n,n \times n}$  and then design  $Q(s)$  to satisfy

$\tilde{N}_{n,n \times m} \cdot Q_{m \times m} \cdot Y_{l,m \times n} = \text{diag}\{J_{ii}\}_{n \times n}$  ( $J_{ii}, i = 1 \sim n$  are low-pass filters) to reject

input/output disturbances in minimum-phase system. However, in thin plant cases

( $n > m$ ), we can not obtain the solutions of parameter matrix,  $Q_{m \times m}(s)$ , which contains

only  $m^2$  parameters to satisfy  $n^2$  desire functions ( $m^2 < n^2$ ). One must design

$Q(s)$  which satisfies the following equation.

$$I_{m \times m} - Q_{m \times m} \cdot Y_{l,m \times n} \cdot \tilde{N}_{n,n \times m} = S_{i,m \times m} \quad (3.25)$$

where  $S_{i,m \times m}$  is an input sensitivity function matrix with  $m \times m$  dimension and

contains  $m^2$  sensitivity functions. Equation (3.25) indicates that one can design  $m^2$

elements of  $Q_{m \times m}$  matrix to satisfy  $m^2$  linear independent sensitivity functions of  $S_{i,m \times m}$ , that is, for thin plant cases, a suitable  $Q_{m \times m}$  matrix can suppress input disturbances of all input channels. On the other hand, for rejecting output disturbances, the following equation must be satisfied.

$$I_{n \times n} - P_{n,n \times m} \cdot Q_{m \times m} \cdot M_{n,m \times m} \cdot Y_{r,m \times n} = S_{o,n \times n} \quad (3.26)$$

where  $S_{o,n \times n}$  is output sensitivity function matrix composed of  $n^2$  linear independent sensitivity functions. Obviously, Eq. (3.26) is also an *overdetermined system* ( $m^2 < n^2$ ), there exist no exact solutions which satisfy Eq. (3.26). Although the designer can select  $m^2$  significant output sensitivity functions and solve these functions by  $m^2$  elements of  $Q_{m \times m}$  matrix, however, the influences of others ( $n^2 - m^2$ ) sensitivity functions will not be guaranteed.

### 3.4.2 The wide plant case

For a wide plant, we can not modify input sensitivity function as

$\tilde{N}_{n,m \times n}^{-1} (I_{n \times n} - \tilde{N}_{n,n \times m} \cdot Q_{m \times m} \cdot Y_{l,m \times n}) \tilde{N}_{n,n \times m}$ , since  $\tilde{N}_n$  is a right invertible matrix, i.e.


$$\tilde{N}_{n,m \times n}^{-1} \cdot \tilde{N}_{n,n \times m} \neq I_{m \times m}.$$

**Lemma 3.2** [47]:

Suppose **A** be an  $m \times n$  matrix, if there exists an  $n \times m$  matrix **B** such that

$\mathbf{BA} = \mathbf{I}_{n \times n}$ , where  $\mathbf{I}_{n \times n}$  is an  $n \times n$  identity matrix, the matrix  $\mathbf{B}$  is called the left inverse of the left invertible matrix  $\mathbf{A}$ . If there exists another  $n \times m$  matrix  $\mathbf{B}$  such that  $\mathbf{AB} = \mathbf{I}_{m \times m}$ , where  $\mathbf{I}_{m \times m}$  is an  $m \times m$  identity matrix, the matrix  $\mathbf{B}$  is called the right inverse of the right invertible matrix  $\mathbf{A}$ . If there exist an operator  $\mathbf{B}$ , such that  $\mathbf{AB} = \mathbf{BA} = \mathbf{I}$ ,  $\mathbf{A}$  is called invertible.  $\square$

Recalling Eq. (3.25), it seems that one can obtain  $m^2$  elements of parameter matrix to satisfy  $m^2$  desire sensitivity functions, however, in wide plant cases, if we modify  $\mathbf{I}_{m \times m} - \mathbf{Q}_{m \times m} \cdot \mathbf{Y}_{l, n \times m} \cdot \tilde{\mathbf{N}}_{n, n \times m} = \mathbf{S}_{l, m \times m}$  as a linear equation,  $\mathbf{AX} = \mathbf{B}$ , where



$$\mathbf{A} = \begin{bmatrix} [\tilde{\mathbf{N}}_{n, m \times n}^T \cdot \mathbf{Y}_{l, n \times m}^T]_{m \times m} & [\mathbf{0}]_{m \times m} & \cdots & [\mathbf{0}]_{m \times m} \\ [\mathbf{0}]_{m \times m} & [\tilde{\mathbf{N}}_{n, m \times n}^T \cdot \mathbf{Y}_{l, n \times m}^T]_{m \times m} & & \vdots \\ \vdots & \vdots & \ddots & [\mathbf{0}]_{m \times m} \\ [\mathbf{0}]_{m \times m} & [\mathbf{0}]_{m \times m} & \cdots & [\tilde{\mathbf{N}}_{n, m \times n}^T \cdot \mathbf{Y}_{l, n \times m}^T]_{m \times m} \end{bmatrix}_{m^2 \times m^2} \quad (3.27)$$

$$\mathbf{X} = \begin{bmatrix} Q_{11} \\ Q_{12} \\ \vdots \\ Q_{1m} \\ Q_{21} \\ Q_{22} \\ \vdots \\ Q_{2m} \\ \vdots \\ Q_{m1} \\ \vdots \\ Q_{mm} \end{bmatrix}_{m^2 \times 1}, \quad \mathbf{B} = \begin{bmatrix} \begin{bmatrix} 1 - S_{11} \\ -S_{12} \\ \vdots \\ -S_{1m} \end{bmatrix}_{m \times 1} \\ \begin{bmatrix} -S_{21} \\ 1 - S_{22} \\ \vdots \\ -S_{2m} \end{bmatrix}_{m \times 1} \\ \vdots \\ \begin{bmatrix} -S_{m1} \\ -S_{m2} \\ \vdots \\ 1 - S_{mm} \end{bmatrix}_{m \times 1} \end{bmatrix}_{m^2 \times 1} \approx \begin{bmatrix} \begin{bmatrix} J_{11} \\ 0 \\ \vdots \\ 0 \end{bmatrix}_{m \times 1} \\ \begin{bmatrix} 0 \\ J_{22} \\ \vdots \\ 0 \end{bmatrix}_{m \times 1} \\ \vdots \\ \begin{bmatrix} 0 \\ 0 \\ \vdots \\ J_{mm} \end{bmatrix}_{m \times 1} \end{bmatrix}_{m^2 \times 1} \quad (3.28)$$

**Lemma 3.3** [47]:

A linear system of equations  $\mathbf{AX} = \mathbf{B}$  is consistent if and only if the rank of the matrix  $\mathbf{A}$  is the same as the rank of the augmented matrix of the system  $(\mathbf{A} | \mathbf{B})$ .  $\square$

In Eqs. (3.27) and (3.28), for wide plant cases,  $rank(\mathbf{A}) = n \times m$ ,  $rank(\mathbf{A} | \mathbf{B}) = n \times m + 1$  and  $rank(\mathbf{A}) < rank(\mathbf{A} | \mathbf{B})$ . That is, the wide plant cases are inconsistent and we can not obtain analytical solution that satisfies Eq. (3.25).

To reject output disturbances in wide plant, one modified the output sensitivity function  $I_{n \times n} - P_{n, n \times m} \cdot Q_{m \times m} \cdot M_{n, m \times m} \cdot Y_{r, m \times n}$  as

$\tilde{M}_{n, n \times n}^{-1} (I_{n \times n} - \tilde{N}_{n, n \times m} \cdot Q_{m \times m} \cdot Y_{l, m \times n}) \tilde{M}_{n, n \times n}$  and then design

$$\tilde{N}_{n, n \times m} \cdot Q_{m \times m} \cdot Y_{l, m \times n} = \text{diag}\{j_{ii}\}, (i = 1 \sim n) \quad (3.29)$$

for minimum phase systems. From Eq. (3.29), we knew that there exist  $m^2$  unknown parameters and  $n^2$  linear independent sensitivity functions, namely, we have  $m^2 - n^2$  arbitrary parameters because of  $m > n$  in wide plant cases. Also, the DCFDOB can perform well for eliminating output disturbances in wide plant cases. Based on these discussions, one summarizes the design properties of the DCFDOB for non-square, minimum phase plant cases in table 3.2. For non-square plant topic, how to find the optimum solutions will be an interesting topic in the future.

Table 3.2 Design properties of the DCFDOB for non-square, minimum phase plant cases

Plant type	Input Sensitivity	Output Sensitivity
Thin plant $P_{n \times m}$ ( $n > m$ )	$S_{i,m \times m} = I_{m \times m} - Q_{m \times m} \cdot Y_{l,m \times n} \cdot \tilde{N}_{n,n \times m}$	$S_{o,n \times n} = I_{n \times n} - P_{n,n \times m} \cdot Q_{m \times m} \cdot M_{n,m \times m} \cdot Y_{r,m \times n}$
	<p>One can modify as:</p> $S_{i,m \times m} = \tilde{N}_{n,n \times m}^{-1} (I_{n \times n} - \tilde{N}_{n,n \times m} Q_{m \times m} \cdot Y_{l,m \times n}) \tilde{N}_{n,n \times m}$	<p>One can modify as:</p> $S_{o,n \times n} = \tilde{M}_{n,n \times n}^{-1} (I_{n \times n} - \tilde{N}_{n,n \times m} Q_{m \times m} \cdot Y_{l,m \times n}) \tilde{M}_{n,n \times n}$
	<p>One can not obtain analytic solutions that satisfies</p> $\tilde{N}_{n,n \times m} Q_{m \times m} \cdot Y_{l,m \times n} = \begin{bmatrix} J_{11} & \cdots & 0 \\ \vdots & \ddots & \vdots \\ 0 & \cdots & J_{mm} \end{bmatrix}_{n \times n}$ <p>since the unknown parameters are less than equations.</p>	<p>One can not obtain analytic solutions that satisfies</p> $\tilde{N}_{n,n \times m} Q_{m \times m} \cdot Y_{l,m \times n} = \begin{bmatrix} J_{11} & \cdots & 0 \\ \vdots & \ddots & \vdots \\ 0 & \cdots & J_{mm} \end{bmatrix}_{n \times n},$ <p>since the unknown parameters are less than equations.</p>
	<p>The solutions can be solved from the following equation:</p> $Q_{m \times m} \cdot Y_{l,m \times n} \cdot \tilde{N}_{n,n \times m} = \begin{bmatrix} J_{11} & \cdots & 0 \\ \vdots & \ddots & \vdots \\ 0 & \cdots & J_{mm} \end{bmatrix}_{m \times m}$	<p>The exact solutions for output disturbance elimination: Can not obtained because the unknown parameters are less than the equations.</p> $P_{n,n \times m} \cdot Q_{m \times m} \cdot M_{n,m \times m} \cdot Y_{r,m \times n} = \begin{bmatrix} J_{11} & \cdots & 0 \\ \vdots & \ddots & \vdots \\ 0 & \cdots & J_{nn} \end{bmatrix}_{n \times n}$
Elimination Capability	Completely eliminate the input disturbances of all channels	Only eliminate the same channel numbers as input channel ones (The designer can select the significant channels)

Plant type	Input Sensitivity	Output Sensitivity
Wide plant $P_{n \times m} (n < m)$	$S_{i,m \times m} = I_{m \times m} - Q_{m \times m} \cdot Y_{l,m \times n} \cdot \tilde{N}_{n,n \times m}$	$S_{o,n \times n} = I_{n \times n} - P_{n,n \times m} \cdot Q_{m \times m} \cdot M_{n,m \times m} \cdot Y_{r,m \times n}$
	One can not modify because $\tilde{N}_{n,n \times m}$ is right invertible	One can modify as: $S_{o,n \times n} = \tilde{M}_{n,n \times n}^{-1} (I_{n \times n} - \tilde{N}_{n,n \times m} Q_{m \times m} \cdot Y_{l,m \times n}) \tilde{M}_{n,n \times n}$
	The exact solutions for input disturbance elimination: Can not be obtained because the system is inconsistent, since $rank(\mathbf{A}) < rank(\mathbf{A}   \mathbf{B})$	The solutions can be solved from the following equation: $\tilde{N}_{n,n \times m} Q_{m \times m} \cdot Y_{l,m \times n} = \begin{bmatrix} J_{11} & \cdots & 0 \\ \vdots & \ddots & \vdots \\ 0 & \cdots & J_{nn} \end{bmatrix}_{n \times n} .$ Furthermore, we have $m^2 - n^2$ arbitrary solutions.
Elimination Capability	Only eliminate the channel numbers as many as output channel ones (The designer can select the significant channels)	Completely eliminate the output disturbances of all channels

In summary, to eliminate input disturbances completely, the numbers of output channel must equal/greater than the one of input channel.

In dual, to eliminate output disturbances completely, the numbers of input channel must equal/greater than the one of output channel.

We will give two numerical examples to show these properties of DCFDOB for non-square plant cases in section 5.3.

For non-minimum phase plant, recalling Eqs. (2.15), (3.6), (3.7) and Fig 2.8, the main goal of model matching method is finding the whole solution set that satisfies  $\|I - \tilde{N}_n Q Y_l\|_\infty < 1$ . According to the plant types, the model matching problem can be discussed in two ways [29]:

(1) **1-block** problem: ( $\tilde{N}_n, Y_l$  are both square and invertible)

If  $\tilde{N}_n(s)$  and  $Y_l(s)$  are both invertible, i.e. square plant cases, and they can be decomposed as:

$$\tilde{N}_n = \tilde{N}_{n,i} \cdot \tilde{N}_{n,o}, Y_l = Y_{l,o} \cdot Y_{l,i} \quad (3.30)$$

where  $\tilde{N}_{n,i}/\tilde{N}_{n,o}$  and  $Y_{l,i}/Y_{l,o}$  are inner/outer functions and  $\tilde{N}_{n,i}^{-1} \tilde{N}_{n,i} = Y_{l,i} Y_{l,i}^{-1} = I$ , then the objective  $\|I - \tilde{N}_n Q Y_l\|_\infty < 1$  can be rewritten as:

$$\begin{aligned} & \|I - \tilde{N}_n Q Y_l\|_\infty \\ &= \|I - \tilde{N}_{n,i} \tilde{N}_{n,o} Q Y_{l,o} Y_{l,i}\|_\infty \\ &= \|\tilde{N}_{n,i}^{-1} Y_{l,i} - \tilde{N}_{n,o} Q Y_{l,o}\|_\infty \\ &= \|R_{11} - Q\|_\infty < 1 \end{aligned} \quad (3.31)$$

where  $R_{11} = \tilde{N}_{n,i}^{-1} \cdot Y_{l,i}$ .

(2) **4-block** problem: ( $\tilde{N}_n$  is left invertible and  $Y_l$  is right invertible)

If  $\tilde{N}_n$  is left invertible and  $Y_l$  is right invertible, i.e. non-square plant cases and

under such circumstance, one can select  $F$  and  $L$  such that

$$\tilde{N}_n \tilde{N}_n = Y_l Y_l^T = I \quad (3.32)$$

That is,  $\tilde{N}_n$  is an inner function and  $Y_l$  is a co-inner function. One also can obtain

complementary inner matrices,  $\tilde{N}_{n,\perp}$ ,  $Y_{l,\perp}$ , such that they satisfy

$$\begin{bmatrix} \tilde{N}_n \\ \tilde{N}_{n,\perp} \end{bmatrix} [\tilde{N}_n \quad \tilde{N}_{n,\perp}] = \begin{bmatrix} Y_l \\ Y_{l,\perp} \end{bmatrix} [Y_l^T \quad Y_{l,\perp}^T] = I \quad (3.33)$$

**Lemma 3.3** [29]:

Let  $T = \left[ \begin{array}{c|c} A & B \\ \hline C & D \end{array} \right]$  be an inner function and  $X^+$  be the pseudo-inverse of  $X$ , the

solution of Eq. (1.16), then a complementary inner factor  $T_\perp$  is given by

$$T_\perp = \left[ \begin{array}{c|c} A + BF & -X^+ C^T D_\perp \\ \hline C + DF & D_\perp \end{array} \right] \quad (3.34)$$

where  $D_\perp$  is an orthogonal complement of  $D$  such that  $[D \quad D_\perp]$  is square and

orthogonal. □

**Note:**

The singular value decomposition of  $X$  is  $X = USV^T$ , where  $U$  and  $V$  are

both  $n \times n$  orthogonal matrices and  $S$  is an  $m \times n$  diagonal matrix with singular

values  $\sigma_i$  for  $i=1, \dots, n$ . Then

$$X^+ = V(S^T S)^{-1} S^T U^T \quad (3.35)$$

If the rank of  $X$  is less than  $n$ , the inverse of  $S^T S$  does not exist.



Furthermore, the main objective of non-square, non-minimum phase plants can be rewritten as

$$\begin{aligned}
& \left\| I - \tilde{N}_n Q Y_l \right\|_{\infty} \\
&= \left\| I - \begin{bmatrix} \tilde{N}_n & \tilde{N}_{n,\perp} \end{bmatrix} \begin{bmatrix} Q & 0 \\ 0 & 0 \end{bmatrix} \begin{bmatrix} Y_l \\ Y_{l,\perp} \end{bmatrix} \right\|_{\infty} \\
&= \left\| \begin{bmatrix} \tilde{N}_n \\ \tilde{N}_{n,\perp} \end{bmatrix} \begin{bmatrix} Y_l \\ Y_{l,\perp} \end{bmatrix} - \begin{bmatrix} \tilde{N}_n \\ \tilde{N}_{n,\perp} \end{bmatrix} \begin{bmatrix} \tilde{N}_n & \tilde{N}_{n,\perp} \end{bmatrix} \begin{bmatrix} Q & 0 \\ 0 & 0 \end{bmatrix} \begin{bmatrix} Y_l \\ Y_{l,\perp} \end{bmatrix} \right\|_{\infty} \quad (3.36) \\
&= \left\| \begin{bmatrix} \tilde{N}_n \\ \tilde{N}_{n,\perp} \end{bmatrix} \begin{bmatrix} Y_l \\ Y_{l,\perp} \end{bmatrix} - \begin{bmatrix} Q & 0 \\ 0 & 0 \end{bmatrix} \right\|_{\infty} \\
&= \left\| \begin{bmatrix} R_{11} - Q & R_{12} \\ R_{21} & R_{22} \end{bmatrix} \right\|_{\infty} < 1
\end{aligned}$$

where

$$\begin{bmatrix} R_{11} & R_{12} \\ R_{21} & R_{22} \end{bmatrix} = \begin{bmatrix} \tilde{N}_n Y_l & \tilde{N}_n Y_{l,\perp} \\ \tilde{N}_{n,\perp} Y_l & \tilde{N}_{n,\perp} Y_{l,\perp} \end{bmatrix} \quad (3.37)$$

Please refer to [29, chapters 2, 4 and 5] and [37]—[38] for detail discussions of 1-block problem and [39]—[40] for 4-block problems. The non-square plant with non-minimum phase zeros cases are much more complex than others. In the future, we will look into these complicated cases and find the optimum  $Q(s)$  parameter matrix for non-square, non-minimum phase plant.

In conclusion, when the proposed structure is applied to MIMO systems, the capability of disturbance rejection is good when plants are square and is restricted by the non-square types of plants. How to obtain the optimum  $Q(s)$  parameter matrix for non-square, non-minimum phase plants will be an interesting issue in the future.

## CHAPTER 4

### UNCERTAINTY AND ROBUSTNESS

In this chapter, one will investigate the robust stability of the DCFDOB under plant uncertainties. The small gain theorem is used here to derive robust stability tests and the modeling error  $\Delta(s)$  will be assumed to be stable. Furthermore, one will discuss the robust DCFDOB which satisfies small gain theorem and its design method and procedures in  $H_\infty$  frameworks.

#### 4.1 Coprime Factor Uncertainty

There are numerous ways of representing classes of systems that are close to a nominal model, and in this monograph, one adopt the coprime factor framework to represent both the nominal model transfer function, and a class of close systems. The right coprime factorization of perturbed plant is described as

$$P = (N_n + \Delta_N) \cdot (M_n + \Delta_M)^{-1}, (N_n, M_n, \Delta_N, \Delta_M \in RH_\infty) \quad (4.1)$$

and the block diagram of DCFDOB with system uncertainties is constructed as follows.

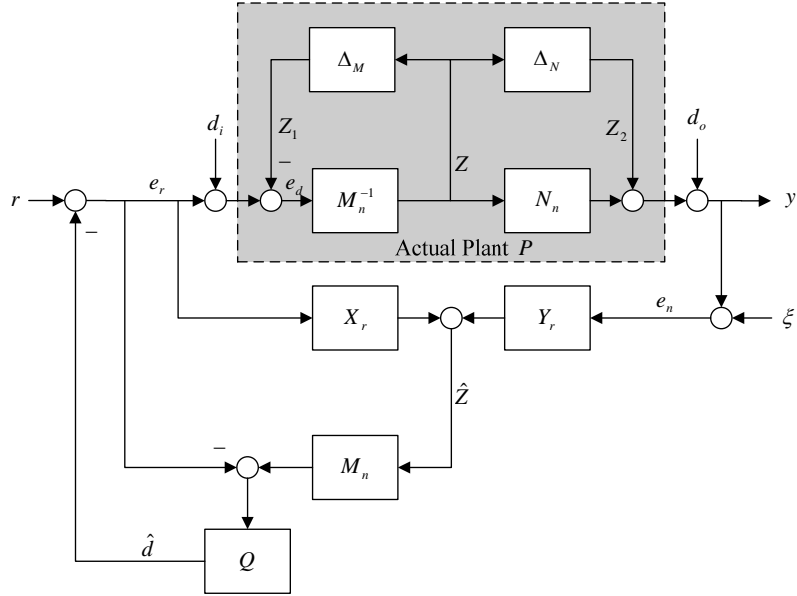


Fig. 4.1 Block diagram of DCFDOB with system uncertainties

Before going into detail, one first introduces an important theorem about robust stability test of system with uncertainty.



#### 4.1.1 Small gain theorem [36]

This chapter considers the stability test of the DCFDOB under model perturbations. The basis for the robust stability criteria derived in the sequel is the so-called small gain theorem. Consider the interconnected system shown in Fig 4.2 with  $M_{\Delta}(s)$  a stable  $p \times q$  transfer matrix and the maximum allowable bound of plant uncertainties  $\varepsilon$  where  $\varepsilon > 0$ . Then the interconnected system shown below is well-posed and guarantee internally stable for all  $\Delta(s) \in RH_{\infty}$  with

$$(a) \quad \|\Delta\|_{\infty} \leq \varepsilon \text{ if and only if } \|M_{\Delta}\|_{\infty} < \varepsilon^{-1} \quad (4.2a)$$

$$(b) \quad \|\Delta\|_{\infty} < \varepsilon \text{ if and only if } \|M_{\Delta}\|_{\infty} \leq \varepsilon^{-1} \quad (4.2b)$$

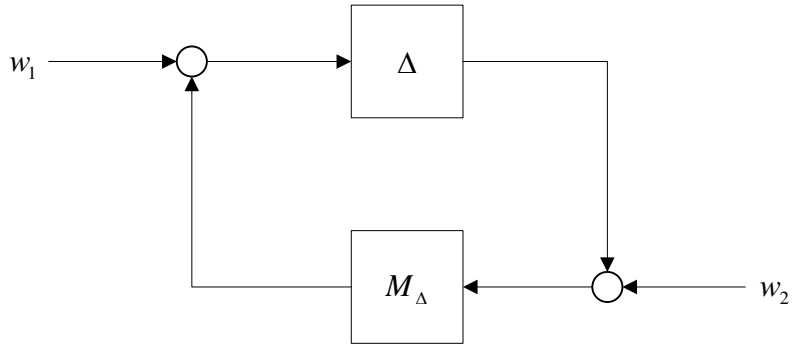


Fig. 4.2  $M_{\Delta} - \Delta$  loop stability analysis

## 4.2 Robust Stability Analysis

### 4.2.1 Robust stability analysis of DCFDOB

According to small gain theorem and Fig. 4.2, one modified Fig. 4.1 as  $M_{\Delta} - \Delta$  loop type and shown in Fig. 4.3.

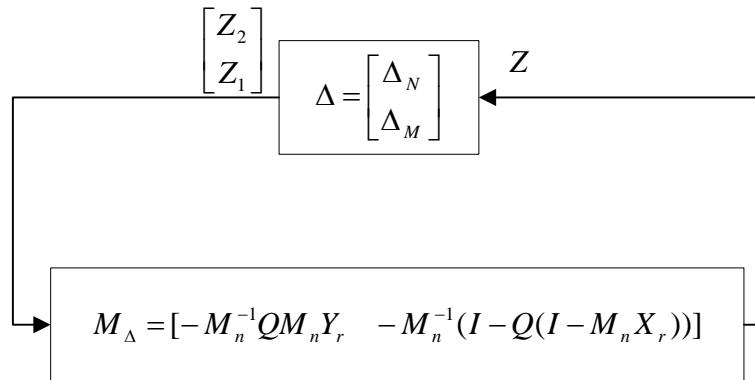


Fig. 4.3  $M_{\Delta} - \Delta$  loop stability analysis of Fig. 4.1

The interconnected system is internally stable if the following inequalities are satisfied :

$$\left\| \begin{bmatrix} \Delta_N \\ \Delta_M \end{bmatrix} \right\|_{\infty} \leq \varepsilon \text{ if and only if } \left\| \begin{bmatrix} -M_n^{-1} Q M_n Y_r & -M_n^{-1} (I - Q(I - M_n X_r)) \end{bmatrix} \right\|_{\infty} < \varepsilon^{-1}$$

(4.3a)

$$\left\| \begin{bmatrix} \Delta_N \\ \Delta_M \end{bmatrix} \right\|_\infty < \varepsilon \text{ if and only if } \left\| \begin{bmatrix} -M_n^{-1}QM_nY_r & -M_n^{-1}(I-Q(I-M_nX_r)) \end{bmatrix} \right\|_\infty \leq \varepsilon^{-1}$$

(4.3b)

If Eq. (4.3b) is pre-multiplied by normalized coprime factorization  $\begin{bmatrix} N_n \\ M_n \end{bmatrix}$ , since

$$\left\| \begin{bmatrix} N_n \\ M_n \end{bmatrix} \right\|_\infty = 1, \text{ the robustness bound of DCFDOB can be obtained from the following}$$

form:

$$\left\| \begin{bmatrix} -P_nQM_nY_r & -P_n(I-Q(I-M_nX_r)) \\ -QM_nY_r & -(I-Q(I-M_nX_r)) \end{bmatrix} \right\|_\infty \leq \varepsilon^{-1} \quad (4.4)$$

In other words, if a small  $\varepsilon^{-1}$  can be achieved by designing an adequate  $Q(s) \in RH_\infty$  for a given nominal plant  $P_n(s)$ , the DCFDOB can be stabilized under

large uncertainties, however,

$$\left\| \begin{bmatrix} -P_nQM_nY_r & -P_n(I-Q(I-M_nX_r)) \\ -QM_nY_r & -(I-Q(I-M_nX_r)) \end{bmatrix} \cdot \begin{bmatrix} N_n \\ M_n \end{bmatrix} \right\|_\infty \leq \varepsilon^{-1} \cdot 1 \quad (4.5)$$

$$\Leftrightarrow \left\| \begin{bmatrix} -P_nQY_l\tilde{M}_nN_n - P_nM_n + P_nQY_l\tilde{N}_nM_n \\ -QY_l\tilde{M}_nN_n - M_n + QY_l\tilde{N}_nM_n \end{bmatrix} \right\|_\infty \leq \varepsilon^{-1} \quad (4.6)$$

$$\Leftrightarrow \left\| \begin{bmatrix} -N_n \\ -M_n \end{bmatrix} \right\|_\infty \leq \varepsilon^{-1} \quad (4.7)$$

$$\Leftrightarrow 1 \leq \varepsilon^{-1} \quad (4.8)$$

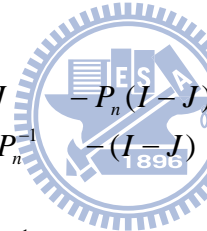
From Eq. (4.8), one knows that the minimum value of  $\varepsilon^{-1}$  will greater than one, that is,

the maximum allowable bound of  $\left\| \begin{bmatrix} \Delta_N \\ \Delta_M \end{bmatrix} \right\|_\infty$  must less than one. Besides, Eq. (4.4) can

be rewritten as follows.

$$\left\| \begin{bmatrix} -\tilde{M}_n^{-1}(\tilde{N}_n Q Y_l) \tilde{M}_n & -\tilde{M}_n^{-1}(I - \tilde{N}_n Q Y_l) \tilde{N}_n \\ -\tilde{N}_n^{-1}(\tilde{N}_n Q Y_l) \tilde{M}_n & -\tilde{N}_n^{-1}(I - \tilde{N}_n Q Y_l) \tilde{N}_n \end{bmatrix} \right\|_\infty \leq \varepsilon^{-1} \quad (4.9)$$

According to Eqs. (3.6) and (3.7), although one can enlarge the bandwidth of  $\tilde{N}_n Q Y_l$  to increase disturbance rejection capability, however, according to Eq. (4.9),  $\varepsilon^{-1}$  increases with increasing the bandwidth of  $\tilde{N}_n Q Y_l$ . For simply explanation, one assumes that the system is SISO, minimum phase and then substitute Eq. (2.9) into Eq. (4.9) to yield Eq. (4.10).



$$\left\| \begin{bmatrix} -J & -P_n(I - J) \\ -J \cdot P_n^{-1} & -(I - J) \end{bmatrix} \right\|_\infty \leq \varepsilon^{-1} \quad (4.10)$$

Obviously, the stability margin  $\varepsilon^{-1}$  can be obtained by designing the low-pass filter  $J(s)$ . If the bandwidth of  $J(s)$  is wider than the one of the nominal plant  $P_n(s)$ , the dominant term  $|-J \cdot P_n^{-1}(j\omega)|$  of Eq. (4.10) will roll up after the cutoff frequency of  $P_n$  and then roll off after the cutoff frequency of  $J(s)$ . The wider bandwidth of the low-pass filter, the larger value of  $|-J \cdot P_n^{-1}(j\omega)|$ , consequently, larger  $\varepsilon^{-1}$  we obtained. A tradeoff must be done between rejection capability and robust stability.

In addition, the output  $y(t)$  of plant with uncertainties is represented as follows.

$$y = P_n \cdot r + P_n(I - Q(I - M_n X_r)) \cdot (d_i - z_1) + (I - P_n Q M_n Y_r) \cdot (d_o + z_2) - P_n Q M_n Y_r \cdot \xi \quad (4.11)$$

Since one design  $P_n(I - Q(I - M_n X_r)) \approx 0$  and  $I - P_n Q M_n Y_r \approx 0$  in low frequency ranges to reject input and output disturbances, Eq. (4.11) can be approximated as follows.

$$y \approx P_n \cdot r - P_n Q M_n Y_r \cdot \xi \quad (4.12)$$

That is, the perturbation will be suppressed as well. Thus, the system will behave like nominal plant in low frequency ranges, and an outer loop controller for stabilizing and better performance can be designed easily. The complete feasible form of DCFDOB is shown in Fig. 4.4.

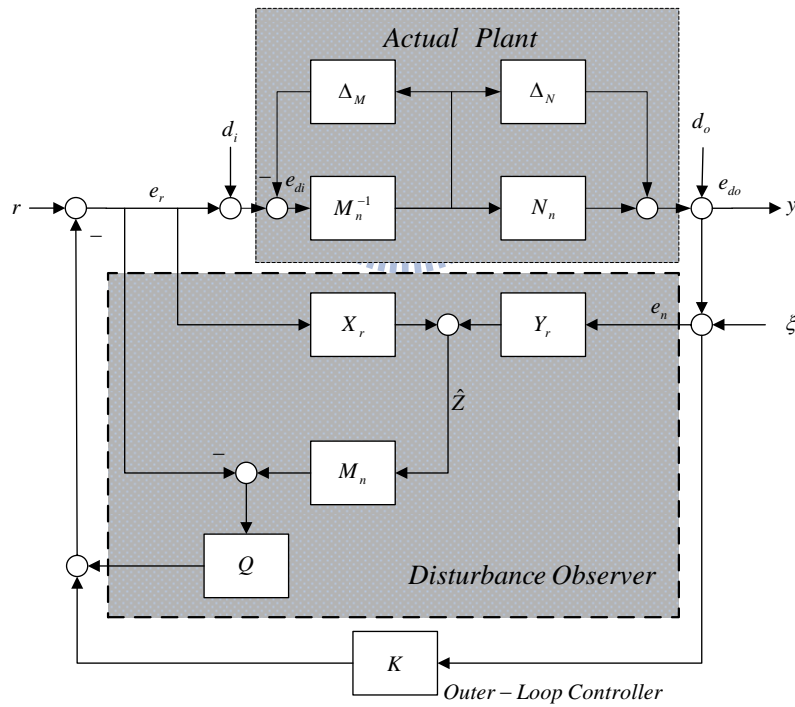


Fig. 4.4 The complete feasible form of DCFDOB with an outer-loop controller

#### 4.2.2 Robust stability analysis of DCFDOB-VS

Recalling the DCFDOB-VS structure shown in Fig. 2.17, we modified it as

$M_\Delta - \Delta$  loop as shown in the following figure.

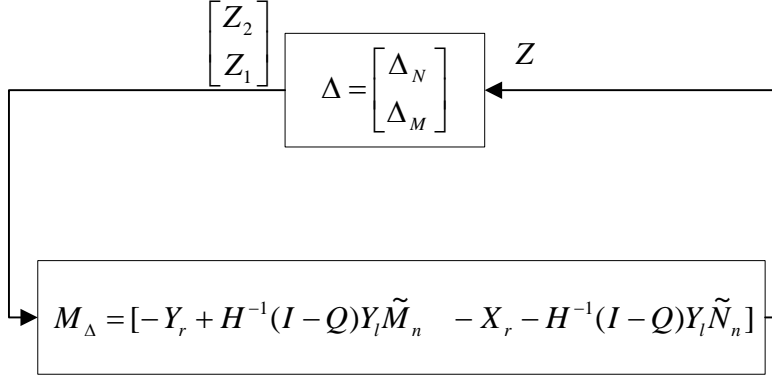


Fig. 4.5  $M_\Delta - \Delta$  loop of DCFDOB-VS

According to small gain theorem, the DCFDOB-VS is guaranteed internally stable for all  $\|\Delta\|_\infty < 1$  if and only if :

$$\left\| \begin{bmatrix} \Delta_N \\ \Delta_M \end{bmatrix} \right\|_\infty \cdot \left\| \begin{bmatrix} -Y_r + H^{-1}(I-Q)Y_l\tilde{M}_n & -X_r - H^{-1}(I-Q)Y_l\tilde{N}_n \end{bmatrix} \right\|_\infty \leq 1 \quad (4.13)$$

If the relation  $Q(s) = I - HQ_Y Y_l^{-1}$  is substituted into  $M_\Delta(s)$  of Eq. (4.13), we can obtain the following equation.

$$\begin{aligned} \|M_\Delta\|_\infty &= \left\| \begin{bmatrix} -Y_r + H^{-1}(I-Q)Y_l\tilde{M}_n & -X_r - H^{-1}(I-Q)Y_l\tilde{N}_n \end{bmatrix} \right\|_\infty \\ &= \left\| \begin{bmatrix} -Y_r + Q_Y\tilde{M}_n & -X_r - Q_Y\tilde{N}_n \end{bmatrix} \right\|_\infty \end{aligned} \quad (4.14)$$

We found that the parameter  $H(s)$  does not appear in Eq. (4.14) and the value of  $\|M_\Delta(s)\|_\infty$  is only influenced by the independent parameter  $Q_Y(s)$ . That is, the advantage is that it will simplify the robustness tuning procedure and disturbances rejection by using only one independent instead of two parameters  $H(s)$  and  $Q(s)$ .

Furthermore, we can modify Fig. 2.17 as Fig. 4.6, which is further equaled to Figs. 4.7(a)



and 4.7(b) through I/O equivalence.

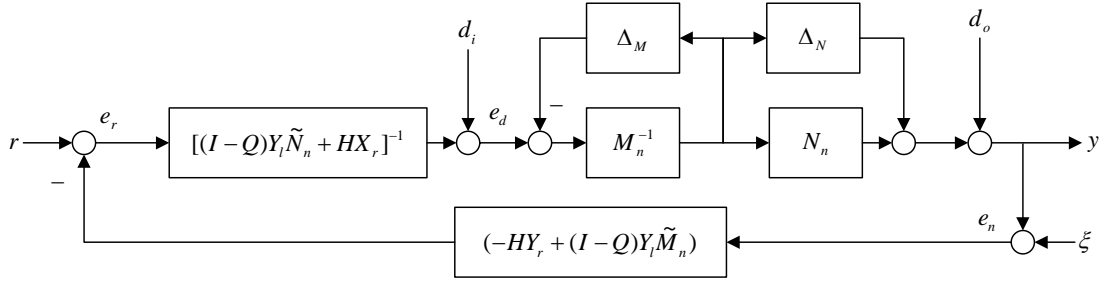


Fig. 4.6 The modification of DCFDOB-VS

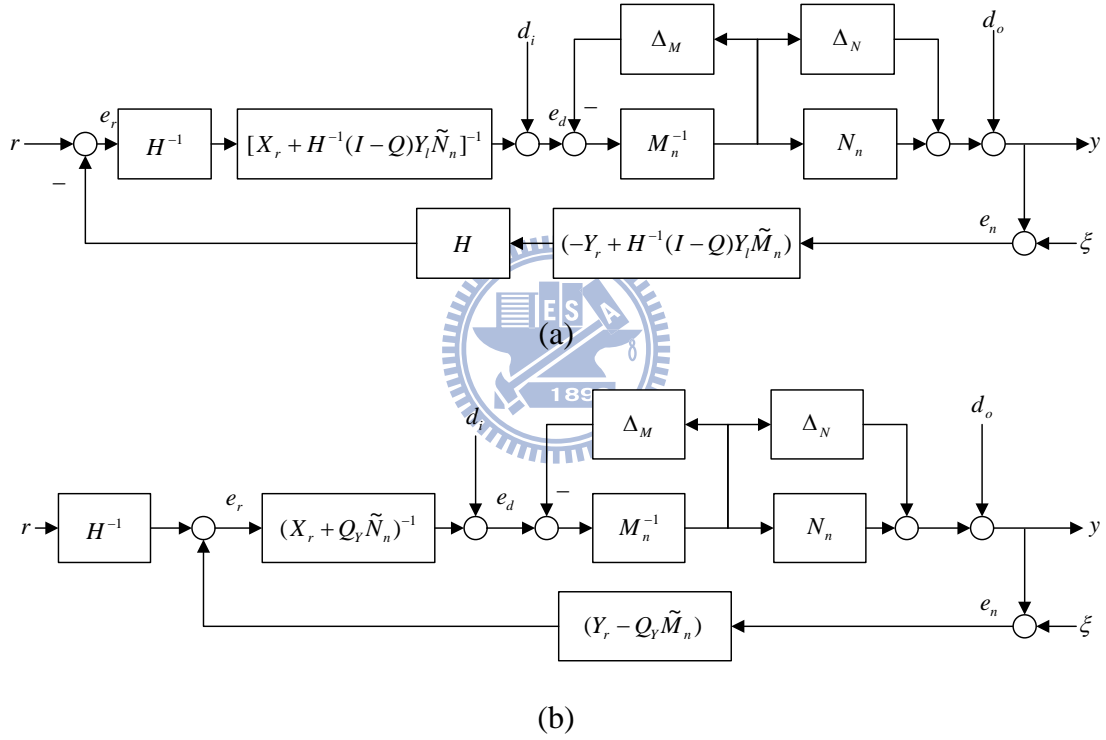


Fig. 4.7 (a) The modification of DCFDOB-VS

(b) the equivalent block diagram of Fig. 4.7 (a) with two independent parameters,

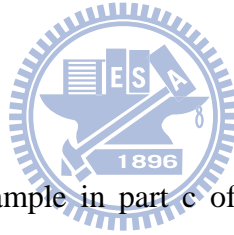
$$H(s) \text{ and } Q_Y(s)$$

According to Fig. 4.7(b), we knew that the DCFDOB-VS can be modified as the well-known Youla-Kucera controller structure with a pre-filter  $H^{-1}(s)$  when

$Q_Y(s) = H^{-1}(I - Q)Y_l$ . Moreover, Fig. 4.7(b) can explain more clearly why the loop properties, e.g.  $\|M_\Delta(s)\|_\infty$ , is only influenced by the independent parameter  $Q_Y(s)$ .

These modifications from DCFDOB-VS to Fig. 4.7(b) can further validate the following properties that we stated and provided in the forgoing sections.

1. Vidyasagar's structure has the subset stabilizing solutions of the Youla-Kucera parameterization and provides the tracking properties [33].
2. The last two columns of Eq. (2.46), i.e. the loop properties of Youla-Kucera parameterization structure are the same as those of Eq. (2.48) when  $Q_{YK}(s) = Q_Y(s)$ .



Recalling the numerical example in part c of paragraph 2.4.2.2, we gave three different bandwidth low-pass filters and three different  $\alpha(s)$ s, i.e. three different  $H(s)$  parameters to observe  $\|M_\Delta\|_\infty$  behaviors. Table 4.1 shows the results for nine cases, which indicate the robust stability is only influenced by the low-pass filter  $J(s)$ , i.e. the independent parameter  $Q_Y(s)$ .

Table 4.1 Plots of  $|M_{\Delta}(j\omega)|$  with different bandwidth of  $J(s)$ ,  $\alpha(s)$  and corresponding  $\|M_{\Delta}\|_{\infty}$

$J(s)$ \ $\alpha(s)$	$\begin{bmatrix} \frac{1}{s^2 + 1.414s + 1} & 0 \\ 0 & \frac{1}{s^2 + 1.414s + 1} \end{bmatrix}$	$\begin{bmatrix} \frac{100}{s^2 + 14.14s + 100} & 0 \\ 0 & \frac{100}{s^2 + 14.14s + 100} \end{bmatrix}$	$\begin{bmatrix} \frac{10000}{s^2 + 141.4s + 10000} & 0 \\ 0 & \frac{10000}{s^2 + 141.4s + 10000} \end{bmatrix}$
$\begin{bmatrix} s+1 & 0 \\ 0 & s+1 \end{bmatrix}$			
$\begin{bmatrix} 0.1s+1 & 0 \\ 0 & 0.1s+1 \end{bmatrix}$			
$\begin{bmatrix} 0.01s+1 & 0 \\ 0 & 0.01s+1 \end{bmatrix}$			

Table 4.1 shows that  $\alpha(s)$ , i.e.  $H(s)$  will not influence the robust stability.

### 4.3 Robust DCFDOB

One discussed the robust stability of DCFDOB and DCFDOB-VS in sections 4.1 and 4.2. The maximum allowable bound of plant uncertainties  $\varepsilon$  can be obtained by designing an adequate  $Q(s)$  and system robustness can be guaranteed when the small gain theorem is satisfied. In this section, one will discuss the design method of robust DCFDOB in  $H_\infty$  frameworks. Consider again Eq. (4.3a), one rearranges the inequality as follows.

$$\left\| \left[ M_n^{-1}(I - Q(I - M_n X_r))[(I - Q(I - M_n X_r))^{-1} Q M_n Y_r \quad \vdots \quad I] \right] \right\|_\infty < \varepsilon^{-1} \quad (4.15)$$

$$\Leftrightarrow \left\| M_n^{-1} S_i [K_{DOB} \quad \vdots \quad I] \right\|_\infty < \varepsilon^{-1} \quad (4.16)$$

where  $S_i = (I - Q(I - M_n X_r)) = (I - Q Y_l \tilde{N}_n)$  and

$$\begin{aligned} K_{DOB} &= (I - Q(I - M_n X_r))^{-1} \cdot Q M_n Y_r \\ &= (I - Q Y_l \tilde{N}_n)^{-1} Q M_n Y_r \\ &= S_i^{-1} \cdot Q M_n Y_r \end{aligned} \quad (4.17)$$

Moreover

$$\begin{aligned} &(I + K_{DOB} \cdot P_n)^{-1} \\ &= (I + S_i^{-1} Q M_n Y_r N_n M_n^{-1})^{-1} \\ &= (I + S_i^{-1} Q M_n (I - X_r M_n) M_n^{-1})^{-1} \\ &= (I + S_i^{-1} Q (I - M_n X_r))^{-1} \\ &= (I + S_i^{-1} Q Y_l \tilde{N}_n)^{-1} \\ &= (I + S_i^{-1} (I - S_i))^{-1} \\ &= (S_i^{-1})^{-1} \\ &= S_i \end{aligned} \quad (4.18)$$

According Eqs. (4.17) and (4.18), one rewrote Eq. (4.16) as Eq. (4.19) and rearranged DCFDOB in form of an output feedback type in Fig. 4.8.

$$\left\| M_n^{-1} (I + K_{DOB} P_n)^{-1} [K_{DOB} \quad I] \right\|_{\infty} < \varepsilon^{-1} \quad (4.19)$$

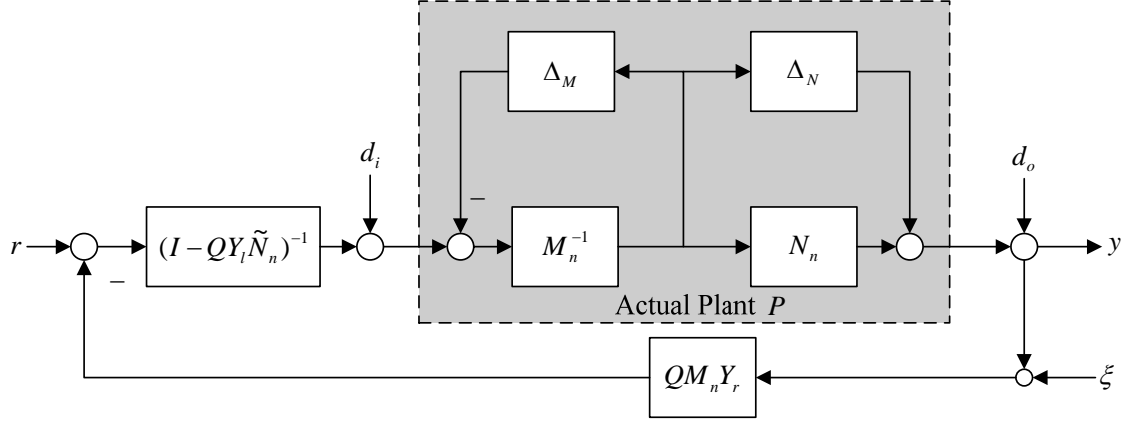


Fig. 4.8 Right coprime factor perturbed system with reduced DCFDOB



**Theorem 4.1**[36, chapter 8]: Consider a right coprime factor perturbed plant described in Fig. 4.8 and  $P = (N_n + \Delta_N) \cdot (M_n + \Delta_M)^{-1}$  with  $N_n$ ,  $M_n$ ,  $\Delta_N$  and  $\Delta_M \in RH_{\infty}$ .

Assume the output feedback controller  $K_{DOB}$  internally stabilizes the nominal system  $P_n$ , then the closed-loop system is well-posed and internally stable for all  $\|\Delta\|_{\infty} \leq \varepsilon$  if and only if

$$\left\| M_n^{-1} (I + K_{DOB} P_n)^{-1} [K_{DOB} \quad I] \right\|_{\infty} < \varepsilon^{-1} \quad (4.20) \square$$

A design objective is to find a reduced DCFDOB  $K_{DOB}(s)$  which satisfied Eq. (4.20) for a given  $\varepsilon$ . Suppose the stable nominal plant  $P_n$  has the minimal realization  $(A, B, C, D)$ . A state-space construction for the normalized right coprime factorization can be obtained in terms of solution to the generalized control (respectively,

filter) algebraic Riccati equation as follows, i.e. Generalized Control Algebraic Riccati

Equation (GCARE):

$$(A - BR_\infty^{-1}D^*C)^* X_\infty + X_\infty(A - BR_\infty^{-1}D^*C) - X_\infty BR_\infty^{-1}B^* X_\infty + C^* \tilde{R}_\infty^{-1}C = 0 \quad (4.21)$$

and Generalized Filter Algebraic Riccati Equation (GFARE):

$$(A - BR_\infty^{-1}D^*C)Y_\infty + Y_\infty(A - BR_\infty^{-1}D^*C)^* - Y_\infty C^* \tilde{R}_\infty^{-1}CY_\infty + BR_\infty^{-1}B^* = 0 \quad (4.22)$$

where  $\tilde{R}_\infty = I + DD^*$  and  $R_\infty = I + D^*D$ . Then, the normalized RCF is given as

$$\begin{bmatrix} M_n \\ N_n \end{bmatrix} := \left[ \begin{array}{c|c} A + BF & BR_\infty^{-1/2} \\ \hline F & R_\infty^{-1/2} \\ C + DF & DR_\infty^{-1/2} \end{array} \right] \in RH_\infty \quad (4.23)$$

where  $F = -R_\infty^{-1}(B^*X_\infty + D^*C)$ . The normalized RCF of  $P_n$  means

$$M_n^T(-j\omega)M_n(j\omega) + N_n^T(-j\omega)N_n(j\omega) = I \quad \text{for all } \omega. \quad (4.24)$$

Moreover, [41] showed that the solution satisfying Eq. (4.20) is obtained as follows:

$$K_{DOB} = \left[ \begin{array}{c|c} A + BF + \gamma^2(W_\infty^*)^{-1}Y_\infty C^*(C + DF) & -\gamma^2(W_\infty^*)^{-1}Y_\infty C^* \\ \hline B^*X_\infty & D^* \end{array} \right] \quad (4.25)$$

where  $W_\infty = I + (X_\infty Y_\infty - \gamma^2 I)$ ,  $F = -R_\infty^{-1}(D^*C + B^*X_\infty)$  and  $\gamma = \varepsilon^{-1}$ . Also, a

maximum value of  $\varepsilon$  can be obtained by a non-iterative method, and is given by

$$\varepsilon_{\max} = (1 - \left\| \begin{bmatrix} N_n \\ M_n \end{bmatrix} \right\|_H^2)^{1/2} = \gamma_{\min}^{-1} \quad (4.26)$$

where  $\|\bullet\|_H$  denotes the Hankel norm, and  $\varepsilon_{\max}$  is called the maximum stability margin.

That is, the stability of the closed-loop can be guaranteed for all

$$\left\| \begin{bmatrix} \Delta_N \\ \Delta_M \end{bmatrix} \right\|_\infty < \varepsilon_{\max} \quad (4.27)$$

The parameter  $Q(s)$  of robust DCFDOB can be obtained.

$$K_{DOB}(s) = (I - QY_l\tilde{N}_n)^{-1} \cdot QM_nY_r \quad (4.28)$$

$$Q(s) = K_{DOB} \cdot (Y_l(\tilde{M}_n + \tilde{N}_nK_{DOB}))^{-1} \quad (4.29)$$

In the above section, one discussed the design method of robust DCFDOB that satisfied (4.15) in  $H_\infty$  frameworks. In the following section, one will introduce the loop - shaping methods to obtain performance / robust stability tradeoffs, and a particular  $H_\infty$  optimization problem to guarantee closed - loop stability and a level of robust stability at all frequencies.

#### 4.4 Robust DCFDOB using $H_\infty$ - loop shaping design

This section considers the  $H_\infty$  - loop shaping design which is developed by McFarlane and Glover [42] to obtain the robust DCFDOB. The objective of the  $H_\infty$  - loop shaping is to incorporate simple performance / robustness tradeoff obtained in the loop - shaping with the guaranteed stability properties of  $H_\infty$  design methods. The  $H_\infty$  - loop shaping is an open - loop shaping approach, which follows the elementary open - loop shaping principles specifying the closed - loop objectives in terms of requirements on the open - loop singular values, denoted  $\sigma(\bullet)$ .  $\bar{\sigma}(\bullet)$  and  $\underline{\sigma}(\bullet)$  denote the maximum and minimum singular values, respectively. To complete a robust DCFDOB, we have to consider the following objectives:

1) Input sensitivity: Recall from Eq. (4.18) that minimizing  $\bar{\sigma}((I + K_{DOB} \cdot P_n)^{-1})$  minimizes the effect of input disturbance on the plant input. The following inequality relates this objective to an open - loop singular value condition:

$$\begin{aligned}\bar{\sigma}((I + K_{DOB} \cdot P_n)^{-1}) &= \frac{1}{\underline{\sigma}(I + K_{DOB} \cdot P_n)} \\ &\leq \frac{1}{\underline{\sigma}(K_{DOB} P_n) - 1} \\ &\approx \frac{1}{\underline{\sigma}(K_{DOB} P_n)} \text{ for frequencies: } \underline{\sigma}(K_{DOB} P_n) \gg 1\end{aligned}\tag{4.30}$$

2) Similar, the inequality of output sensitivity:

$$\begin{aligned}\bar{\sigma}((I + P_n \cdot K_{DOB})^{-1}) &= \frac{1}{\underline{\sigma}(I + P_n \cdot K_{DOB})} \\ &\leq \frac{1}{\underline{\sigma}(P_n K_{DOB}) - 1} \\ &\approx \frac{1}{\underline{\sigma}(P_n K_{DOB})} \text{ for frequencies: } \underline{\sigma}(P_n K_{DOB}) \gg 1\end{aligned}\tag{4.31}$$

3) Robustness of coprime uncertainty on the nominal plant can be obtained by minimizing both  $\bar{\sigma}(K_{DOB}(I + P_n K_{DOB})^{-1} P_n)$  and  $\bar{\sigma}(P_n(I + K_{DOB} P_n)^{-1} K_{DOB})$ . One also has that:

$$\begin{aligned}\bar{\sigma}(K_{DOB}(I + P_n K_{DOB})^{-1} P_n) &= \bar{\sigma}(((K_{DOB} P_n)^{-1} + I)^{-1}) \\ &\leq \frac{1}{\underline{\sigma}((K_{DOB} P_n)^{-1}) + 1} \\ &\approx \frac{1}{\underline{\sigma}((K_{DOB} P_n)^{-1})} \text{ for frequencies: } \bar{\sigma}(K_{DOB} P_n) \ll 1\end{aligned}\tag{4.32}$$

Similar, one has  $\bar{\sigma}(P_n K_{DOB}) \ll 1$ .



In each of cases 1) - 3), one has approximated a closed - loop objective by a condition on the singular values of  $P_n$  and  $K_{DOB}$  over a particular frequency range.

1) and 2) are rejection performance objectives, while 3) is robust stability objective.

Good rejection performance requires that

$$\underline{\sigma}(P_n K_{DOB}) \gg 1, \underline{\sigma}(K_{DOB} P_n) \gg 1, \underline{\sigma}(K_{DOB}) \gg 1 \quad (4.33)$$

in a low frequency range  $[0, \omega_l]$ .

Good robustness requires that

$$\overline{\sigma}(P_n K_{DOB}) \ll 1, \overline{\sigma}(K_{DOB} P_n) \ll 1, \overline{\sigma}(K_{DOB}) \leq \delta \quad (4.34)$$

in a high frequency range  $[\omega_u, \infty]$  where  $\delta$  is not too large. Figure 4.9 indicates

graphically how the requirements on these closed - loop objective constrain the shape of the open - loop singular values in design.

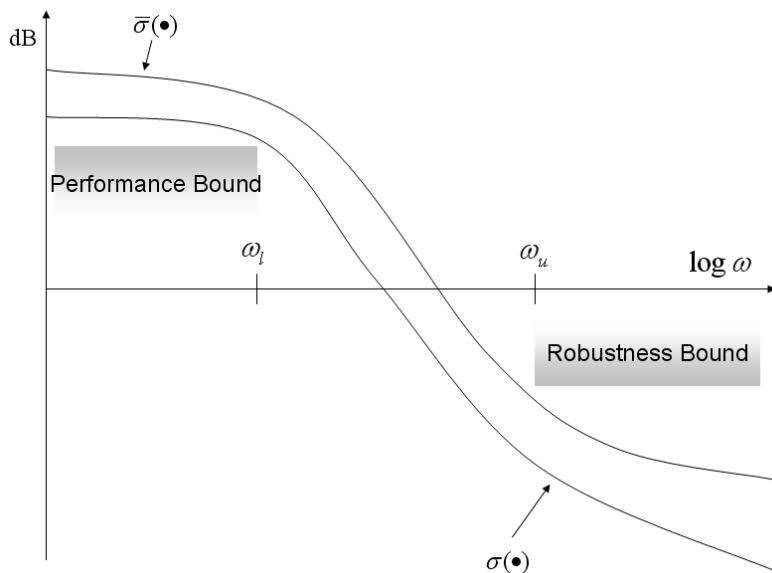


Fig. 4.9 Open - loop singular value shaping

#### 4.4.1 The $H_\infty$ - loop shaping design procedure of the robust DCFDOB

The  $H_\infty$  - loop shaping design procedure which we utilize to develop the robust DCFDOB is developed by McFarlane and Glover [41] and is stated next.

(1) The  $H_\infty$  - loop shaping uses a pre-weighting matrix  $W_1$  and/or a post-weighting matrix  $W_2$  to shape the singular values of the nominal plant  $P_n$  as a desired open-loop shape  $P_S = W_2 P_n W_1$  and its normalized right coprime factor  $P_S = N_S M_S^{-1}$ .  $W_1$  and  $W_2$  are selected such that  $P_S$  contains no hidden modes.

(2) Robust Stability:

a) Calculate  $\varepsilon_{S,\max}$ , where

$$\begin{aligned} \varepsilon_{S,\max} &= \left( \inf_{K_\infty \in RH_\infty} \left\| M_S^{-1} (I + K_\infty P_S)^{-1} \begin{bmatrix} K_\infty & I \end{bmatrix} \right\|_\infty \right)^{-1} \\ &= \left( 1 - \left\| \begin{bmatrix} N_S \\ M_S \end{bmatrix} \right\|_H^2 \right)^{1/2} < 1 \end{aligned} \quad (4.35)$$

If  $\varepsilon_{S,\max} \ll 1$  return to step (1) and adjust  $W_1$  and  $W_2$ .

b) Select  $\varepsilon_S \leq \varepsilon_{S,\max}$ ; then synthesize the solution  $K_\infty$  that satisfies

$$\left\| M_S^{-1} (I + K_\infty P_S)^{-1} \begin{bmatrix} K_\infty & I \end{bmatrix} \right\|_\infty \leq \varepsilon_S^{-1} = \gamma_S \quad (4.36)$$

(3) The final reduced DCFDOB  $K_{DOB}$  is constructed by combining the solution  $K_\infty$  with the shaping functions  $W_1$  and  $W_2$ .

$$K_{DOB} = W_1 K_\infty W_2 \quad (4.37)$$

(4) The final parameter  $Q(s)$  can be obtained according to Eqs. (4.28), (4.29) and (4.37).

$$\begin{aligned}
K_{DOB} &= W_1 K_\infty W_2 \\
\Leftrightarrow (I - Q Y_l \tilde{N}_n)^{-1} \cdot Q M_n Y_r &= W_1 K_\infty W_2 \\
\Leftrightarrow Q(s) &= W_1 K_\infty W_2 (M_n Y_r + Y_l \tilde{N}_n W_1 K_\infty W_2)^{-1}
\end{aligned} \tag{4.38}$$

After introducing the solving steps of  $K_{DOB}(s)$ , i.e.  $Q(s)$  that satisfies Eq. (4.36) and forms the robust DCFDOB, we will explain how all the closed-loop objectives of Eqs. (4.33) and (4.34) are incorporated. Note that Eq. (4.36) is not only the criterion for robustness but implicitly considers minimizing the  $H_\infty$  norm of the transfer functions from  $[\tilde{d}_o \ \tilde{d}_i]^T$  to  $[\tilde{y}_2 \ \tilde{y}_1]^T$  in Figure 4.10(a) as follows.

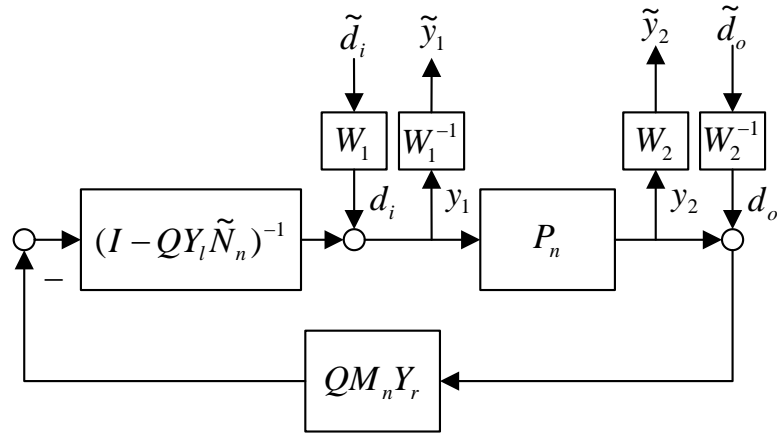
$$\begin{aligned}
\|M_S^{-1}(I + K_\infty P_S)^{-1}[K_\infty \ I]\|_\infty &= \left\| \begin{bmatrix} P_S \\ I \end{bmatrix} (I + K_\infty P_S)^{-1} [K_\infty \ I] \right\|_\infty \\
&= \left\| \begin{bmatrix} W_2 P_n \\ W_1^{-1} \end{bmatrix} (I + K_{DOB} P_n)^{-1} [K_{DOB} W_2^{-1} \ W_1] \right\|_\infty
\end{aligned} \tag{4.39}$$

where the inner function  $\begin{bmatrix} N_S \\ M_S \end{bmatrix}$  is pre-multiplied to go to the four-block problem.

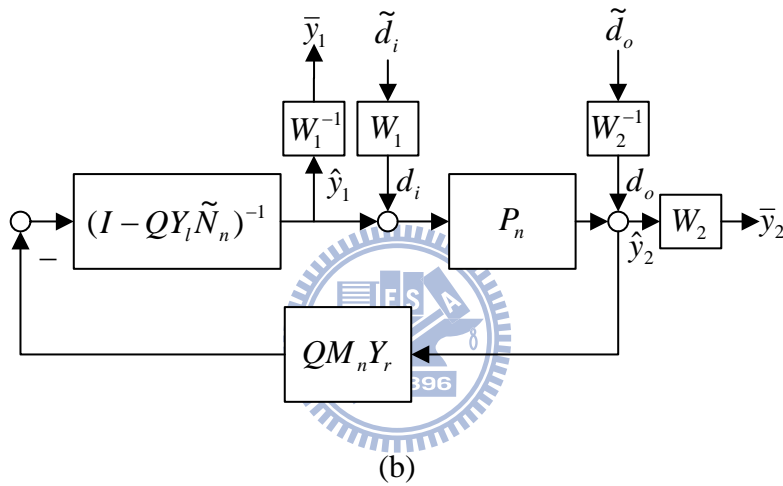
The corollary 16.7 of [36] shows the Eq. (4.39) also equals Eq. (4.40) by interchanging  $K_\infty$  and  $P_S$ .

$$\begin{aligned}
\left\| \begin{bmatrix} P_S \\ I \end{bmatrix} (I + K_\infty P_S)^{-1} [K_\infty \ I] \right\|_\infty &= \left\| \begin{bmatrix} K_\infty \\ I \end{bmatrix} (I + P_S K_\infty)^{-1} [P_S \ I] \right\|_\infty \\
&= \left\| \begin{bmatrix} W_1^{-1} K_{DOB} \\ W_2 \end{bmatrix} (I + P_n K_{DOB})^{-1} [P_n W_1 \ W_2^{-1}] \right\|_\infty
\end{aligned} \tag{4.40}$$

Equation (4.40) presents the transfer functions from  $[\tilde{d}_i \ \tilde{d}_o]^T$  to  $[\bar{y}_1 \ \bar{y}_2]^T$  in Figure 4.10(b)



(a)



(b)

Fig. 4.10 Two cases of the transfer functions from  $(\tilde{d}_i \ \tilde{d}_o)$  to

$$(\tilde{y}_1 \ \tilde{y}_2) \text{ and } (\bar{y}_1 \ \bar{y}_2)$$

Equations (4.39) and (4.40) show how all the closed-loop objectives of Eqs. (4.33) and (4.34) are incorporated.

#### 4.4.2 On the achieved loop shape

As described above, the desired loop shaped was specified as  $W_2 P_n W_1$ , but the finally achieving loop shape is in fact given by  $W_1 K_\infty W_2 P_n$  at plant input and  $P_n W_1 K_\infty W_2$  at plant output. Figure 4.11 illustrates the discrepancies that may occur

between specified and achieved loop shapes. It can be seen in Figure 4.11 that, at low frequency (in particular  $\omega \in (0, \omega_l)$ ), the deterioration in loop shape at plant output can be obtained by comparing  $\underline{\sigma}(P_n W_1 K_\infty W_2)$  with  $\underline{\sigma}(W_2 P_n W_1)$ .

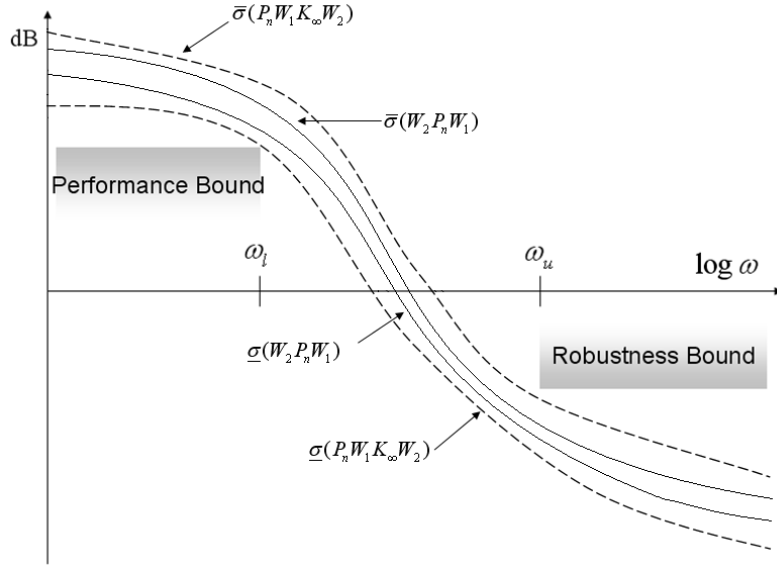


Fig. 4.11 Specified and achieved loop shapes

Note that:

$$\begin{cases} \underline{\sigma}(P_n K_{DOB}) = \underline{\sigma}(P_n W_1 K_\infty W_2) \geq \underline{\sigma}(W_2 P_n W_1) \underline{\sigma}(K_\infty) / \kappa(W_2) \\ \overline{\sigma}(P_n K_{DOB}) = \overline{\sigma}(P_n W_1 K_\infty W_2) \leq \overline{\sigma}(W_2 P_n W_1) \overline{\sigma}(K_\infty) / \kappa(W_2) \end{cases} \quad (4.41)$$

where  $\kappa(\bullet) = \overline{\sigma}(\bullet) / \underline{\sigma}(\bullet)$  denotes the condition number. Similarly, for loop shape deterioration at plant input, one compares  $\underline{\sigma}(W_1 K_\infty W_2 P_n)$  with  $\underline{\sigma}(W_2 P_n W_1)$  and we have

$$\begin{cases} \underline{\sigma}(K_{DOB} P_n) = \underline{\sigma}(W_1 K_\infty W_2 P_n) \geq \underline{\sigma}(W_2 P_n W_1) \underline{\sigma}(K_\infty) / \kappa(W_1) \\ \overline{\sigma}(K_{DOB} P_n) = \overline{\sigma}(W_1 K_\infty W_2 P_n) \leq \overline{\sigma}(W_2 P_n W_1) \overline{\sigma}(K_\infty) / \kappa(W_1) \end{cases} \quad (4.42)$$

Equations (4.41) and (4.42) present that  $\underline{\sigma}(K_\infty) / \overline{\sigma}(K_\infty)$  require a bound on the deterioration of the loop shapes at low / high frequencies. Note that the condition

numbers  $\kappa(W_1)$  and  $\kappa(W_2)$  are selected by the designer. Moreover, theorems 4.2 and 4.3 show that  $\underline{\sigma}(K_\infty) / \bar{\sigma}(K_\infty)$  is bounded by function of  $\gamma_s$  and  $\underline{\sigma}(P_s) / \bar{\sigma}(P_s)$ . Hence by Eqs. (4.41) and (4.42),  $K_\infty$  will only have a limited effect on the specified loop shape at low-frequency.

**Theorem 4.2** [36]:

Any  $K_\infty$  satisfying Eq. (4.36), where  $P_s$  is assumed square, also satisfies

$$\underline{\sigma}(K_\infty(j\omega)) \geq \frac{\underline{\sigma}(P_s(j\omega)) - \sqrt{\gamma_s^2 - 1}}{\sqrt{\gamma_s^2 - 1} \underline{\sigma}(P_s(j\omega)) + 1} \quad (4.43)$$

for all  $\omega$  such that  $\underline{\sigma}(P_s(j\omega)) > \sqrt{\gamma_s^2 - 1}$ . Furthermore, if  $\underline{\sigma}(P_s) \gg \sqrt{\gamma_s^2 - 1}$ , then

$\underline{\sigma}(K_\infty(j\omega)) \approx \frac{1}{\sqrt{\gamma_s^2 - 1}}$ , where  $\approx$  denotes asymptotically greater than or equal to as

$\underline{\sigma}(P_s) \rightarrow \infty$ . □

**Theorem 4.3** [36]:

Any  $K_\infty$  satisfying Eq. (4.36), where  $P_s$  is assumed square, also satisfies

$$\bar{\sigma}(K_\infty(j\omega)) \leq \frac{\sqrt{\gamma_s^2 - 1} + \bar{\sigma}(P_s(j\omega))}{1 - \sqrt{\gamma_s^2 - 1} \bar{\sigma}(P_s(j\omega))} \quad (4.44)$$

for all  $\omega$  such that  $\bar{\sigma}(P_s(j\omega)) < \frac{1}{\sqrt{\gamma_s^2 - 1}}$ . Furthermore, if  $\bar{\sigma}(P_s) \ll \frac{1}{\sqrt{\gamma_s^2 - 1}}$ , then

$\bar{\sigma}(K_\infty(j\omega)) \approx \sqrt{\gamma_s^2 - 1}$ , where  $\approx$  denotes asymptotically less than or equal to as

$\bar{\sigma}(P_s) \rightarrow 0$ . □

#### 4.4.3 Bounds of the robust DCFDOB

In this paragraph, we discuss each bounded magnitudes of the robust DCFDOB via  $H_\infty$  - loop shaping design procedure. Let  $P_n$  be the nominal plant and let  $K_{DOB} = W_1 K_\infty W_2$  be the associated reduced DCFDOB obtained from the loop shaping design procedure. Then if  $\|M_S^{-1}(I + K_\infty P_S)^{-1}[K_\infty \quad I]\|_\infty \leq \gamma_S$  one has

$$\bar{\sigma}(S_i) \leq \min\{\gamma_S \kappa(W_1), \gamma_S \bar{\sigma}(M_S) \kappa(W_1)\} \quad (4.45)$$

where  $\bar{\sigma}(S_i)$  notes the gain from input disturbance  $d_i$  to plant input  $y_1$  of Figure 4.10(a),  $\kappa(\bullet) = \bar{\sigma}(\bullet)/\underline{\sigma}(\bullet)$  denotes the condition number and

$$\bar{\sigma}(M_S) = \bar{\sigma}(\tilde{M}_S) = \left( \frac{1}{1 + \underline{\sigma}^2(W_2 P_n W_1)} \right)^{1/2}. \quad \text{One also has}$$

$$\bar{\sigma}(P_n S_i) \leq \min\left\{ \frac{\gamma_S \bar{\sigma}(N_S)}{\underline{\sigma}(W_1) \underline{\sigma}(W_2)}, \frac{\gamma_S \bar{\sigma}(N_S)}{\underline{\sigma}(W_1) \underline{\sigma}(W_2)} \right\} \quad (4.46)$$

where  $\bar{\sigma}(P_n S_i)$  denotes the gain from input disturbance  $d_i$  to plant output  $y_2$  of

Figure 4.10(a) and  $\bar{\sigma}(N_S) = \bar{\sigma}(\tilde{N}_S) = \left( \frac{\bar{\sigma}^2(W_2 P_n W_1)}{1 + \bar{\sigma}^2(W_2 P_n W_1)} \right)^{1/2}$ . Furthermore, one has

$$\bar{\sigma}(S_i K_{DOB}) \leq \min\{\gamma_S \bar{\sigma}(W_1) \bar{\sigma}(W_2), \gamma_S \bar{\sigma}(M_S) \bar{\sigma}(W_1) \bar{\sigma}(W_2)\} \quad (4.47)$$

where  $\bar{\sigma}(S_i K_{DOB})$  denotes the gain from output disturbance  $d_o$  to plant input  $y_1$  of

Figure 4.10(a).

$$\bar{\sigma}(P_n S_i K_{DOB}) \leq \min\{\gamma_S \kappa(W_2), \gamma_S \bar{\sigma}(N_S) \kappa(W_2)\} \quad (4.48)$$

where  $\bar{\sigma}(P_n S_i K_{DOB})$  denotes the gain from output disturbance  $d_o$  to plant output  $y_2$  of Figure 4.10(a).

Moreover, we also can obtain Eqs. (4.49)-(4.52).

$$\bar{\sigma}(K_{DOB}S_oP_n) \leq \min\{\gamma_s \kappa(W_1), \gamma_s \bar{\sigma}(\tilde{N}_s) \kappa(W_1)\} \quad (4.49)$$

$$\bar{\sigma}(K_{DOB}S_o) \leq \min\{\gamma_s \bar{\sigma}(W_1) \bar{\sigma}(W_2), \gamma_s \bar{\sigma}(\tilde{M}_s) \bar{\sigma}(W_1) \bar{\sigma}(W_2)\} \quad (4.50)$$

$$\bar{\sigma}(S_oP_n) \leq \min\left\{\frac{\gamma_s}{\underline{\sigma}(W_1)\underline{\sigma}(W_2)}, \frac{\gamma_s \bar{\sigma}(\tilde{N}_s)}{\underline{\sigma}(W_1)\underline{\sigma}(W_2)}\right\} \quad (4.51)$$

$$\bar{\sigma}(S_o) \leq \min\{\gamma_s \kappa(W_2), \gamma_s \bar{\sigma}(\tilde{M}_s) \kappa(W_2)\} \quad (4.52)$$

where  $\bar{\sigma}(K_{DOB}S_oP_n)$ ,  $\bar{\sigma}(K_{DOB}S_o)$ ,  $\bar{\sigma}(S_oP_n)$  and  $\bar{\sigma}(S_o)$  denotes the gain from input disturbance  $d_i$  to DCFDOB output  $\hat{y}_1$ , output disturbance  $d_o$  to DCFDOB output  $\hat{y}_1$ , input disturbance  $d_i$  to system output  $\hat{y}_2$  and output disturbance  $d_o$  to system output  $\hat{y}_2$  of Figure 4.10(b), respectively.

These following derivations present how these boundaries in Eqs. (4.45)-(4.52) be obtained. Firstly, note that

$$\|M_s^{-1}(I + K_\infty P_s)^{-1}[K_\infty \quad I]\|_\infty \leq \gamma_s \quad (4.53)$$

If Eq. (4.53) is pre-multiplied by normalized coprime factorization  $\begin{bmatrix} N_s \\ M_s \end{bmatrix}$ . Since

$\left\| \begin{bmatrix} N_s \\ M_s \end{bmatrix} \right\|_\infty = 1$ , one can obtained Eq. (4.54).



$$\begin{aligned}
& \left\| M_S^{-1}(I + K_\infty P_S)^{-1} \begin{bmatrix} K_\infty & I \end{bmatrix} \right\|_\infty \leq \gamma_S \\
\Leftrightarrow & \left\| \begin{bmatrix} N_S \\ M_S \end{bmatrix} \cdot M_S^{-1}(I + K_\infty P_S)^{-1} \begin{bmatrix} K_\infty & I \end{bmatrix} \right\|_\infty \leq \gamma_S \\
\Leftrightarrow & \left\| \begin{bmatrix} P_S \\ I \end{bmatrix} (I + K_\infty P_S)^{-1} \begin{bmatrix} K_\infty & I \end{bmatrix} \right\|_\infty \leq \gamma_S \tag{4.54} \\
\Leftrightarrow & \left\| \begin{bmatrix} W_2 P_n \\ W_1^{-1} \end{bmatrix} (I + K_{DOB} P_n)^{-1} \begin{bmatrix} K_{DOB} W_2^{-1} & W_1 \end{bmatrix} \right\|_\infty \leq \gamma_S \\
\Leftrightarrow & \left\| \begin{bmatrix} W_2 P_n \\ W_1^{-1} \end{bmatrix} \cdot S_i \cdot \begin{bmatrix} K_{DOB} W_2^{-1} & W_1 \end{bmatrix} \right\|_\infty \leq \gamma_S
\end{aligned}$$

Noting that  $\bar{\sigma}(\bullet) \leq \|\bullet\|_\infty$  for all frequencies, one can obtain Eqs (4.45)-(4.48) because

by Eq. (4.54), one has

$$\begin{aligned}
\bar{\sigma}(W_2 P_n S_i K_{DOB} W_2^{-1}) & \leq \gamma_S \\
\Rightarrow \bar{\sigma}(P_n S_i K_{DOB}) & \leq \gamma_S \kappa(W_2) \tag{4.55}
\end{aligned}$$

and

$$\begin{aligned}
\bar{\sigma}(W_1^{-1} S_i W_1) & \leq \gamma_S \\
\Rightarrow \bar{\sigma}(S_i) & \leq \gamma_S \kappa(W_1) \tag{4.56}
\end{aligned}$$

Next recall that

$$\begin{aligned}
\left\| \begin{bmatrix} P_S \\ I \end{bmatrix} (I + K_\infty P_S)^{-1} \begin{bmatrix} K_\infty & I \end{bmatrix} \right\|_\infty & = \left\| \begin{bmatrix} K_\infty \\ I \end{bmatrix} (I + P_S K_\infty)^{-1} \begin{bmatrix} P_S & I \end{bmatrix} \right\|_\infty \leq \gamma_S \\
\Leftrightarrow \left\| \begin{bmatrix} W_1^{-1} K_{DOB} \\ W_2 \end{bmatrix} \cdot S_o \cdot \begin{bmatrix} P_n W_1 & W_2^{-1} \end{bmatrix} \right\|_\infty & \leq \gamma_S \tag{4.57}
\end{aligned}$$

Then by Eq. (4.57), one can obtain Eqs. (4.49)-(4.52). Furthermore, recalling Eq.

(4.57), we have

$$\begin{aligned}
& \left\| M_S^{-1}(I + K_\infty P_S)^{-1} \begin{bmatrix} K_\infty & I \end{bmatrix} \right\|_\infty \leq \gamma_S \\
\Leftrightarrow & \left\| M_S^{-1} W_1^{-1} (I + K_{DOB} P_n)^{-1} \begin{bmatrix} K_{DOB} W_2^{-1} & W_1 \end{bmatrix} \right\|_\infty \leq \gamma_S \tag{4.58}
\end{aligned}$$

and we can immediately show (4.59) and (4.60).

$$\begin{aligned} \bar{\sigma}(M_S^{-1}W_1^{-1}(I + K_{DOB}P_n)^{-1}W_1)) &\leq \gamma_S \\ \Rightarrow \bar{\sigma}(S_i) &\leq \gamma_S \bar{\sigma}(M_S)\kappa(W_1) \end{aligned} \quad (4.59)$$

and

$$\begin{aligned} \bar{\sigma}(M_S^{-1}W_1^{-1}(I + K_{DOB}P_n)^{-1}K_{DOB}W_2^{-1})) &\leq \gamma_S \\ \Rightarrow \bar{\sigma}(S_i K_{DOB}) &\leq \gamma_S \bar{\sigma}(M_S)\bar{\sigma}(W_1)\bar{\sigma}(W_2) \end{aligned} \quad (4.60)$$

Next, recall that  $P_S = W_2 P_n W_1 = N_S M_S^{-1}$ . Then by Eq. (4.53) we have

$$\begin{aligned} \left\| M_S^{-1}(I + K_\infty P_S)^{-1} \begin{bmatrix} K_\infty & I \end{bmatrix} \right\|_\infty &\leq \gamma_S \\ \Leftrightarrow \left\| N_S^{-1}W_2 P_n (I + K_{DOB}P_n)^{-1} \begin{bmatrix} K_{DOB}W_2^{-1} & W_1 \end{bmatrix} \right\|_\infty &\leq \gamma_S \end{aligned} \quad (4.61)$$

and

$$\begin{aligned} \bar{\sigma}(N_S^{-1}W_2 P_n (I + K_{DOB}P_n)^{-1}W_1)) &\leq \gamma_S \\ \Rightarrow \bar{\sigma}(P_n S_i) &\leq \frac{\gamma_S \bar{\sigma}(N_S)}{\underline{\sigma}(W_1)\underline{\sigma}(W_2)} \end{aligned} \quad (4.62)$$

$$\begin{aligned} \bar{\sigma}(N_S^{-1}W_2 P_n (I + K_{DOB}P_n)^{-1}K_{DOB}W_2^{-1})) &\leq \gamma_S \\ \Rightarrow \bar{\sigma}(P_n S_i K_{DOB}) &\leq \gamma_S \bar{\sigma}(N_S)\kappa(W_2) \end{aligned} \quad (4.63)$$

Similarly, one can obtain

$$\bar{\sigma}(S_o) \leq \gamma_S \bar{\sigma}(\tilde{M}_S)\kappa(W_2) \quad (4.64)$$

$$\bar{\sigma}(K_{DOB}S_o) \leq \gamma_S \bar{\sigma}(\tilde{M}_S)\bar{\sigma}(W_1)\bar{\sigma}(W_2) \quad (4.65)$$

$$\bar{\sigma}(S_o P_n) \leq \frac{\gamma_S \bar{\sigma}(\tilde{N}_S)}{\underline{\sigma}(W_1)\underline{\sigma}(W_2)} \quad (4.66)$$

$$\bar{\sigma}(K_{DOB}S_o P_n) \leq \gamma_S \bar{\sigma}(\tilde{N}_S)\kappa(W_1) \quad (4.67)$$

By (3.4), (3.5) and (4.17) one also has

$$\begin{aligned}
& I - P_n \cdot S_i \cdot K_{DOB} \\
&= I - N_n M_n^{-1} \cdot (I - QY_l \tilde{N}_n) \cdot [(I - QY_l \tilde{N}_n)^{-1} QM_n Y_r] \\
&= I - N_n M_n^{-1} QM_n Y_r \\
&= S_o
\end{aligned} \tag{4.68}$$

and

$$\begin{aligned}
\bar{\sigma}(S_o) &= \bar{\sigma}(I - P_n S_i K_{DOB}) \\
&\leq 1 + \gamma_S \kappa(W_2)
\end{aligned} \tag{4.69}$$

Similar, one has

$$\begin{aligned}
& I - K_{DOB} \cdot S_o \cdot P_n \\
&= I - S_i^{-1} QM_n Y_r \cdot (I - N_n M_n^{-1} QM_n Y_r) \cdot N_n M_n^{-1} \\
&= I - S_i^{-1} QM_n Y_r N_n M_n^{-1} \cdot (I - QM_n Y_r N_n M_n^{-1}) \\
&= I - S_i^{-1} Q(I - M_n X_r) \cdot [I - Q(I - M_n X_r)] \\
&= I - S_i^{-1} Q(Y_l \tilde{N}_n) \cdot (I - QY_l \tilde{N}_n) \\
&= I - [(I - QY_l \tilde{N}_n)^{-1} QY_l \tilde{N}_n] \cdot (I - QY_l \tilde{N}_n) \\
&= I - QY_l \tilde{N}_n \cdot (I - QY_l \tilde{N}_n)^{-1} \cdot (I - QY_l \tilde{N}_n) \\
&= I - QY_l \tilde{N}_n \\
&= S_i
\end{aligned} \tag{4.70}$$

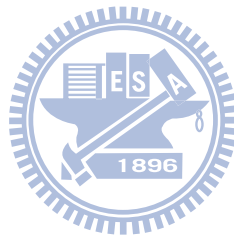
and

$$\begin{aligned}
\bar{\sigma}(S_i) &= \bar{\sigma}(I - K_{DOB} S_o P_n) \\
&\leq 1 + \gamma_S \kappa(W_1)
\end{aligned} \tag{4.71}$$

The shaping functions  $W_1$  and  $W_2$  are selected by the designer, then it can be seen that, by (4.45)-(4.52), all of the closed – loop objectives are guaranteed to have bounded magnitude and the bounds depend only on  $\gamma_S$ ,  $W_1$ ,  $W_2$  and  $P_n$ .

In this paragraph, one has incorporated the normalized DCFDOB into a loop shaping based systematic design technique. This enables both performance and robust stability objective to be traded off, and preserves the exact solution associated with this

particular  $H_\infty$  problem. The following chapter, we will give some numerical examples and one experimental result to demonstrate the design steps and verify the correctness of our derivations of the DCFDOB structure.



## CHAPTER 5

### NUMERICAL EXAMPLES AND EXPERIMENTAL RESULTS

In this chapter, we demonstrate four parts numerical examples and an experimental result to illustrate the design steps for each plant case. In part 1, two examples, SISO and MIMO, of minimum phase systems are given. In part 2, we show the design steps for a SISO, non-minimum phase plant in part 2-example 1, and for MIMO, non-minimum phase plant in part 2-example 2. In part 3, two types of non-square plant, thin and wide systems, are given to express the inherent restriction on input / output disturbances rejections. In part 4, a robust DCFDOB developed by  $H_\infty$ -loop shaping design procedures are presented. Finally, an experimental result of a positioning control for an AC brushless servomotor system and cogging force suppressing is illustrated.

#### 5.1 Numerical example part 1: minimum phase plants

In the first example of part 1, a stable, minimum phase, SISO plant with uncertainty is used and the second example of part 1, a stable, minimum phase, MIMO plant is considered.

**Example 1:** Assume the actual plant  $P(s)$  and the nominal plant  $P_n(s)$  are given as follows.

$$P_n(s) = \frac{40}{15s + 60}, P(s) = \frac{42}{30s + 65} \quad (5.1)$$

The control gain matrix and observer gain matrix are given as  $F = [-55.75]$ ,  $L = [-475.91]$ , the corresponding coprime factors are obtained as:

$$\begin{aligned} M_n &= \frac{s + 4}{s + 60}, N_n = \frac{2.667}{s + 60}, \\ X_r &= \frac{s + 176}{s + 120}, Y_r = \frac{2436}{s + 120} \end{aligned} \quad (5.2)$$

Two low-pass filters,  $J_1(s)$  with  $400 \text{ rad/sec}$  bandwidth and  $J_2(s)$  with  $40 \text{ rad/sec}$  bandwidth, are given and the corresponding parameters  $Q_1(s)$  and  $Q_2(s)$  are obtained in Eq. (5.4) and Eq. (5.6), respectively.

$$J_1(s) = \frac{1.6 \times 10^5}{s^2 + 565.6s + 1.6 \times 10^5} \quad (5.3)$$

$$Q_1(s) = \frac{24.6305(s + 120)(s + 60)}{(s^2 + 565.6s + 1.6 \times 10^5)} \quad (5.4)$$

$$J_2(s) = \frac{1600}{s^2 + 56.56s + 1600} \quad (5.5)$$

$$Q_2(s) = \frac{0.24627(s + 120)(s + 60)}{(s^2 + 56.56s + 1600)} \quad (5.6)$$

Figure 5.1 illustrates frequency response of input sensitivity. From Fig. 5.1, obviously, the rejection capability and rejection bandwidth are directly related to the bandwidth of low-pass filter. However, Fig. 5.2 displays that the bandwidth from measurement noise  $\xi$  to system output  $y$  also increase with an increase in bandwidth of  $J(s)$ . That is, bandwidth of the low-pass filter is a basic criterion to be considered and tradeoff when designs a DOB.

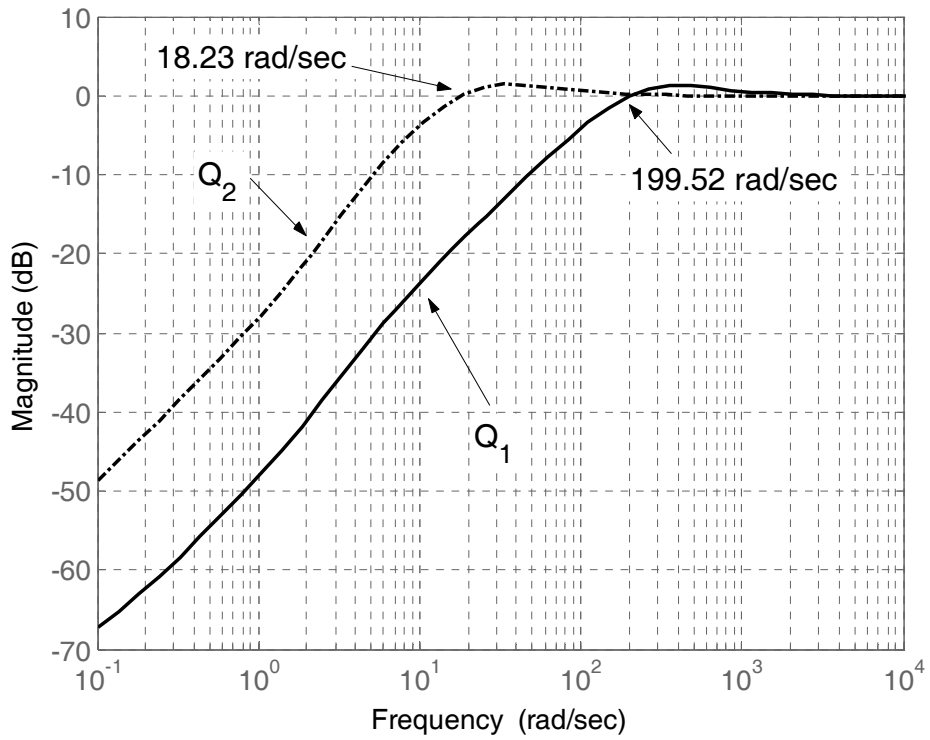


Fig. 5.1 Frequency responses of input sensitivity of part 1 - example 1

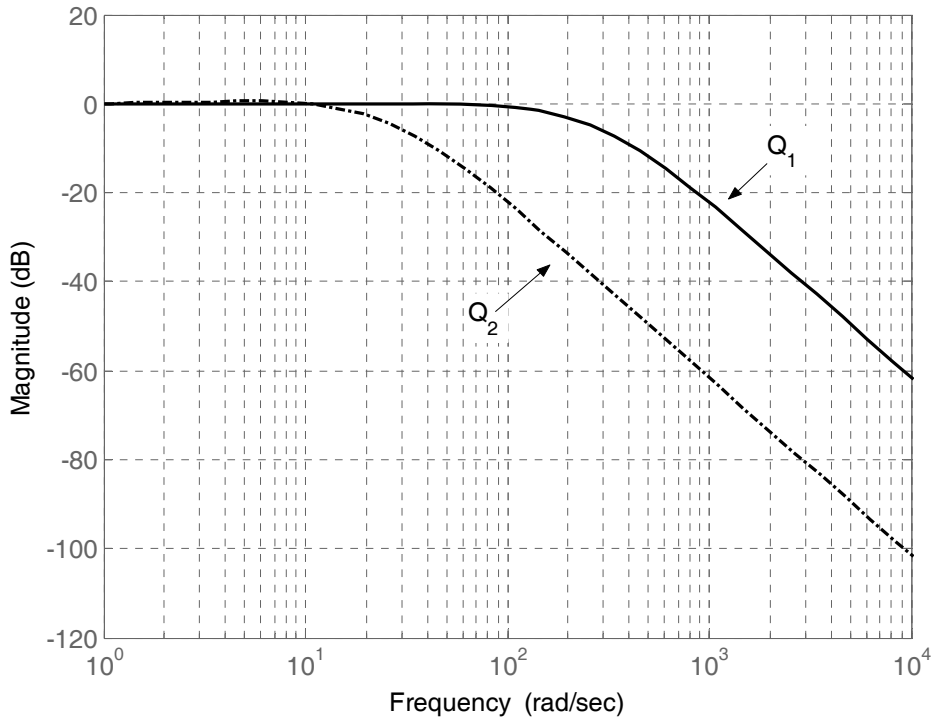


Fig. 5.2 Frequency responses from noise to system output of part 1 – example 1

In time domain simulation, a unit-step input disturbance  $d_i(t) = u(t-5)$  is given,

where  $u(t-\tau)$  denotes a unit-step and  $u(t) = 1, t \geq \tau \text{ sec}$  and  $u(t) = 0, t < \tau \text{ sec}$ .

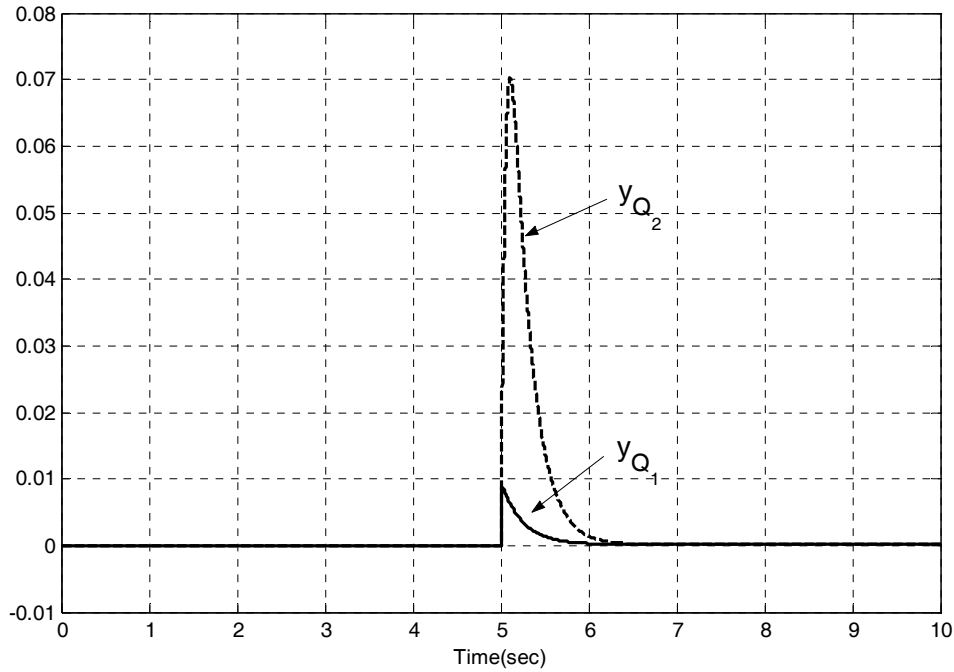


Fig. 5.3 Simulation results of part 1 – example 1

In Fig. 5.3,  $y_{Q_1}$  and  $y_{Q_2}$  denote system outputs of DCFDOB with parameters  $Q_1$  and  $Q_2$ , respectively and this figure demonstrates that when a wide bandwidth

low-pass filter is adopted, the disturbance eliminate rate is faster than a narrow one. In

the following, we consider both input and output disturbances and a unit-step  $u(t-7)$

is given as an output disturbance, where  $u(t) = 1, t \geq 7 \text{ sec}$  and  $u(t) = 0, t < 7 \text{ sec}$ .

The simulation results are shown in Fig. 5.4(a)-(c).



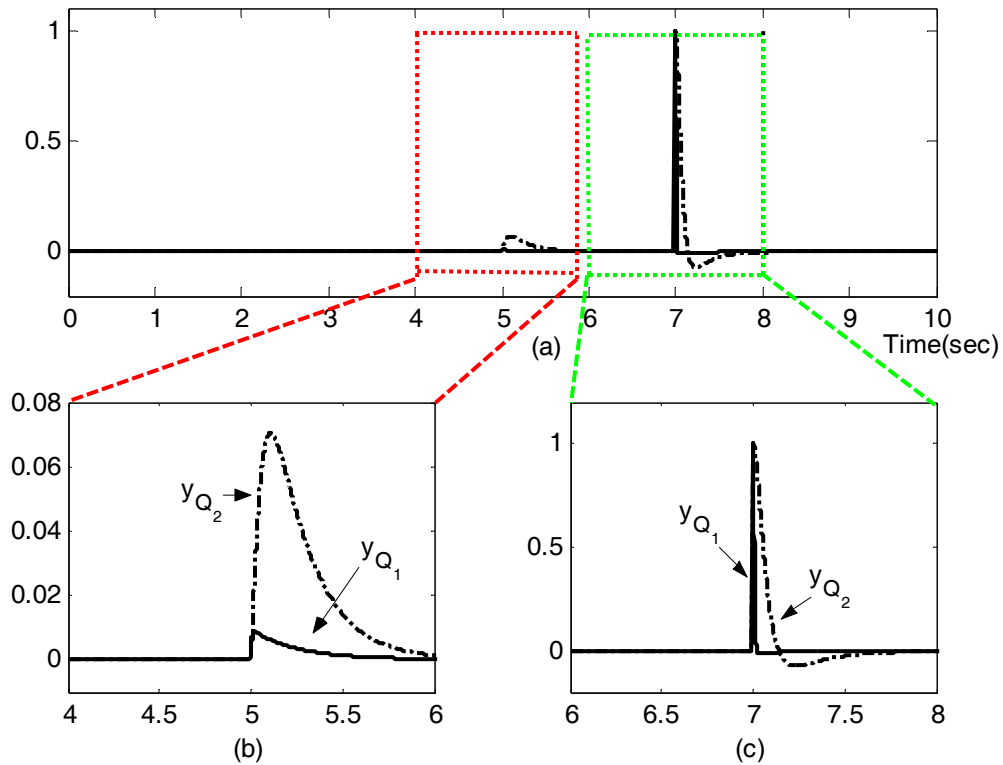


Fig. 5.4 (a) Simulation results when considered both input and output disturbances of part 1 – example 1

(b) Detailed response from 4 sec to 6 sec of Fig. 5.4(a)

(c) Detailed response from 6 sec to 8 sec of Fig. 5.4(a)

In Fig. 5.4(a)-(c), we observe that suppressing the input disturbance will also reduce the influence of the output disturbance. That is because the output sensitivity function is the same as the input sensitivity function in SISO system. Consequently, large bandwidth low-pass filter, i.e.  $Q_1(s)$  indicates better disturbance rejection. In Fig. 5.5(a)-(b), we plot the frequency responses and phases of the nominal plant and the ones from I/O points of DCFDOB with  $Q_1(s)$  and  $Q_2(s)$ .

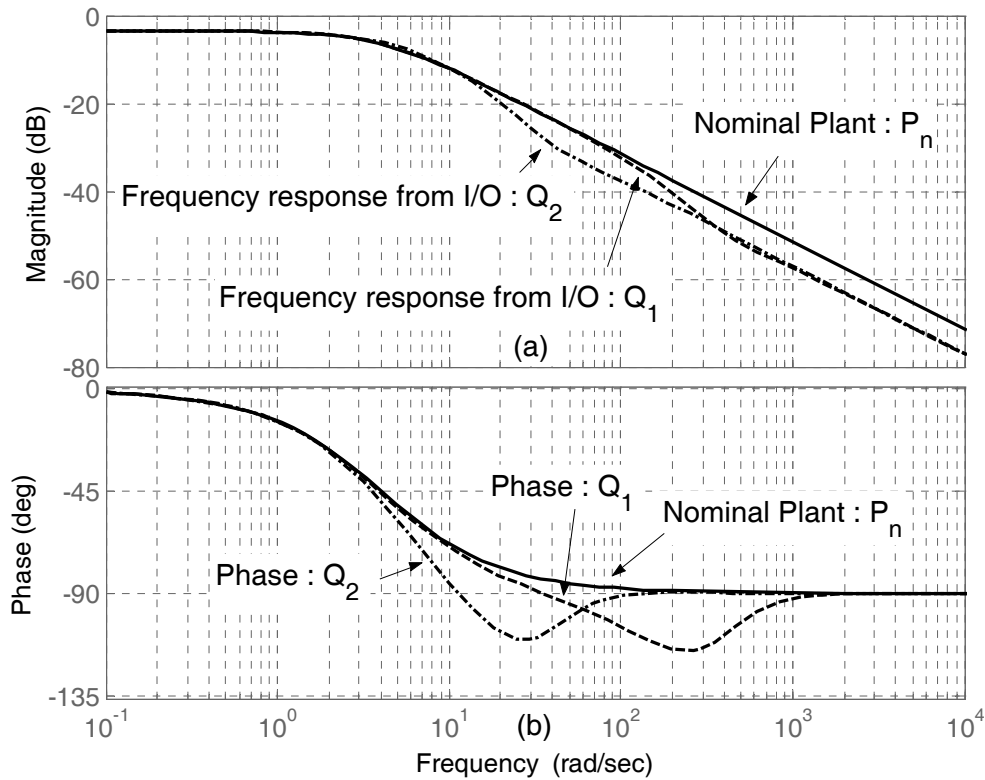


Fig. 5.5 (a) Frequency responses (b) phase plots of nominal plant and the ones from I/O points of DCFDOB with  $Q_1(s)$  and  $Q_2(s)$

Fig. 5.5(a)-(b) show that the DCFDOB can push the actual plant to nominal plant within the rejection bandwidth. In Fig. 5.5(a), the frequency response from I/O points of DCFDOB with  $Q_1(s)$  and overlaps the one of nominal plant before  $100 \text{ rad/sec}$ , but the one with  $Q_2(s)$  overlaps only before  $50 \text{ rad/sec}$ . In Fig. 5.5(b), the phase of DCFDOB with  $Q_1(s)$  overlaps the one of nominal plant before  $10 \text{ rad/sec}$  while the one with  $Q_2(s)$  overlaps only before  $2 \text{ rad/sec}$ . In general, the wider bandwidth the filter has, the closer the approximation will be.

Next, we will apply the DCFDOB to a MIMO, stable, minimum phase system in

numerical part 1-example 2.

**Example 2:** Suppose a simple MIMO system with  $2 \times 2$  dimension is given as follows.

$$P_n = \begin{bmatrix} \frac{1}{s+5} & \frac{2}{s+6} \\ \frac{5}{s+7} & \frac{3}{s+8} \end{bmatrix} = \left[ \begin{array}{c|c} A & B \\ \hline C & D \end{array} \right]$$

$$= \left[ \begin{array}{cccc|cc} -5 & 0 & 0 & 0 & 1 & 0 \\ 0 & -7 & 0 & 0 & 2.2361 & 0 \\ 0 & 0 & -6 & 0 & 0 & 1.4142 \\ 0 & 0 & 0 & -8 & 0 & 1.7321 \\ \hline 1 & 0 & 1.4142 & 0 & 0 & 0 \\ 0 & 2.2361 & 0 & 1.7321 & 0 & 0 \end{array} \right] \quad (5.7)$$

The transmission zeros of the system lie in  $-8.2527$  and  $-4.7373$  and the control gain matrix  $F$  and the observer gain matrix  $L$  are given as follows.

$$F = \begin{bmatrix} -0.0176 & -0.4815 & 0.2848 & 0.1536 \\ 0.1660 & 0.2416 & -2.1122 & -1.1077 \end{bmatrix} \quad (5.8)$$

$$L = \begin{bmatrix} -30 & 0 \\ 0 & -0.8944 \\ 14.1421 & 0 \\ 0 & 3.4641 \end{bmatrix} \quad (5.9)$$

The corresponding coprime factorization factors can be obtained by Eqs. (1.10)-(1.11).

To eliminate both input and output disturbances, we adopt the solution,  $Q = \tilde{N}_n^{-1} \cdot J \cdot Y_l^{-1}$ ,

which stated in section 3.1 to achieve this aim and is shown in Eq. (5.10).

$$\begin{aligned}
Q &= \tilde{N}_n^{-1} \cdot J \cdot Y_l^{-1} \\
&= \begin{bmatrix} Q_{11} & Q_{12} \\ Q_{21} & Q_{22} \end{bmatrix} \\
Q_{11}(s) &= \frac{24200(s+12)(s+11)(s+10)(s+5.672)(s^2+10s+24.5)(s^2+11.75s+36.86)}{(s+200)^2(s+8.547)(s+3.742)(s^2+11s+30.61)(s^2+21.29s+126.4)} \\
Q_{12}(s) &= \frac{3562(s+12)(s+11)(s+10)(s^2+10s+24.81)(s^2+13.58s+46.1)(s^2+12.27s+46.48)}{(s+200)^2(s+8.21)(s+8.006)(s+3.742)(s^2+11s+30.61)(s^2+21.29s+126.4)} \\
Q_{21}(s) &= \frac{-15592(s+12)(s+11)(s+10)(s+5.662)(s^2+9.985s+24.93)(s^2+14.78s+60)}{(s+200)^2(s+8.547)(s+3.742)(s^2+11s+30.61)(s^2+21.29s+126.4)} \\
Q_{22}(s) &= \frac{-2786(s+10)(s+11)(s+12)(s+7)(s+5)^2(s^2+15.78s+74.7)}{(s+200)^2(s+8.547)(s+3.742)(s^2+11s+30.61)(s^2+21.29s+126.4)} \\
J &= \begin{bmatrix} \frac{(200)^2}{(s+200)^2} & 0 \\ 0 & \frac{(200)^2}{(s+200)^2} \end{bmatrix}
\end{aligned} \tag{5.10}$$

The frequency responses from  $\begin{bmatrix} d_{i,1} \\ d_{i,2} \end{bmatrix}$  and  $\begin{bmatrix} d_{o,1} \\ d_{o,2} \end{bmatrix}$  to  $\begin{bmatrix} y_1 \\ y_2 \end{bmatrix}$  of Fig 3.1 are shown in

Fig. 5.6(a)-(d) and the simulation results are shown in Fig. 5.6(e) where the input

disturbances are  $D_i = \begin{bmatrix} d_{i,1} \\ d_{i,2} \end{bmatrix} = \begin{bmatrix} u(t-5) \\ \sin 5 \cdot t \end{bmatrix}$ , output disturbances are given as

$D_o = \begin{bmatrix} d_{o,1} \\ d_{o,2} \end{bmatrix} = \begin{bmatrix} t \\ 5 \sin t \end{bmatrix}$  and the reference command  $\begin{bmatrix} r_1 \\ r_2 \end{bmatrix} = 0$ .

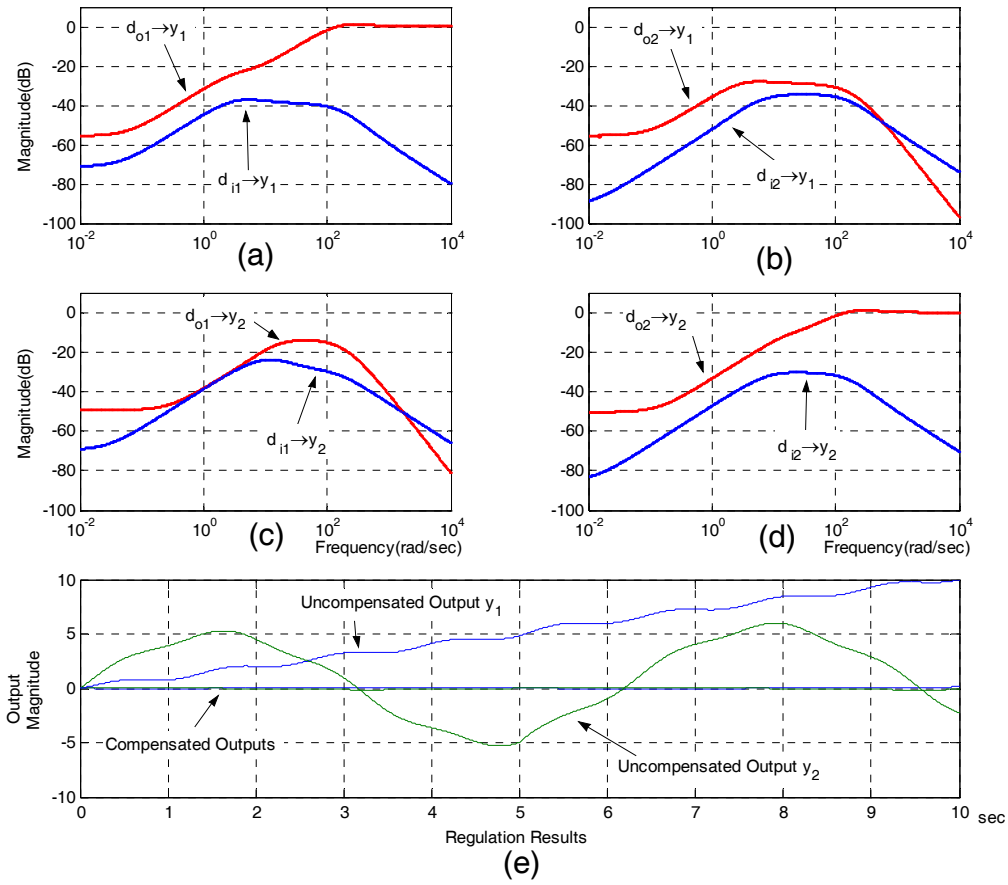


Fig. 5.6 Frequency responses from (a)  $\begin{bmatrix} d_{i,1} \\ d_{o,1} \end{bmatrix} \rightarrow y_1$  (b)  $\begin{bmatrix} d_{i,2} \\ d_{o,2} \end{bmatrix} \rightarrow y_1$

(c)  $\begin{bmatrix} d_{i,1} \\ d_{o,1} \end{bmatrix} \rightarrow y_2$  (d)  $\begin{bmatrix} d_{i,2} \\ d_{o,2} \end{bmatrix} \rightarrow y_2$  and (e) simulation results of part 1 - example 2

From Figs. 5.6(a)-(d) it is clear that in low frequency ranges, the DCFOB attenuates both input and output disturbances to system outputs very well. In Figs. 5.6 (a) and (d), we observe that the magnitudes of frequency responses from  $d_{o,1}$  to  $y_1$  and  $d_{o,2}$  to  $y_2$  close to 0dB in high frequency ranges, i.e. high frequency output disturbances will directly influence the outputs beyond rejection bandwidth. From Fig. 5.6(e), the uncompensated outputs i.e. the open loop, are much larger than the ones compensated

by DCFDOB, it reveals that the DCFDOB structure can not only apply to MIMO system but also eliminate various kinds of input and output disturbances at the same time.

## 5.2 Numerical example part 2: non-minimum phase plants

In the first example of part 2, an unstable, non-minimum phase, SISO plant with output feedback controller is used and the second example of part 2, a stable, non-minimum phase, MIMO plant is considered.

**Example 1:** An unstable and non-minimum phase SISO plant is given as

$$P_n(s) = \frac{0.2s - 20}{s - 20} \quad (5.11)$$

Its unstable pole locates at 20 and a single real RHP-zero locates at 100. The control gain matrix and observer gain matrix are given as  $F = [-80]$ ,  $L = [38.75]$  and then the corresponding coprime factorization factors are obtained as:

$$\begin{aligned} M_n &= \frac{s - 20}{s + 60} \in RH_\infty, N_n = \frac{0.2s - 20}{s + 60} \in RH_\infty \\ X_r &= \frac{s + 1300}{s + 600} \in RH_\infty, Y_r = \frac{-3100}{s + 600} \in RH_\infty \end{aligned} \quad (5.12)$$

In this example, one gives two different weighting functions as in Eqs. (5.13) and (5.14)

to show the flexibility in designing  $Q(s)$ .

$$W_1 = \frac{1 \times 10^8}{5 \times 10^6 s + 10} \quad (5.13)$$

$$W_2 = \frac{16.78(s^2 + 1.6s + 120)}{(s + 2 \times 10^{-6})(s^2 + 0.1 + 100)} \quad (5.14)$$

$W_1$  is a low-pass filter with high DC-gain and  $W_2$  contains large magnitude peak at  $10 \text{ rad/sec}$ . According to paragraph 2.2.2, one obtains the corresponding optimum parameters  $Q_{w_1}(s)$  and  $Q_{w_2}(s)$  in Eqs (5.15) and (5.16), respectively.

$$Q_{w_1} = \frac{(s + 4 \times 10^4)(s + 6)^2}{(s + 301)(s^2 + 289s + 2.17 \times 10^4)} \quad (5.15)$$

$$Q_{w_2} = \frac{(s + 3.52 \times 10^4)(s + 6)^2(s^2 + 1.972s + 113.8)}{(s + 278.3)(s^2 + 1.6s + 120)(s^2 + 267.8s + 1.97 \times 10^4)} \quad (5.16)$$

Moreover, model reduction method proposed by [15] is also applied to this example and the approximated minimum phase plant  $G_{approx}$  is

$$G_{approx} = \frac{38.3913}{s + 1.6356} \quad (5.17)$$

and its corresponding parameter is  $Q_{reduction} = G_{approx}^{-1} \cdot J(s)$ ,  $J(s) = \frac{1000}{s^2 + 44.71s + 1000}$ .

To stabilize this unstable system, an output feedback controller  $K(s) = \frac{0.75}{s + 15}$  is given. Figure 5.7 shows these three corresponding input sensitivity functions. From

Fig. 5.7, it reveals that the sensitivity functions which added  $W_1(s), W_2(s)$  are almost the same in the whole frequency ranges except a notch response located at  $10 \text{ rad/sec}$ ,

and the rejection capability of our method is better than the one proposed by [15]. The

waterbed effect caused by the RHP-zero is obviously and the limitation of crossover

frequency  $\omega_c$  is  $47 \text{ rad/sec}$ . In time domain simulation, the reference  $r = 0$  and a

complex input disturbance  $d_i = 0.2 \times \sin(10 \cdot t) + u(t - 5)$  is given and output responses

are shown in Fig. 5.8(a)-(c).

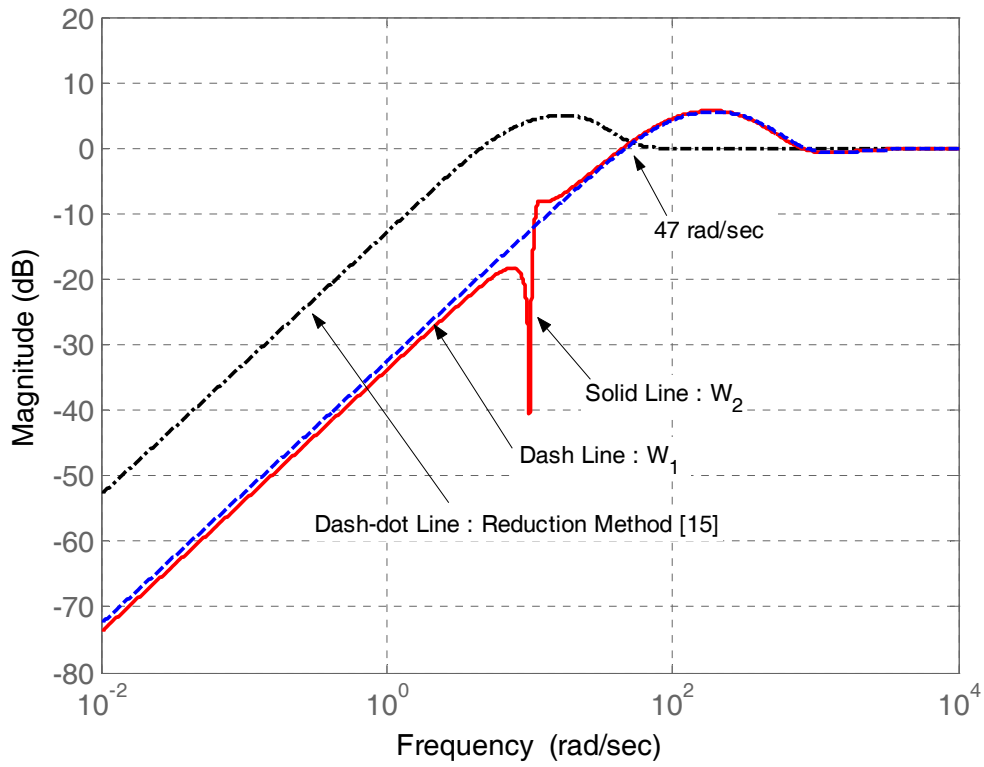


Fig. 5.7 Frequency responses of part 2 – example 1

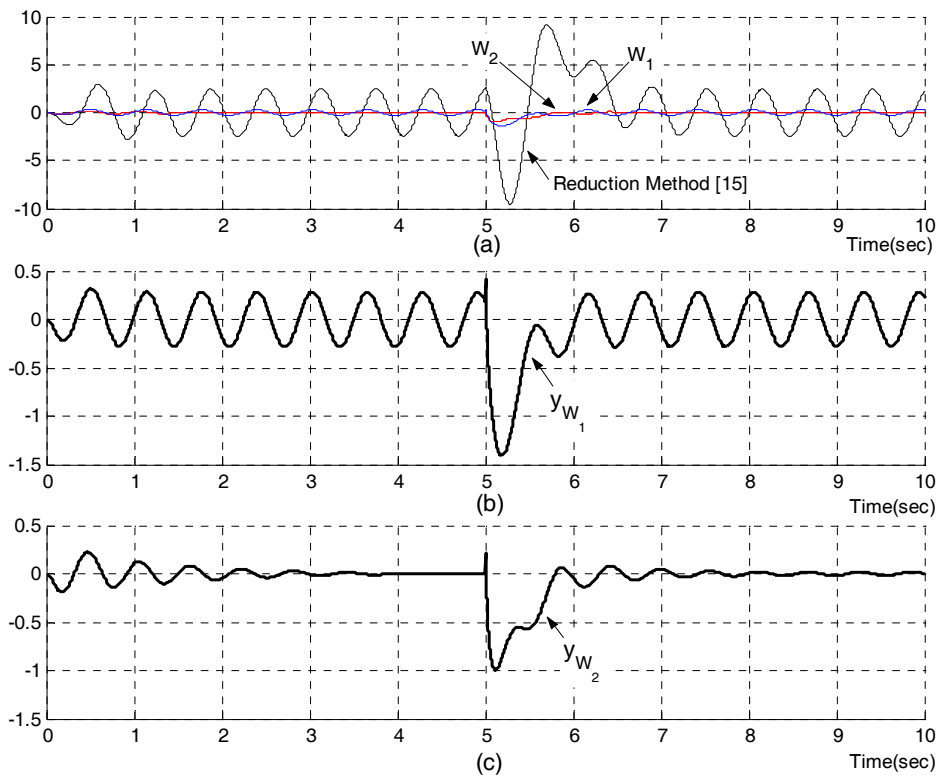


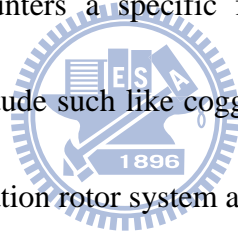


Fig. 5.8 (a) System outputs of simulation results of part 2 – example 1

(b) System output  $y_{w_1}$  of DCFDOB with parameter  $Q_{w_1}(s)$

(c) System output  $y_{w_2}$  of DCFDOB with parameter  $Q_{w_2}(s)$

In Fig. 5.8(a), a large disturbance influence also remains in the output by using reduction method [15] but almost be reduced in the ones by our structure. In Figs. 5.8 (b) and (c), the output  $y_{w_1}$  compensated by DCFDOB with parameter  $Q_{w_1}(s)$  remains slight oscillation caused by the specific sinusoid disturbance and  $y_{w_2}$  decays toward zero when  $Q_{w_2}(s)$  is adopted in DCFDOB. This is beneficial and flexible in designing when a system encounters a specific frequency of sinusoid wave type disturbance with unknown magnitude such like cogging force of constant speed motor, unbalance force of magnetic levitation rotor system and cutting force of milling system.



**Example 2:** In the second example of part 2, one gives a simple  $2 \times 2$  MIMO, stable and non-minimum phase plant as a numerical example and the nominal plant and its state-space realization are given as follows.

$$P_n = \begin{bmatrix} \frac{s-10}{s^2+5s+6} & \frac{1}{s+4} \\ \frac{1}{s+3} & \frac{1}{s^2+5s+12} \end{bmatrix} =$$

$$\left[ \begin{array}{cccccc|cc} -0.5384 & -1.8968 & 0 & 0 & 0 & 0 & -1.076 & 0 \\ 1.8968 & -4.4616 & 0 & 0 & 0 & 0 & 1.469 & 0 \\ 0 & 0 & -3 & 0 & 0 & 0 & 1 & 0 \\ 0 & 0 & 0 & -4 & 0 & 0 & 0 & 1 \\ 0 & 0 & 0 & 0 & -0.8329 & -2.9205 & 0 & 1.4088 \\ 0 & 0 & 0 & 0 & 2.9205 & -4.1671 & 0 & -1.7276 \\ \hline 1.076 & 1.469 & 0 & 1 & 0 & 0 & 0 & 0 \\ 0 & 0 & 1 & 0 & -1.4088 & -1.7276 & 0 & 0 \end{array} \right]$$

(5.18)

The system poles locate at  $-3, -2, -4, -2.5 \pm 2.3979i$  and it contains a LHP-zero locates at  $-4.0494$  and a RHP-zero locates at  $5.8070$ . The corresponding coprime factors are obtained and given in appendix A and then the parameter  $Q(s)$  can be obtained according to section 3.2. Furthermore, assume the input disturbances is

$$D_i = \begin{bmatrix} d_{i,1} \\ d_{i,2} \end{bmatrix} = \begin{bmatrix} 2 \times \sin\left(\frac{t}{5}\right) \\ 5 \cdot u(t-25) \end{bmatrix}, \quad \text{where } u(t) = 1, t \geq 25 \text{ sec} \quad \text{and} \quad u(t) = 0, t < 25 \text{ sec} .$$

$$\text{Output disturbances are given as } D_o = \begin{bmatrix} d_{o,1} \\ d_{o,2} \end{bmatrix} = \begin{bmatrix} \frac{t}{5} \\ 5 \times \sin\left(\frac{t}{2}\right) \end{bmatrix}. \quad \text{For eliminating low}$$

frequency disturbances and keeping small DC-gain of  $S_i$  and  $S_o$ , a weighting

function matrix  $W_{2 \times 2} = \text{diag} \left[ \frac{3}{s + 0.05} \quad \frac{3}{s + 0.05} \right]_{2 \times 2}$  with  $3 \text{ rad/sec}$  crossover

frequency and  $35.6 \text{ dB}$  DC-gain is given. The frequency responses of sensitivity

functions from  $D_i$  and  $D_o$  to system outputs  $\begin{bmatrix} y_1 \\ y_2 \end{bmatrix}$  of Fig. 3.1 and the regulation

results are shown in Figures 5.9(a)-(e).

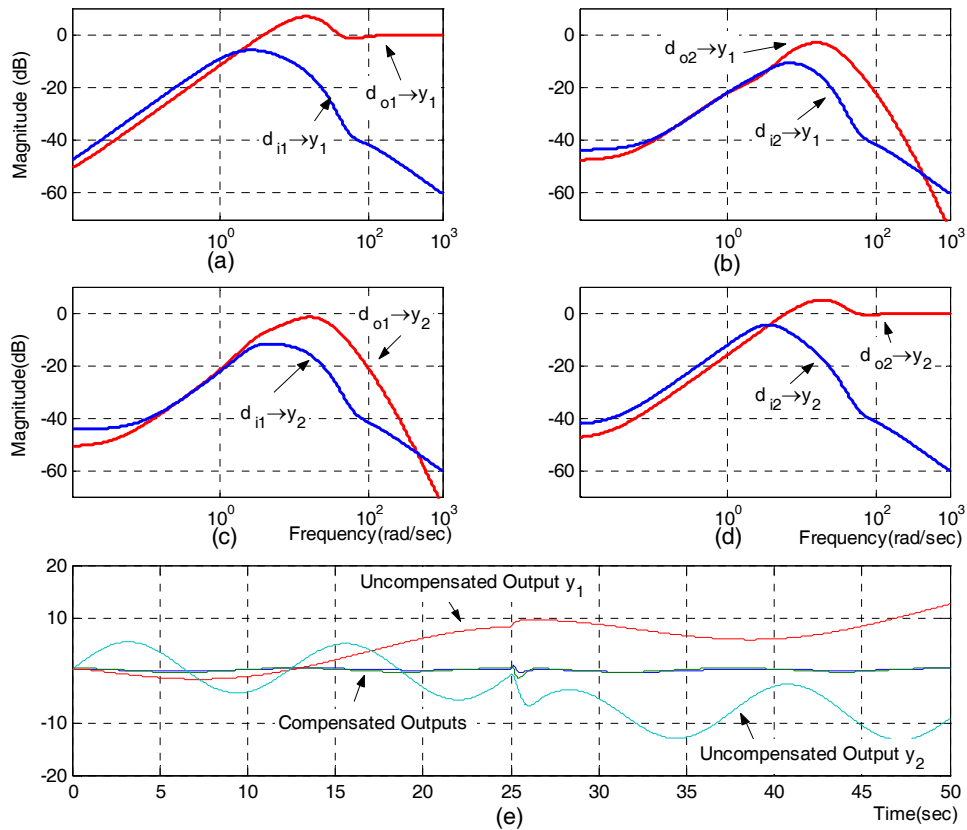


Fig. 5.9 Frequency responses from (a)  $\begin{bmatrix} d_{i,1} \\ d_{o,1} \end{bmatrix} \rightarrow y_1$  (b)  $\begin{bmatrix} d_{i,2} \\ d_{o,2} \end{bmatrix} \rightarrow y_1$  (c)  $\begin{bmatrix} d_{i,1} \\ d_{o,1} \end{bmatrix} \rightarrow y_2$

(d)  $\begin{bmatrix} d_{i,2} \\ d_{o,2} \end{bmatrix} \rightarrow y_2$  and (e) simulation results of part 2 - example 2

Obviously, compared Figs. 5.9(a)-(d) with Figs. 5.6(a)-(d) of example 2 of part 1, the sensitivity functions with large peaks caused by RHP-zeros and greater than  $0 \text{ dB}$  are

present. Consequently, the outputs compensated by DCFDOB are better than the ones without compensating.

### 5.3 Numerical example part 3: non-square, minimum phase plants

**Example 1:** a  $3 \times 2$  thin plant case

In this paragraph, a non-square  $3 \times 2$  MIMO, stable, minimum phase plant with 2 inputs and 3 outputs is given as a numerical example and we discuss input disturbance rejection and output disturbance rejection, respectively. In output disturbance rejection issue, we demonstrate three solving methods, in the first design, we use the same solution obtained from input disturbance rejection. In the second design, we focus on eliminating some selected channels disturbances. In the third design, we focus on eliminating the diagonal terms of output sensitivity functions. The nominal plant and its state-space realization are given as follows.

$$P_{n,3 \times 2} = \begin{bmatrix} \frac{1}{s+5} & \frac{2}{s+6} \\ \frac{4}{s+7} & \frac{3}{s+8} \\ \frac{2}{s+5} & \frac{5}{s+4} \end{bmatrix} = \left[ \begin{array}{cccccc|cc} -5 & 0 & 0 & 0 & 0 & 0 & 1 & 0 \\ 0 & -7 & 0 & 0 & 0 & 0 & 2 & 0 \\ 0 & 0 & -5 & 0 & 0 & 0 & 1.4142 & 0 \\ 0 & 0 & 0 & -6 & 0 & 0 & 0 & 1.4142 \\ 0 & 0 & 0 & 0 & -8 & 0 & 0 & 1.7321 \\ 0 & 0 & 0 & 0 & 0 & -4 & 0 & 2.2361 \\ \hline 1 & 0 & 0 & 1.4142 & 0 & 0 & 0 & 0 \\ 0 & 2 & 0 & 0 & 1.7321 & 0 & 0 & 0 \\ 0 & 0 & 1.4142 & 0 & 0 & 2.2361 & 0 & 0 \end{array} \right] \quad (5.19)$$

and the control gain matrix,  $F$ , and observer gain matrix,  $L$ , are

$$F = \begin{bmatrix} -0.71741 & -1.0721 & -1.0146 & 0 & 0 & 0 \\ 0 & 0 & 0 & -0.75888 & -0.73805 & -1.6646 \end{bmatrix}$$

$$L = \begin{bmatrix} -0.82658 & 0 & 0 & -0.98894 & 0 & 0 \\ 0 & -1.1319 & 0 & 0 & -0.86947 & 0 \\ 0 & 0 & -0.90878 & 0 & 0 & -1.7212 \end{bmatrix} \quad (5.20)$$

The corresponding coprime factors are obtained and given in appendix B. According to Table 3.2, the design objective of input disturbances elimination is

$$Q_{2 \times 2} \cdot Y_{1,2 \times 3} \cdot \tilde{N}_{n,3 \times 2} = \begin{bmatrix} J_{11} & 0 \\ 0 & J_{22} \end{bmatrix}, \text{ where } J_{ii} (i=1 \sim 2) \text{ are low pass filters with desired}$$

bandwidth and the parameter  $Q_{2 \times 2}(s)$  is shown in appendix B. Assume the input

$$\text{disturbances are } D_i = \begin{bmatrix} d_{i,1} \\ d_{i,2} \end{bmatrix} = \begin{bmatrix} u_1(t-2) \\ u_2(t-7) \end{bmatrix}, \text{ where } u_1(t) = 1, t \geq 2 \text{ sec and}$$

$u_2(t) = 1, t \geq 7 \text{ sec}$  and the simulation block is shown in Fig 5.10.

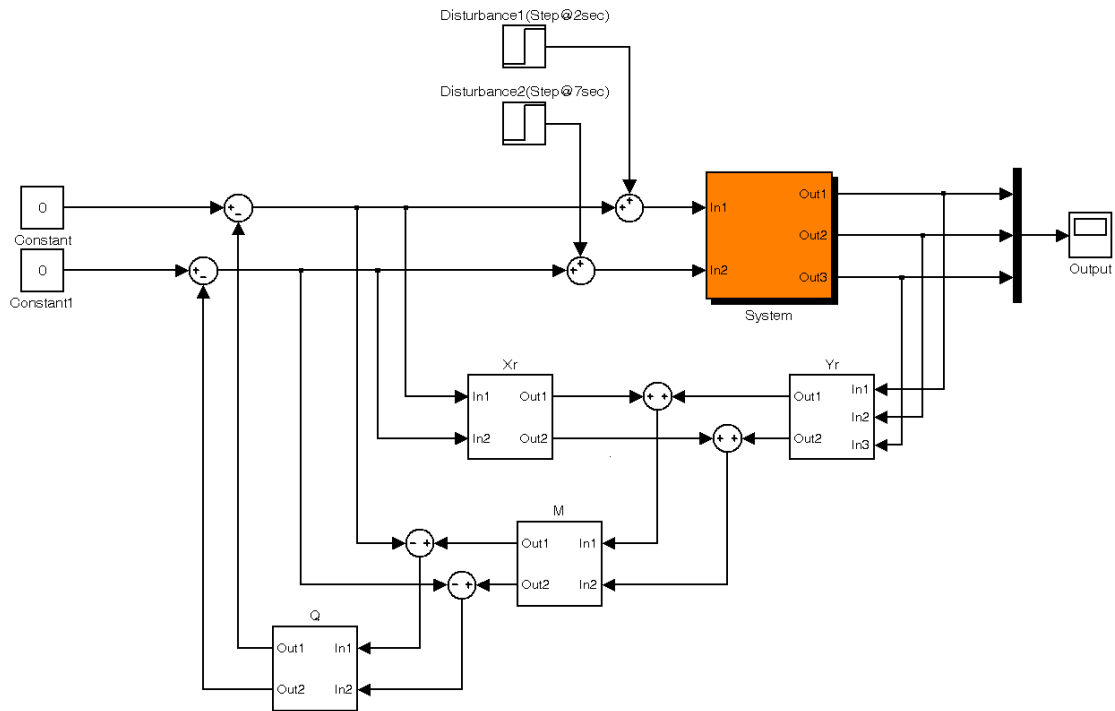


Fig. 5.10 Simulation block of numerical example part 3 – example 1

Figure 5.11(a) show the input disturbances rejection results with/without DCFDOB and Figs. 5.11 (b) and (c) display the detailed output response from 1.5 sec to 3.5 sec and from 6.5 sec to 8.5 sec, respectively. Fig. 5.11(d) shows the system outputs without DCFDOB. From these figures, we knew that even in non-square plant, the DCFDOB performed very well in eliminating input disturbances.

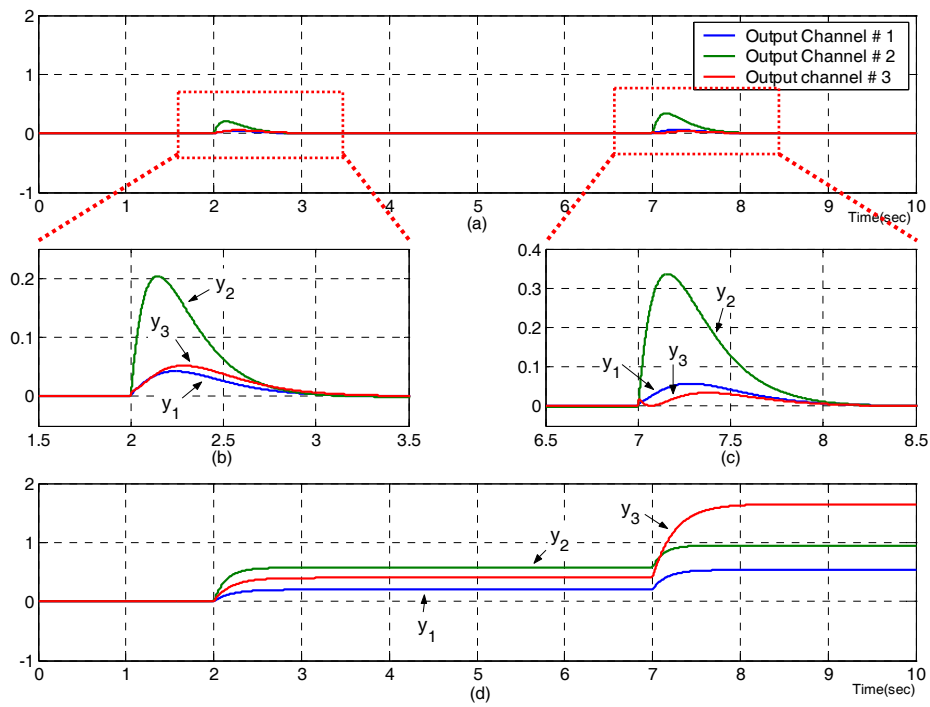


Fig. 5.11

- (a) Simulation results of non-square thin plant with DCFDOB and input disturbance
- (b) Detailed responses from 1.5 sec to 3.5 sec of Fig. 5.1(a)
- (c) Detailed responses from 6.5 sec to 8.5 sec of Fig. 5.1(a)
- (d) Simulation results of non-square thin plant without DCFDOB

Figures 5.12(a)-(d) show the frequency responses of input sensitivity functions.

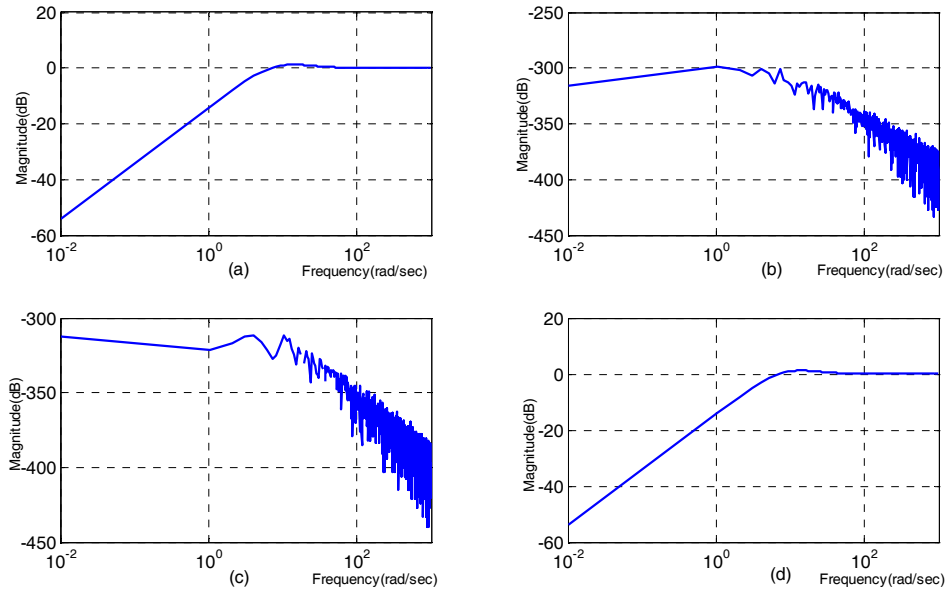


Fig. 5.12 Frequency responses of input sensitivity functions of part 3 – example 1

$$(a) S_{i,11} : d_{i,1} \rightarrow y_1 \quad (b) S_{i,12} : d_{i,2} \rightarrow y_1$$

$$(c) S_{i,21} : d_{i,2} \rightarrow y_1 \quad (d) S_{i,22} : d_{i,2} \rightarrow y_2$$

In Figs 5.12(a) and (d), i.e. the diagonal terms, hold low magnitudes (-50dB) in low frequency ranges and the magnitude of the couple terms shown in Figs. 5.12 (b) and (c) are almost zeros (-300dB).

After that, we will discuss the influence of output disturbance on non-square thin plant. In the first design of output disturbance elimination on non-square thin plant, we use the same solutions that obtained in example 1 of part 3 and shown in Eq. (B.7) in appendix B.

$$\text{Output disturbances are given as } D_o = \begin{bmatrix} d_{o,1} \\ d_{o,2} \\ d_{o,3} \end{bmatrix} = \begin{bmatrix} u_1(t-2) \\ u_2(t-5) \\ u_3(t-7) \end{bmatrix}, \text{ where } u_1(t) = 1, t \geq 2 \text{ sec},$$



$u_2(t) = 1, t \geq 5 \text{ sec}$  and  $u_3(t) = 1, t \geq 7 \text{ sec}$ . The simulation results are shown in Figs.

5.13.

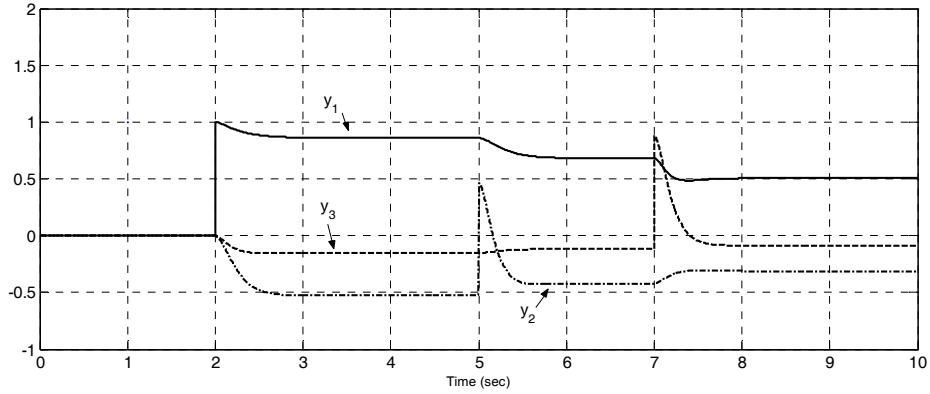


Fig. 5.13 Simulation results of output disturbances on non-square thin plant – design 1

Figure 5.13 illustrates that the capability is not good in rejecting output disturbance in

non-square thin plant case and performance limitation was discussed in paragraph 3.4.1.

Moreover, the frequency responses are shown in Figs. 5.14(a)-(i).

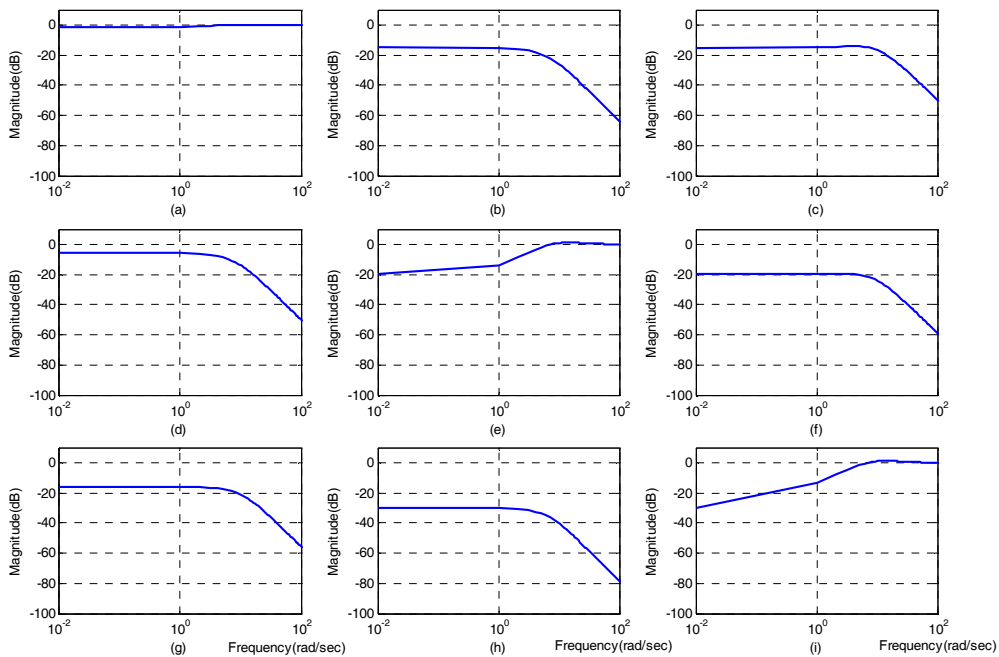


Fig. 5.14 Frequency responses of output sensitivity functions (design 1)

of part 3 – example 1

$$(a) S_{o,11} : d_{o,1} \rightarrow y_1 \quad (b) S_{o,12} : d_{o,2} \rightarrow y_1 \quad (c) S_{o,13} : d_{o,3} \rightarrow y_1$$

$$(d) S_{o,21} : d_{o,1} \rightarrow y_2 \quad (e) S_{o,22} : d_{o,2} \rightarrow y_2 \quad (f) S_{o,23} : d_{o,3} \rightarrow y_2$$

$$(g) S_{o,31} : d_{o,1} \rightarrow y_3 \quad (h) S_{o,32} : d_{o,2} \rightarrow y_3 \quad (i) S_{o,33} : d_{o,3} \rightarrow y_3$$

From Figs. 5.14(a)-(i), although these sensitivity functions are all below 0dB in low frequency ranges, the magnitudes of some sensitivity functions in low frequency ranges are still too large, e.g.,  $S_{o,11}$  and  $S_{o,21}$ . Moreover, the coupling terms of input sensitivity functions shown in Figs. 5.12(a) and (d) are almost zero (-300dB) but the ones of output sensitivity functions are not small enough. That is, coupling effects will worsen the eliminating performance. According to Table 3.2, in the second design, we focus on eliminating the output disturbances of the first and the second channels. The solutions can be obtained by reducing the influence from  $[d_{o,1} \ d_{o,2}]^T$  to  $[y_1 \ y_2]^T$ , that is,

$$\begin{cases} (\tilde{N}_{11}Q_{11} + \tilde{N}_{12}Q_{21})Y_{l,11} + (\tilde{N}_{11}Q_{11} + \tilde{N}_{12}Q_{22})Y_{l,21} = J \\ (\tilde{N}_{11}Q_{11} + \tilde{N}_{12}Q_{21})Y_{l,12} + (\tilde{N}_{11}Q_{12} + \tilde{N}_{12}Q_{22})Y_{l,22} = 0 \\ (\tilde{N}_{21}Q_{11} + \tilde{N}_{22}Q_{21})Y_{l,11} + (\tilde{N}_{21}Q_{12} + \tilde{N}_{22}Q_{22})Y_{l,21} = 0 \\ (\tilde{N}_{21}Q_{11} + \tilde{N}_{22}Q_{21})Y_{l,12} + (\tilde{N}_{21}Q_{12} + \tilde{N}_{22}Q_{22})Y_{l,22} = J \end{cases} \quad (5.21)$$

where  $J = \frac{10^2}{(s+10)^2}$  and  $Q_{2 \times 2}(s)$  are obtained as follows.

$$\begin{bmatrix} Q_{11} & Q_{12} \\ Q_{21} & Q_{22} \end{bmatrix} = \begin{aligned} Q_{11} &= \frac{129.2(s+10.52)(s+7.86)(s+5.78)(s+5.04)(s^2+15.76s+62.48)}{(s+10)^2(s+8.42)(s+8.36)(s+4.64)(s+4.58)} \\ Q_{12} &= -\frac{182.1(s+11.29)(s+8.16)(s+7.01)(s+7)(s+5.43)(s+5.27)(s+5)}{(s+10)^2(s+8.42)(s+8.36)(s+4.64)(s+4.58)(s+4)} \\ Q_{21} &= -\frac{125.1(s+10.52)(s+8.14)(s+8)(s+6.35)(s+6)(s+5.78)}{(s+10)^2(s+8.42)(s+8.36)(s+4.64)(s+4.58)} \\ Q_{22} &= \frac{205.48(s+11.79)(s+8.25)(s+7.81)(s+7.01)(s+5.27)(s^2+10.77s+29.21)}{(s+10)^2(s+8.42)(s+8.36)(s+4.64)(s+4.58)(s+4)} \end{aligned} \quad (5.22)$$

The time domain simulations are given in Fig.5.15, where the output disturbances are

given as  $D_o = \begin{bmatrix} u_1(t-2) \\ u_2(t-5) \\ u_3(t-7) \end{bmatrix}$  and reference commands are zeros.

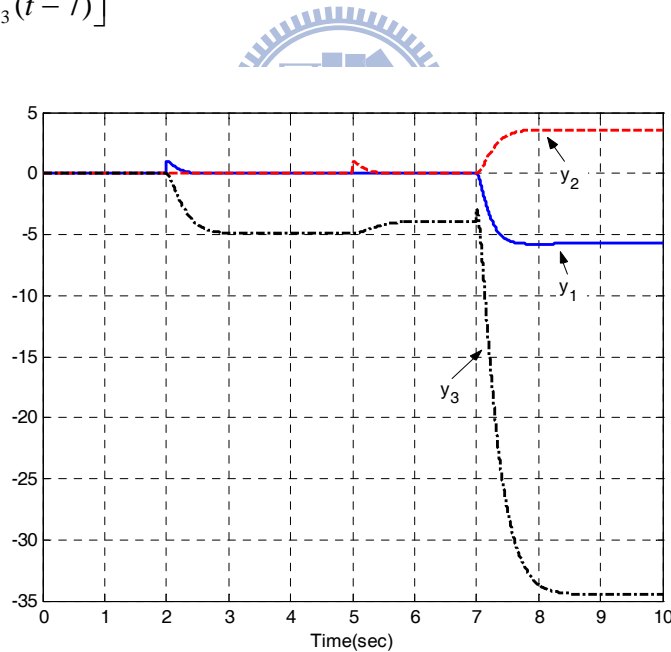


Fig. 5.15 Simulation results of output disturbances on non-square thin plant – design 2

The simulation plots show that the influences from  $[d_{o,1} \ d_{o,2}]^T$  to  $[y_1 \ y_2]^T$  are reduced when  $t < 7$ sec. However, the third output channel,  $y_3$ , is coupled by the compensated signals of the first and the second input channels. All channels are

influenced after the disturbance of third channel raised after 7 seconds. The frequency responses of the nine channels are shown in Fig 5.16(a)-(i). In Figs. 5.16(a), (b), (d) and (e), the magnitudes of output sensitivity functions from  $\begin{bmatrix} d_{o,1} \\ d_{o,2} \end{bmatrix}$  to  $\begin{bmatrix} y_1 \\ y_2 \end{bmatrix}$  are all below -40dB in low frequency ranges but the others output sensitivity functions are all greater than 0dB. As we mentioned in section 3.4, the sensitivity functions from  $d_{o,3}$  to  $[y_1 \ y_2 \ y_3]^T$  and the ones from  $[d_{o,1} \ d_{o,2}]^T$  to  $y_3$  are not guaranteed.

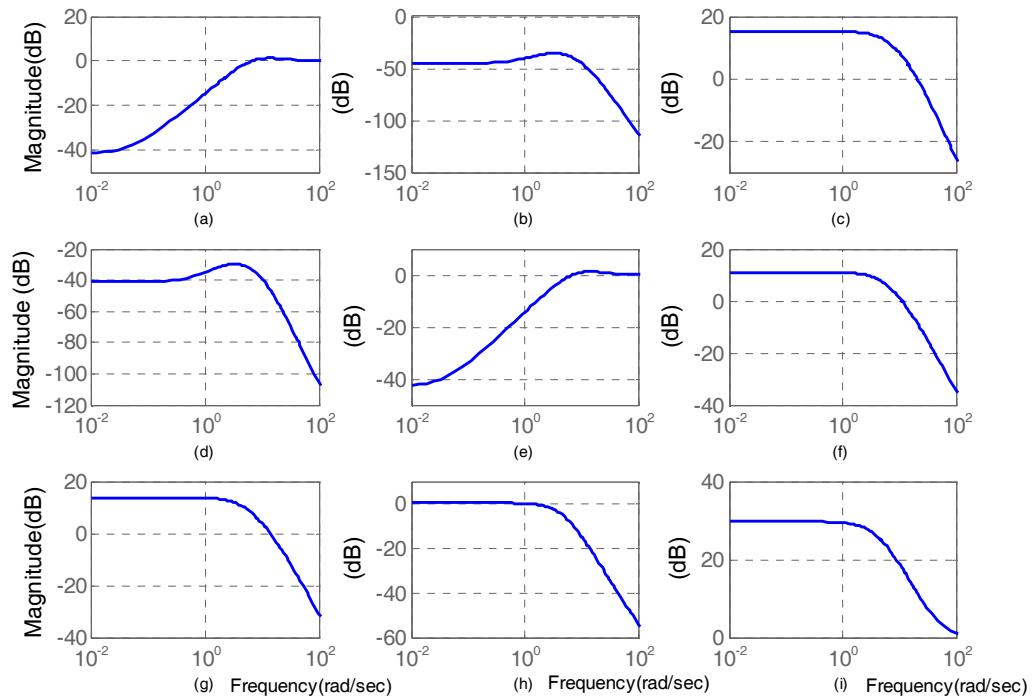


Fig. 5.16 Frequency responses of output sensitivity functions (design 2)

of part 3 - example 1

$$(a) S_{o,11} : d_{o,1} \rightarrow y_1 \quad (b) S_{o,12} : d_{o,2} \rightarrow y_1 \quad (c) S_{o,13} : d_{o,3} \rightarrow y_1$$

$$(d) S_{o,21} : d_{o,1} \rightarrow y_2 \quad (e) S_{o,22} : d_{o,2} \rightarrow y_2 \quad (f) S_{o,23} : d_{o,3} \rightarrow y_2$$

$$(g) S_{o,31} : d_{o,1} \rightarrow y_3 \quad (h) S_{o,32} : d_{o,2} \rightarrow y_3 \quad (i) S_{o,33} : d_{o,3} \rightarrow y_3$$

In the third design for output disturbance rejection, we focus on reducing the diagonal terms of output sensitivity function matrix to eliminate the direct disturbance effect on each channel. The solutions can be obtained by solving the following equations.

$$\begin{cases} (\tilde{N}_{11}Q_{11} + \tilde{N}_{12}Q_{21})Y_{l,11} + (\tilde{N}_{11}Q_{11} + \tilde{N}_{12}Q_{22})Y_{l,21} = J \\ (\tilde{N}_{21}Q_{11} + \tilde{N}_{22}Q_{21})Y_{l,12} + (\tilde{N}_{21}Q_{12} + \tilde{N}_{22}Q_{22})Y_{l,22} = J \\ (\tilde{N}_{31}Q_{11} + \tilde{N}_{32}Q_{21})Y_{l,13} + (\tilde{N}_{31}Q_{12} + \tilde{N}_{32}Q_{22})Y_{l,23} = J \end{cases} \quad (5.23)$$

$$J = \frac{10^2}{(s+10)^2}$$

The time domain simulations are given in Fig 5.17, where the output disturbances are

also given as  $D_o = \begin{bmatrix} u_1(t-2) \\ u_2(t-5) \\ u_3(t-7) \end{bmatrix}$  and reference commands are zeros.

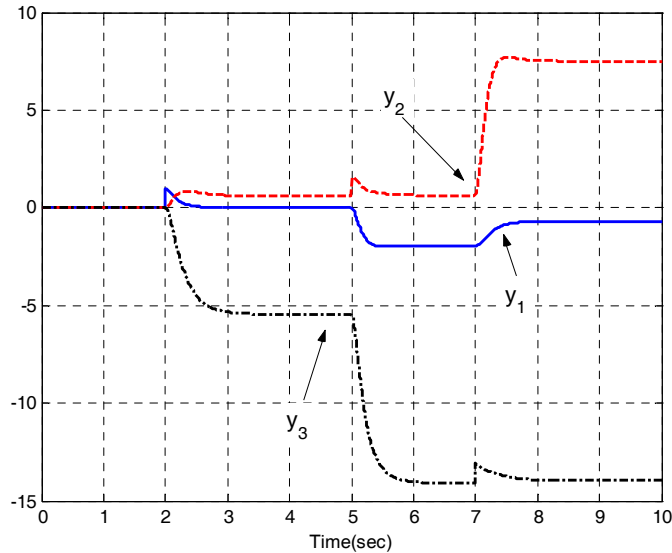


Fig. 5.17 Simulation results of example 5.3 part 1 – design 3

From Fig. 5.17, we obtain that the influence from  $d_{o,1}$  to  $y_1$  of is eliminated when

$2 \leq t < 5$ , however the others channels outputs will be coupled. Also, the same phenomenon in the second and the third channels can be obtained when  $5 \leq t < 7$  and  $7 \leq t \leq 10$ , respectively. The frequency responses of design 3 are shown in Figs 5.18(a)-(i).

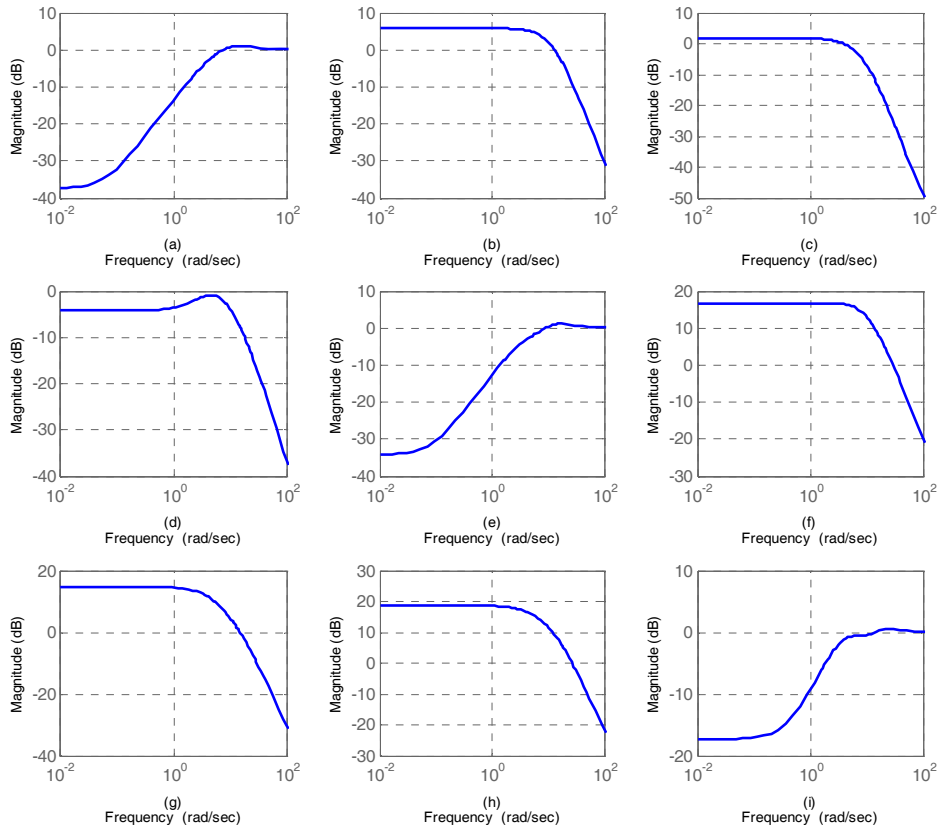


Fig. 5.18 Frequency responses of output sensitivity functions (design 3)

of part 3 – example 1

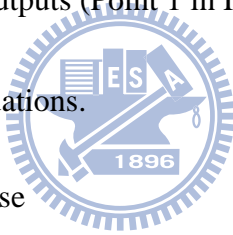
$$(a) S_{o,11} : d_{o,1} \rightarrow y_1 \quad (b) S_{o,12} : d_{o,2} \rightarrow y_1 \quad (c) S_{o,13} : d_{o,3} \rightarrow y_1$$

$$(d) S_{o,21} : d_{o,1} \rightarrow y_2 \quad (e) S_{o,22} : d_{o,2} \rightarrow y_2 \quad (f) S_{o,23} : d_{o,3} \rightarrow y_2$$

$$(g) S_{o,31} : d_{o,1} \rightarrow y_3 \quad (h) S_{o,32} : d_{o,2} \rightarrow y_3 \quad (i) S_{o,33} : d_{o,3} \rightarrow y_3$$

After these three demonstrations of output disturbance rejection for non-square, thin plant case which contains  $n$  input channels and  $m$  output channels ( $n < m$ ), we knew that only  $n^2$  output sensitivity functions can be considered and the others  $m^2 - n^2$  ones are not guaranteed.

Moreover, the transfer function matrix from input disturbances  $d_i$  to estimated input disturbances  $\hat{d}_i$  is  $Q_{2 \times 2} \cdot Y_{l, 2 \times 3} \cdot \tilde{N}_{n, 3 \times 2}$  and its matrix rank is 2, that is, it is full rank and there exist exact solutions of  $Q_{2 \times 2}$ . In contrast, one can not obtain the exact solutions since the number of unknown parameters of transfer functions matrix from output disturbances  $d_o$  to plant outputs (Point 1 in Fig. 3.1),  $P_{n, 3 \times 2} \cdot Q_{2 \times 2} \cdot M_{n, 2 \times 2} \cdot Y_{r, 2 \times 3}$ , are less than the one of desired equations.



**Example 2:** a  $2 \times 3$  wide plant case

For wide plant case, a  $2 \times 3$  non-square, stable, minimum phase plant with 3 inputs and 2 outputs is given as the second numerical example. The nominal plant and its state-space realization are given as follows.

$$\begin{aligned}
P_{n,2 \times 3} &= \begin{bmatrix} \frac{1}{s+5} & \frac{7}{s+7} & \frac{2}{s+5} \\ \frac{2}{s+6} & \frac{3}{s+8} & \frac{5}{s+4} \end{bmatrix} \\
\left[ \begin{array}{c|c} A & B \\ \hline C & D \end{array} \right] &= \left[ \begin{array}{cccccc|ccc} -5 & 0 & 0 & 0 & 0 & 0 & 1 & 0 & 0 \\ 0 & -6 & 0 & 0 & 0 & 0 & 1.4142 & 0 & 0 \\ 0 & 0 & -7 & 0 & 0 & 0 & 0 & 2 & 0 \\ 0 & 0 & 0 & -8 & 0 & 0 & 0 & 1.732 & 0 \\ 0 & 0 & 0 & 0 & -5 & 0 & 0 & 0 & 1.4142 \\ 0 & 0 & 0 & 0 & 0 & -4 & 0 & 0 & 2.2361 \\ \hline 1 & 0 & 2 & 0 & 1.4142 & 0 & 0 & 0 & 0 \\ 0 & 1.4142 & 0 & 1.732 & 0 & 2.2361 & 0 & 0 & 0 \end{array} \right]
\end{aligned}
\tag{5.24}$$

and the control gain matrix,  $F$ , and observer gain matrix,  $L$ , are given as follows.

$$\begin{aligned}
F &= \begin{bmatrix} -0.82658 & -0.98894 & 0 & 0 & 0 & 0 \\ 0 & 0 & -1.1319 & -0.86947 & 0 & 0 \\ 0 & 0 & 0 & 0 & -0.90878 & -1.7212 \end{bmatrix} \\
L &= \begin{bmatrix} -0.71741 & 0 \\ 0 & -0.75888 \\ -1.0721 & 0 \\ 0 & -0.73805 \\ -1.0146 & 0 \\ 0 & -1.6646 \end{bmatrix}
\end{aligned}
\tag{5.25}$$

And the corresponding coprime factorization factors can be obtained by Eqs. (1.10) and

(1.11). According to Table 3.2, the design objective of output disturbances elimination

is  $\tilde{N}_{n,2 \times 3} \cdot Q_{3 \times 3} \cdot Y_{l,3 \times 2} = \begin{bmatrix} J_{11} & 0 \\ 0 & J_{22} \end{bmatrix}_{2 \times 2}$ , where  $J_{ii} (i=1 \sim 2)$  are low pass filters with

desired bandwidth. Obviously, there are 9 unknowns parameters,  $Q_{11} \sim Q_{33}$ , and only

4 equations, namely, only four parameters are needed. In this case, we choose  $Q_{11}$ ,

$Q_{22}$ ,  $Q_{31}$  and  $Q_{32}$  which are solved as follows.



$$\begin{aligned}
\mathcal{Q}_{3 \times 3}(s) &= \begin{bmatrix} \mathcal{Q}_{11} & 0 & 0 \\ 0 & \mathcal{Q}_{22} & 0 \\ \mathcal{Q}_{31} & \mathcal{Q}_{32} & 0 \end{bmatrix} \\
\left\{ \begin{aligned} \mathcal{Q}_{11}(s) &= \frac{J_{22} \tilde{N}_{n,13} Y_{l,21} + J_{11} \tilde{N}_{n,23} Y_{l,22}}{(\tilde{N}_{n,13} \tilde{N}_{n,21} - \tilde{N}_{n,11} \tilde{N}_{n,23})(Y_{l,12} Y_{l,21} - Y_{l,11} Y_{l,22})} \\ \mathcal{Q}_{22}(s) &= \frac{J_{22} \tilde{N}_{n,13} Y_{l,11} + J_{11} \tilde{N}_{n,23} Y_{l,12}}{(\tilde{N}_{n,13} \tilde{N}_{n,22} - \tilde{N}_{n,12} \tilde{N}_{n,23})(Y_{l,11} Y_{l,22} - Y_{l,12} Y_{l,21})} \\ \mathcal{Q}_{31}(s) &= \frac{-J_{22} \tilde{N}_{n,11} Y_{l,21} - J_{11} \tilde{N}_{n,21} Y_{l,22}}{(\tilde{N}_{n,13} \tilde{N}_{n,21} - \tilde{N}_{n,11} \tilde{N}_{n,23})(Y_{l,12} Y_{l,21} - Y_{l,11} Y_{l,22})} \\ \mathcal{Q}_{32}(s) &= \frac{J_{22} \tilde{N}_{n,12} Y_{l,11} + J_{11} \tilde{N}_{n,22} Y_{l,12}}{(\tilde{N}_{n,13} \tilde{N}_{n,22} - \tilde{N}_{n,12} \tilde{N}_{n,23})(Y_{l,12} Y_{l,21} - Y_{l,11} Y_{l,22})} \end{aligned} \right. \quad (5.26)
\end{aligned}$$

where  $J_{11}(s) = J_{22}(s) = \frac{100}{(s+10)^2}$ . The output disturbances are given as

$$D_o = \begin{bmatrix} d_{o,1} \\ d_{o,2} \end{bmatrix} = \begin{bmatrix} u_1(t-2) \\ u_2(t-5) \end{bmatrix}, \quad \text{where } u_1(t) = 1, t \geq 2 \text{ sec and } u_2(t) = 1, t \geq 5 \text{ sec}. \quad \text{The}$$

simulation result is shown in Fig. 5.19 and frequency responses of output sensitivity functions are shown in Fig. 5.20.

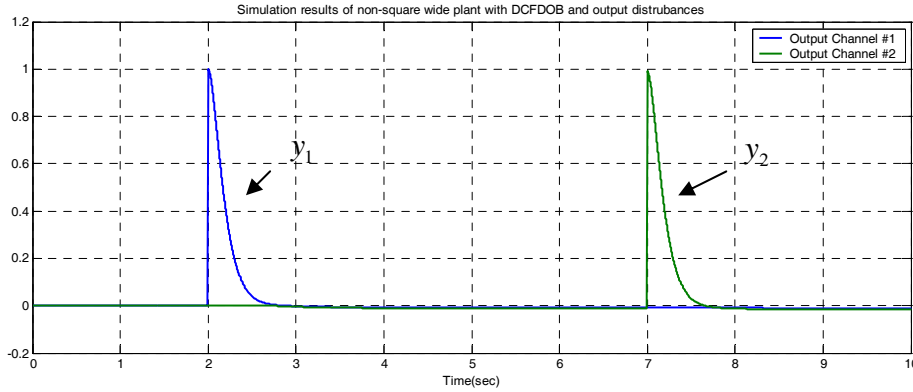


Fig. 5.19 Simulation results of output disturbances for non-square wide plant

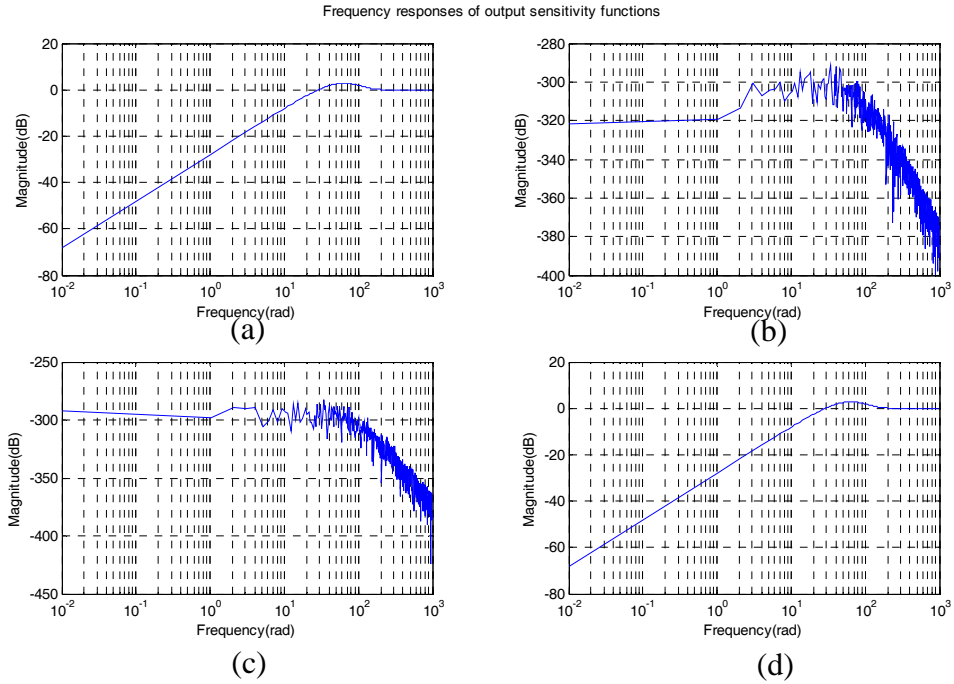


Fig. 5.20 Frequency responses of output sensitivity functions of part 3 – example 2

$$\begin{aligned}
 & \text{(a)} S_{o,11} : d_{o,1} \rightarrow y_1 \quad \text{(b)} S_{o,12} : d_{o,2} \rightarrow y_1 \\
 & \text{(c)} S_{o,21} : d_{o,2} \rightarrow y_1 \quad \text{(d)} S_{o,22} : d_{o,2} \rightarrow y_2
 \end{aligned}$$

To eliminate the input disturbance, the design objective becomes

$$Q_{3 \times 3} \cdot Y_{l,3 \times 2} \cdot \tilde{N}_{n,2 \times 3} = \begin{bmatrix} J_{11} & 0 & 0 \\ 0 & J_{22} & 0 \\ 0 & 0 & J_{33} \end{bmatrix}. \quad \text{It seems that we can design nine parameters,}$$

$Q_{11} \sim Q_{33}$ , to satisfy nine equations, however, if we rewrite  $Q_{3 \times 3} \cdot Y_{l,3 \times 2} \cdot \tilde{N}_{n,2 \times 3}$  as a

linear equation,  $\mathbf{AX} = \mathbf{B}$ , where

$$\mathbf{A} = \begin{bmatrix} [\mathbf{A}']_{3 \times 3} & [0]_{3 \times 3} & [0]_{3 \times 3} \\ [0]_{3 \times 3} & [\mathbf{A}']_{3 \times 3} & [0]_{3 \times 3} \\ [0]_{3 \times 3} & [0]_{3 \times 3} & [\mathbf{A}']_{3 \times 3} \end{bmatrix}_{9 \times 9}, \quad \mathbf{X} = \begin{bmatrix} Q_{11} \\ Q_{12} \\ \vdots \\ Q_{33} \end{bmatrix}_{9 \times 1}, \quad \mathbf{B} = \begin{bmatrix} J_{11} \\ 0 \\ 0 \\ 0 \\ J_{22} \\ 0 \\ 0 \\ 0 \\ J_{33} \end{bmatrix}_{9 \times 1} \quad (5.27)$$

$$\text{and } \mathbf{A}' = \begin{bmatrix} \tilde{N}_{n,11}Y_{l,11} + \tilde{N}_{n,21}Y_{l,12} & \tilde{N}_{n,11}Y_{l,21} + \tilde{N}_{n,21}Y_{l,22} & \tilde{N}_{n,11}Y_{l,31} + \tilde{N}_{n,21}Y_{l,32} \\ \tilde{N}_{n,12}Y_{l,11} + \tilde{N}_{n,22}Y_{l,12} & \tilde{N}_{n,12}Y_{l,21} + \tilde{N}_{n,22}Y_{l,22} & \tilde{N}_{n,12}Y_{l,31} + \tilde{N}_{n,22}Y_{l,32} \\ \tilde{N}_{n,13}Y_{l,11} + \tilde{N}_{n,23}Y_{l,12} & \tilde{N}_{n,13}Y_{l,21} + \tilde{N}_{n,23}Y_{l,22} & \tilde{N}_{n,13}Y_{l,31} + \tilde{N}_{n,23}Y_{l,32} \end{bmatrix}$$

Furthermore, matrix  $\mathbf{A}'$  can be reduced as follows by row reduction.

$$\mathbf{A}'_{\text{reduced}} = \begin{bmatrix} 1 & 0 & \frac{Y_{l,22}Y_{l,31} - Y_{l,21}Y_{l,32}}{-Y_{l,12}Y_{l,21} + Y_{l,11}Y_{l,22}} \\ 0 & 1 & \frac{Y_{l,12}Y_{l,31} - Y_{l,11}Y_{l,32}}{Y_{l,12}Y_{l,21} - Y_{l,11}Y_{l,22}} \\ 0 & 0 & 0 \end{bmatrix} \quad (5.28)$$

and  $\text{rank}(\mathbf{A}'_{\text{reduced}}) = 2$ , i.e.  $\text{rank}(\mathbf{A}) = 6$ . Also, matrix  $[\mathbf{A} | \mathbf{B}]$  can be reduced by row reduction and we obtain that  $\text{rank}([\mathbf{A} | \mathbf{B}]) = 7$ , that is, the system is inconsistent and has no analytic solutions. Consequently, the performances of input disturbance rejection in wide plant system will not be good enough and a similar phenomenon as the output disturbance rejection in thin plant system will be obtained. We ignore the numerical simulations for input disturbances rejection in this thesis.

## 5.4 Numerical example part 4: the loop-shaping design method

In part 4, one demonstrates the steps of  $H_\infty$ -loop shaping design method of robust DCFDOB that developed in sections 4.3 and 4.4. A simple MIMO nominal plant is given as

$$P_n = \begin{bmatrix} \frac{1}{s+5} & \frac{2}{s+6} \\ \frac{5}{s+7} & \frac{3}{s+8} \end{bmatrix} \Leftrightarrow \left[ \begin{array}{cccc|cc} -5 & 0 & 0 & 0 & 1 & 0 \\ 0 & -7 & 0 & 0 & 2.236 & 0 \\ 0 & 0 & -6 & 0 & 0 & 1.414 \\ 0 & 0 & 0 & -8 & 0 & 1.732 \\ \hline 1 & 0 & 1.414 & 0 & 0 & 0 \\ 0 & 2.236 & 0 & 1.732 & 0 & 0 \end{array} \right] \quad (5.29)$$

The corresponding normalized coprime factorization factors are given in appendix C.

Figure 5.21(a) shows the singular values of the nominal plant. A dynamic

pre-weighting matrix  $W_1 = \text{diag} \left[ \frac{5(s+0.45)}{s}, \frac{5(s+0.45)}{s} \right]_{2 \times 2}$  contains an integral pole

and a zero at -0.45 is in use to improve low frequency performance and increase the

crossover frequency. The singular values of the shaped plant  $P_S = W_2 P_n W_1$  are shown

in Fig. 5.21(b). Moreover,  $W_2$  is an identity matrix. Figure 5.21(b) displays

$\underline{\sigma}(W_2 P_n W_1) \gg 1$  in low frequency ranges and  $\bar{\sigma}(W_2 P_n W_1) < 1$  in high frequency ranges,

i.e. it satisfies the shaping criteria for good performance and robustness. The

crossover frequency of  $\underline{\sigma}(W_2 P_n W_1)$  and  $\bar{\sigma}(W_2 P_n W_1)$  is  $1 \text{ rad/sec}$  and  $30 \text{ rad/sec}$ ,

respectively.

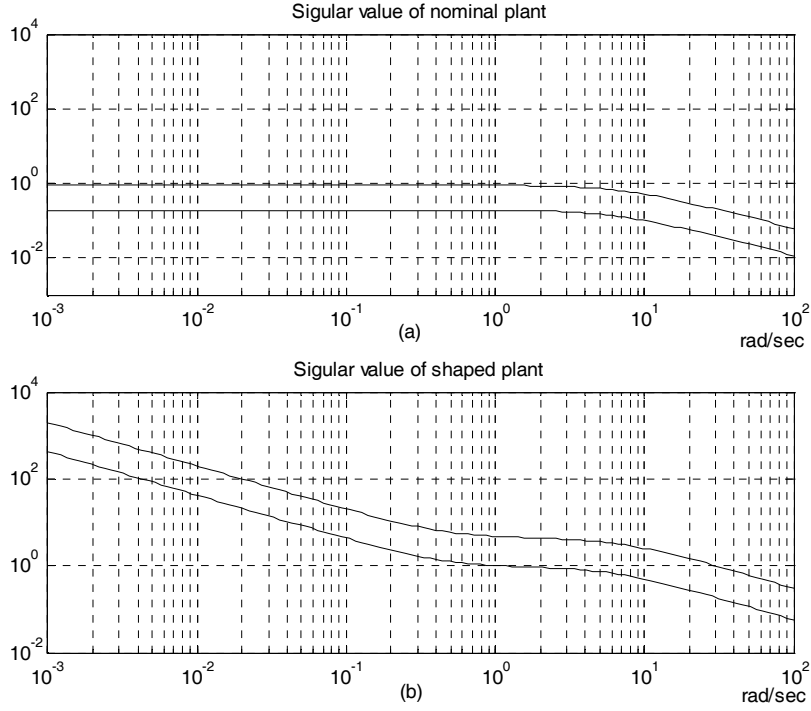


Fig. 5.21 Singular values: (a) the nominal plant (b) the shaped plant  $W_2 P_n W_1$

A solution  $K_\infty$  that satisfies Eq. (4.36) ( $\gamma_s = 1.2894$ ) is obtained by Eq. (4.21) to Eq. (4.25) and the final reduced DCFDOB  $K_{DOB}$  and parameter  $Q$  are derived from Eq. (4.37) and Eq. (4.38), respectively. Figure 5.22(a) and 5.22(b) show the upper / lower singular values of  $K_{DOB} P_n$  and  $P_n K_{DOB}$ , respectively and the crossover frequencies of  $\bar{\sigma}(K_{DOB} P_n)$  and  $\bar{\sigma}(P_n K_{DOB})$  are about  $20 \text{ rad/sec}$ . Figure 5.23(a) and 5.23(b) show the input and output sensitivity functions with the largest peak of 1.0355 and 1.0356, respectively. However, the controller reduction problem is considered to overcome a numerical problem: the extremely high order of parameter  $Q$  that derived from Eq. (4.38). In this example, a reduced parameter  $Q_{2 \times 2}$  matrix containing six orders elements is obtained using frequency matching and shown in appendix C.

Figures 5.24(a) and 5.24(b) plot the frequency responses of the origin parameter matrix  $Q_{2 \times 2}$  and the reduced parameter matrix, respectively.

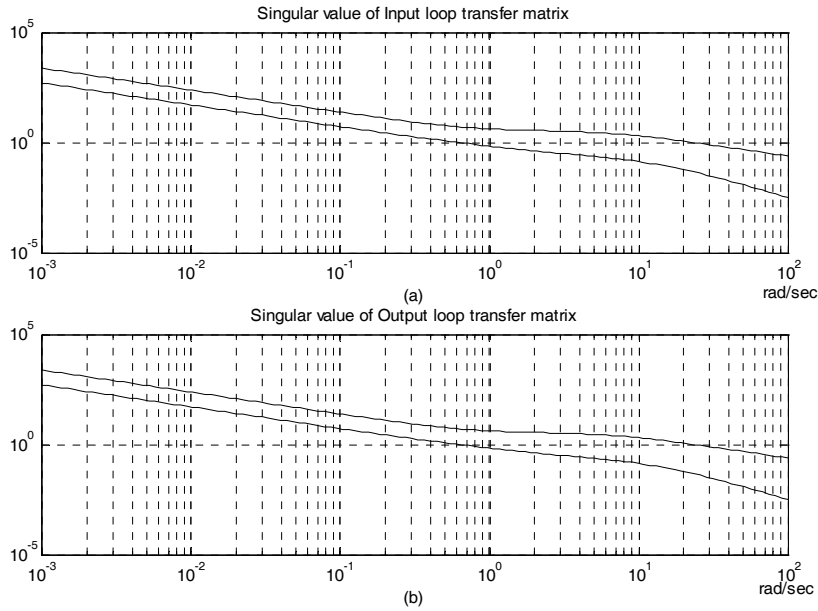


Fig 5.22 Singular values of (a)  $K_{DOB} P_n$  (b)  $P_n K_{DOB}$

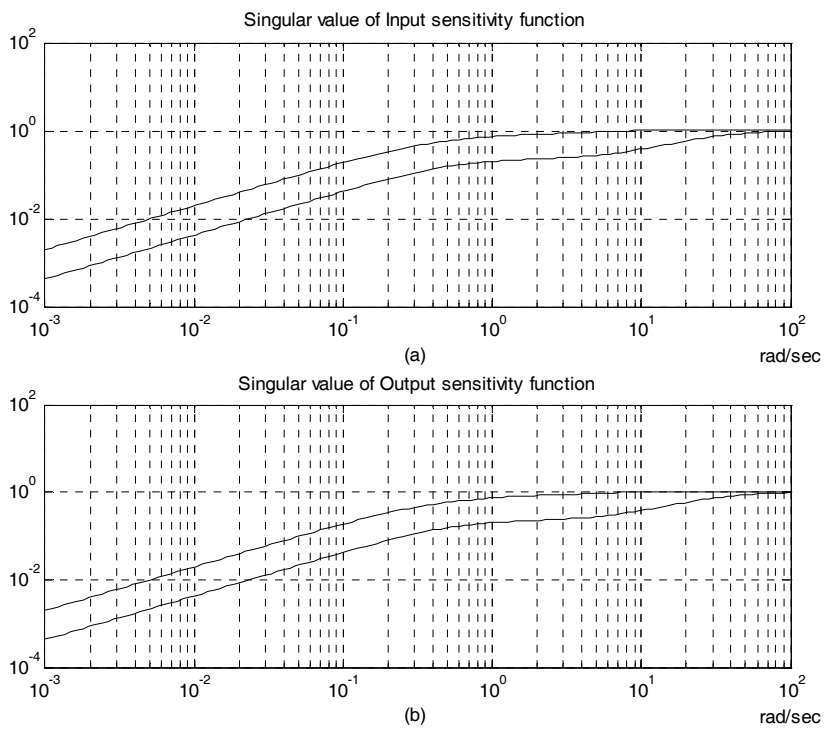


Fig. 5.23 Singular values of (a) input sensitivity function and

(b) output sensitivity function

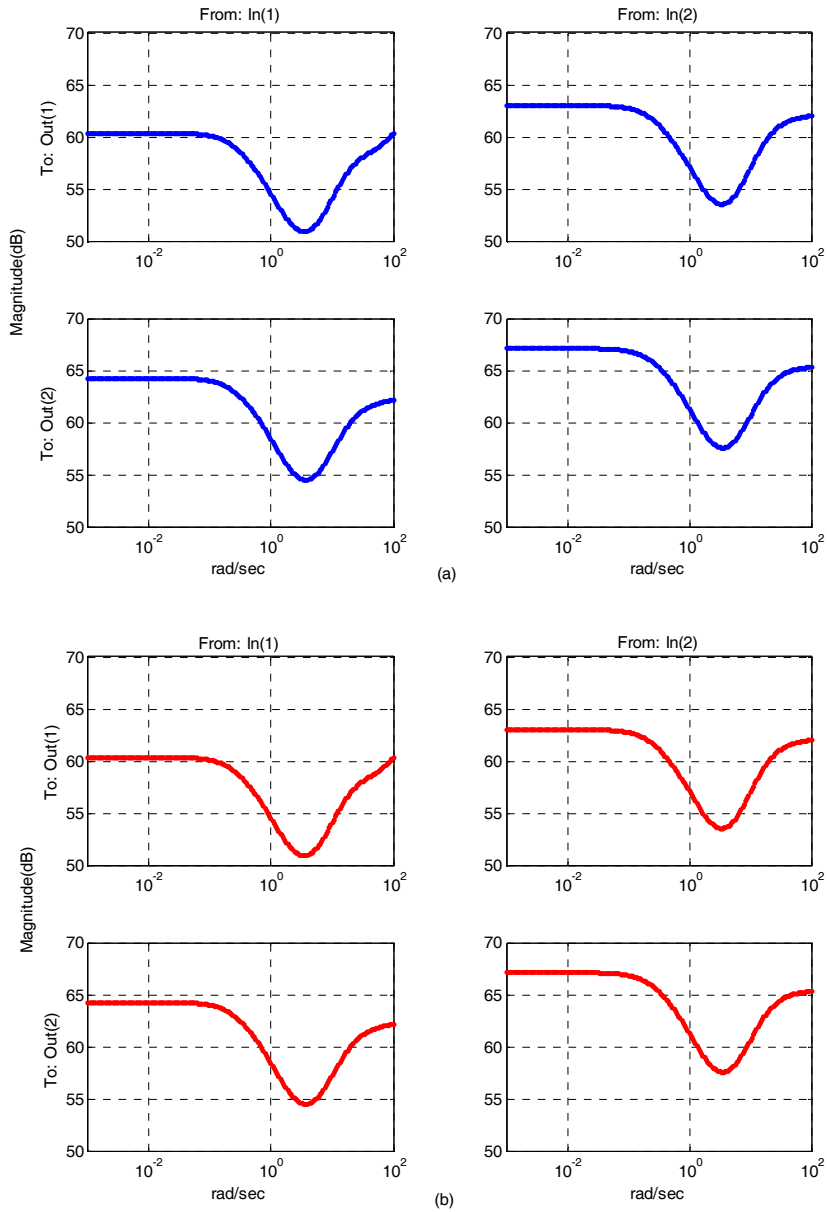


Fig. 5.24 Frequency responses of (a) the origin parameter matrix  $Q_{2 \times 2}$  and

(b) the reduced order parameter matrix

Figures 5.25(a) and 5.25(b) show the singular values of the original parameter matrix and the reduced parameter matrix, respectively. Moreover, the largest peaks of the input and output sensitivity functions with reduced  $Q$  filters are 1.0355 and 1.0356,

respectively. In Fig. 5.25(a), the singular values with original parameter matrix almost overlap with the ones of the reduced parameter matrix except a slight deterioration in low frequency. And a similar phenomenon is observed in Fig. 5.25(b), i.e. the parameter reduction is acceptable. Figures 5.26(a)-(d) present the unit step input /

output disturbances rejection performance with plant uncertainty  $\left\| \begin{bmatrix} \Delta_N \\ \Delta_M \end{bmatrix} \right\|_\infty = 0, 0.2254,$

0.3944 and 0.4111, respectively. Input disturbances  $D_i = \begin{bmatrix} d_{i,1} \\ d_{i,2} \end{bmatrix} = \begin{bmatrix} u_1(t-10) \\ u_2(t-10) \end{bmatrix}$  and

output disturbances  $D_o = \begin{bmatrix} d_{o,1} \\ d_{o,2} \end{bmatrix} = \begin{bmatrix} u_1(t-30) \\ u_2(t-30) \end{bmatrix}$  are given.

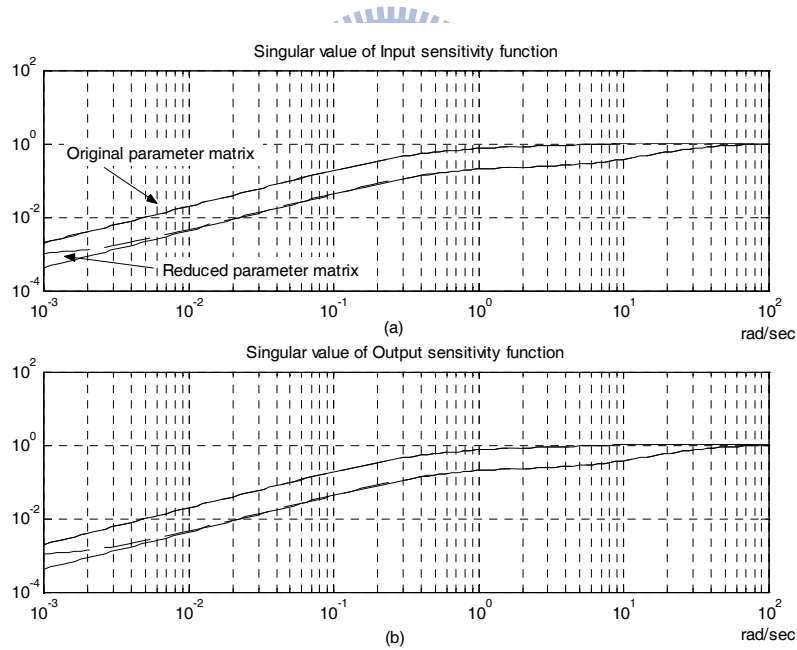


Fig 5.25 The Singular values of (a) the original parameter matrix (solid line) and  
(b) the reduced parameter matrix (dashed line)



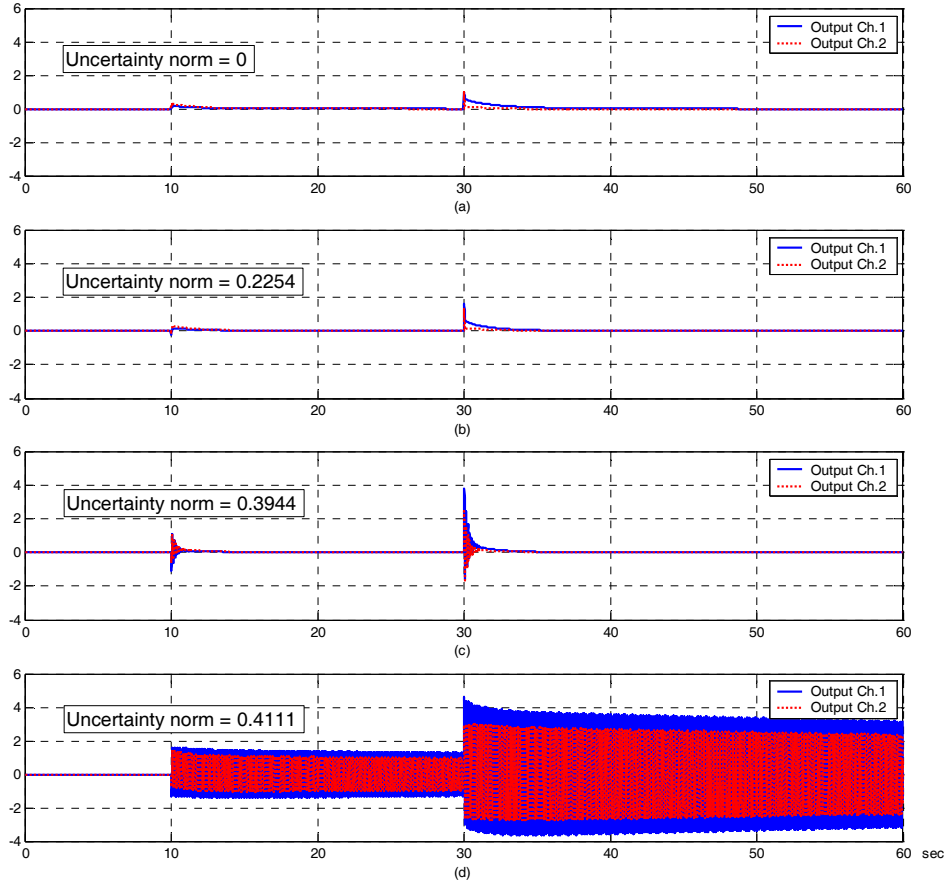


Fig. 5.26 Simulation results with various uncertainty norms of part 4

$$\begin{aligned}
 \text{(a)} \quad \left\| \begin{bmatrix} \Delta_N \\ \Delta_M \end{bmatrix} \right\|_{\infty} &= 0 & \text{(b)} \quad \left\| \begin{bmatrix} \Delta_N \\ \Delta_M \end{bmatrix} \right\|_{\infty} &= 0.2254 \\
 \text{(c)} \quad \left\| \begin{bmatrix} \Delta_N \\ \Delta_M \end{bmatrix} \right\|_{\infty} &= 0.3944 & \text{(d)} \quad \left\| \begin{bmatrix} \Delta_N \\ \Delta_M \end{bmatrix} \right\|_{\infty} &= 0.4111
 \end{aligned}$$

Figures 5.27 - 5.34 show the singular values of achieved loops and corresponding upper boundaries of Eqs. (4.45)-(4.52). According to Eqs. (4.45)-(4.52) and corresponding Figs (5.27)-(5.34), we know that these upper boundaries only depend on  $\gamma_s$ ,  $W_1$ ,  $W_2$  and  $P_n$ , that is the designer can select the weighting functions much more visually and

quickly. Take Fig. 5.27 for example, if a stability margin  $\gamma_s$ , a nominal plant  $P_n$ , i.e.  $M_s$  and weighting function  $W_1$  are given, the upper boundaries of  $\bar{\sigma}(S_i)$  can be obtained immediately without solving the controller  $K_\infty$  in Eq. (4.36).

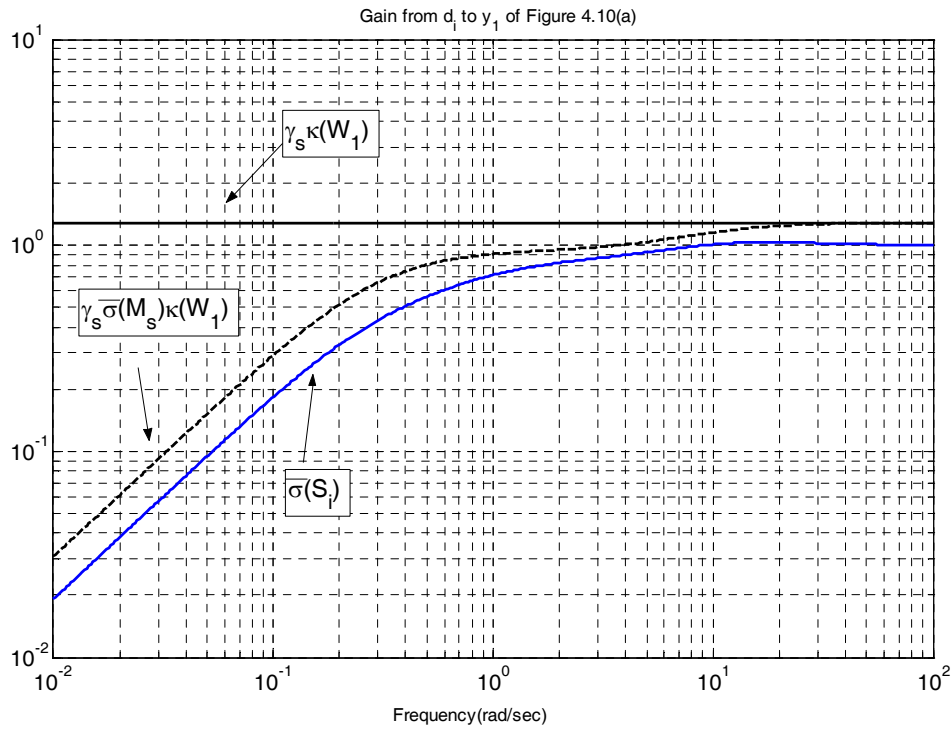


Fig. 5.27 The  $\bar{\sigma}(S_i(j\omega))$  and its corresponding upper boundaries plots of Eq. (4.45)

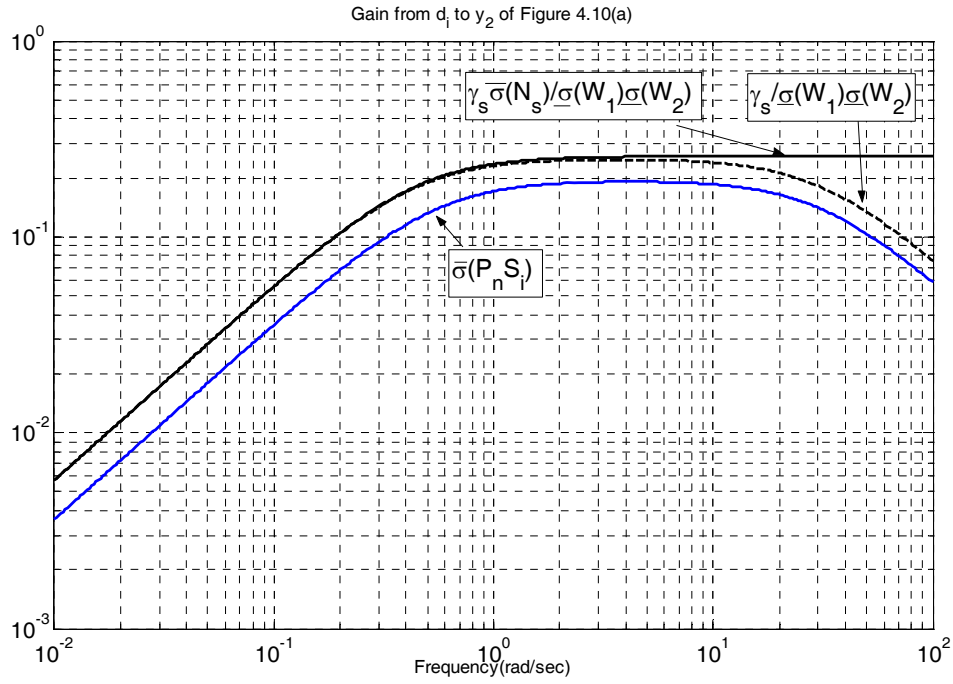


Fig. 5.28 The  $\bar{\sigma}(P_n S_i(j\omega))$  and

its corresponding upper boundaries plots of Eq. (4.46)

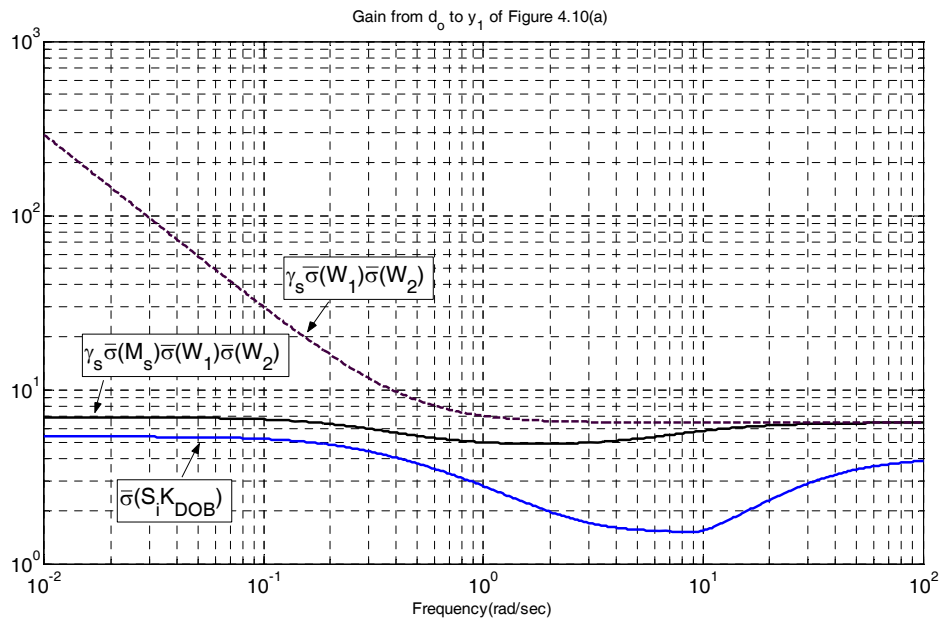


Fig. 5.29 The  $\bar{\sigma}(S_i K_{DOB}(j\omega))$  and

its corresponding upper boundaries plots of Eq. (4.47)

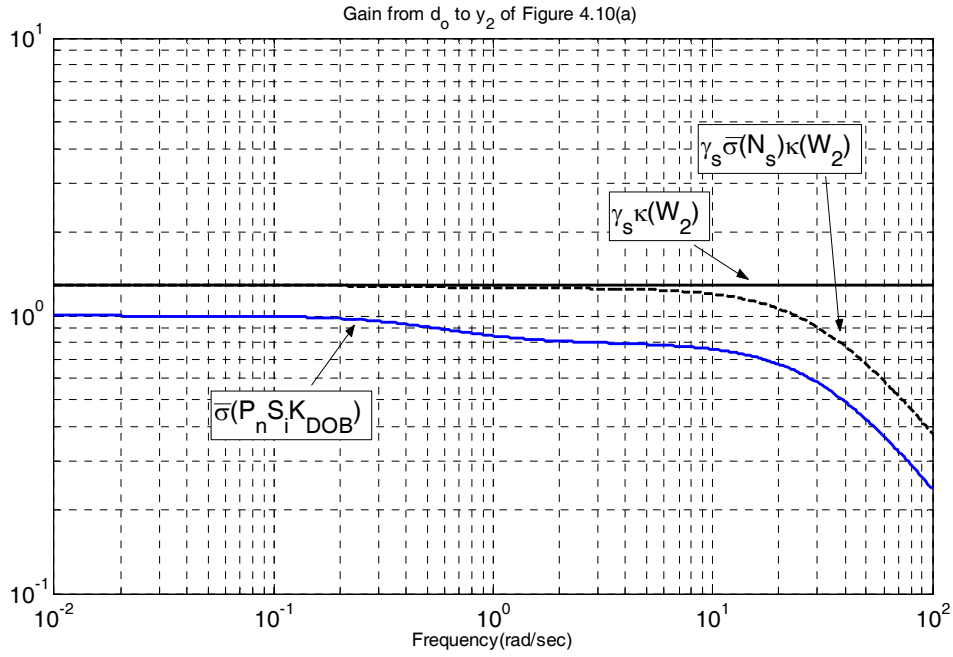


Fig. 5.30 The  $\bar{\sigma}(P_n S_i K_{DOB}(j\omega))$  and

its corresponding upper boundaries plots of Eq. (4.48)

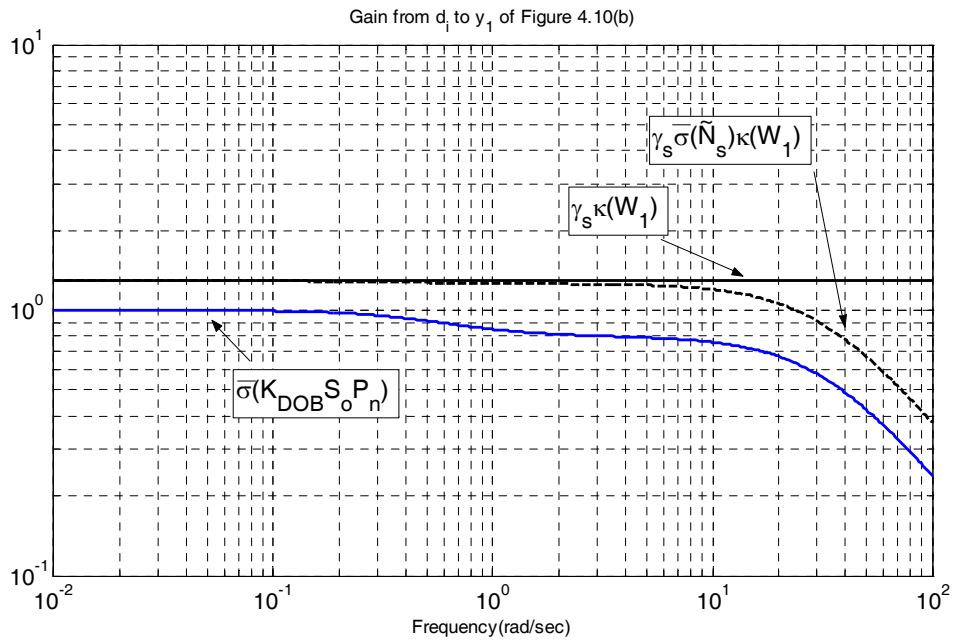
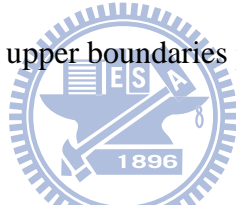


Fig. 5.31 The  $\bar{\sigma}(K_{DOB} S_o P_n(j\omega))$  and

its corresponding upper boundaries plots of Eq. (4.49)

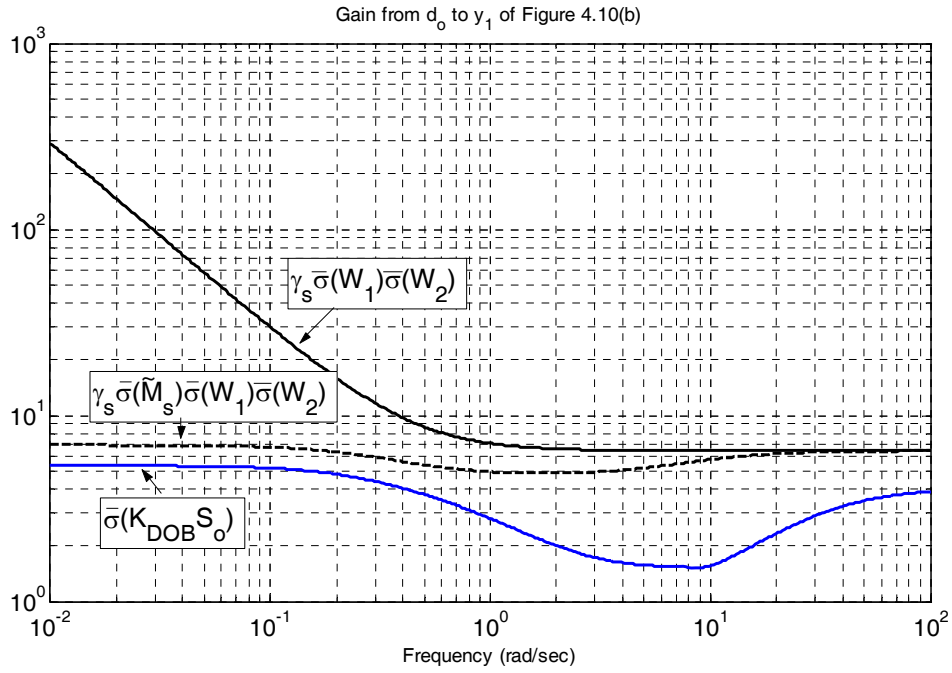


Fig. 5.32 The  $\bar{\sigma}(K_{DOB}S_o(j\omega))$  and

its corresponding upper boundaries plots of Eq. (4.50)

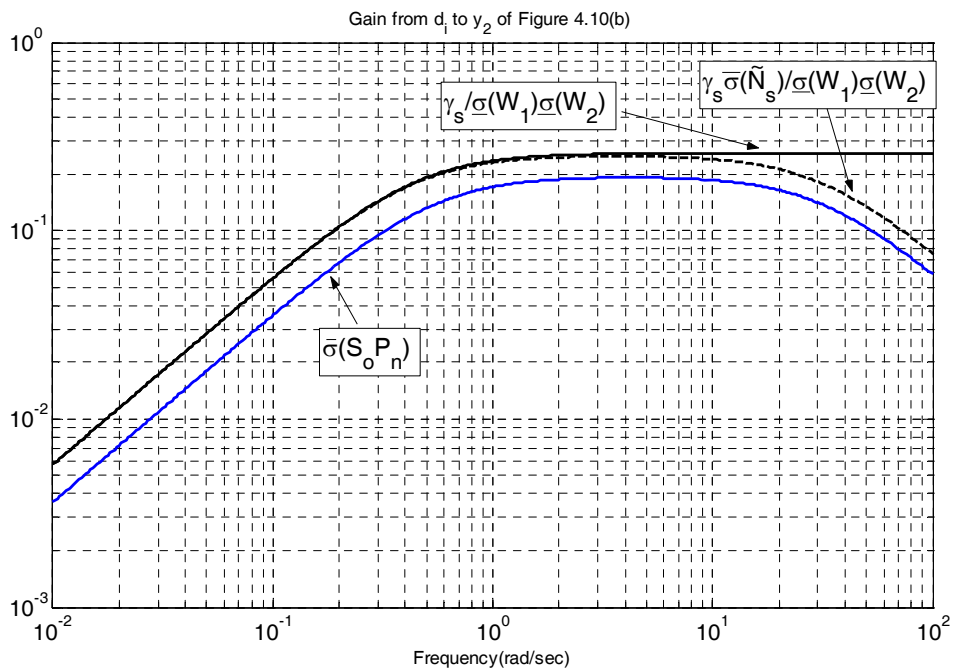
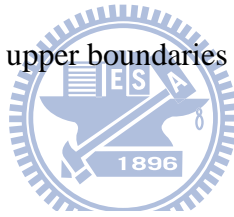


Fig. 5.33 The  $\bar{\sigma}(S_o P_n(j\omega))$  and

its corresponding upper boundaries plots of Eq. (4.51)

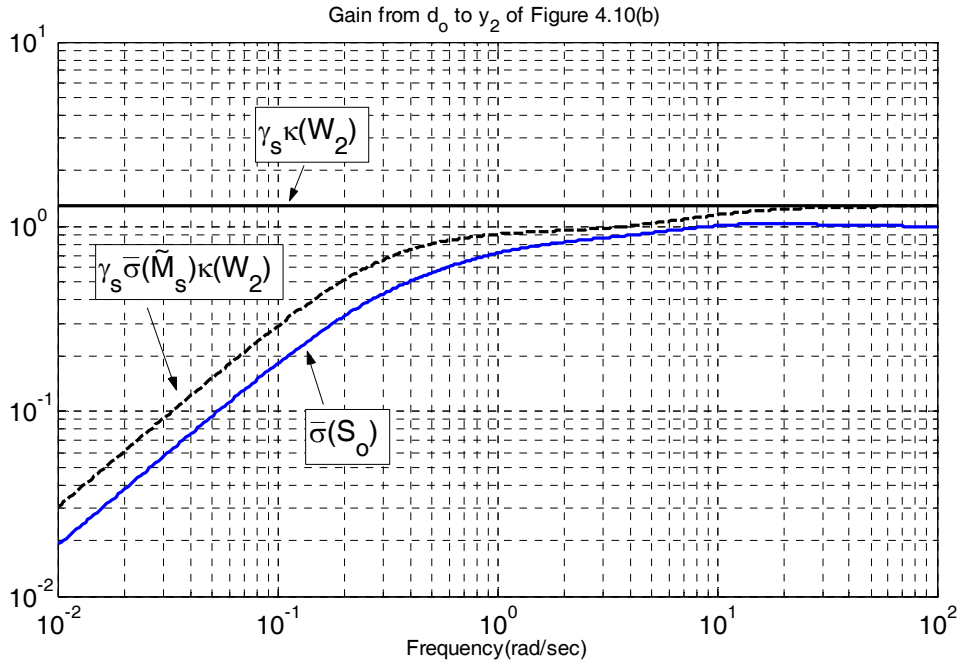


Fig. 5.34 The  $\bar{\sigma}(S_0(j\omega))$  and its corresponding upper boundaries plots of Eq. (4.52)

## 5.5 Part 5: experimental results of an AC servo motor

After showing these numerical examples, one demonstrates that this DCFDOB structure can be applied to general system cases and deal with input and output disturbances.

An experiment result of a rotate positioning control for an AC servomotor system and cogging force suppressing will be shown in the following.

In general, the electronic dynamic is so fast that the transfer function of AC servo driver can be treated as a constant gain. For simplicity, the high frequency modes coming from both the support mechanical structure of the motor and electronic system are ignored. The transfer function from input voltage to output rotating position can be simplified as Eq. (5.30) and the physical parameters of experiment are given in table 5.1.

$$P_n = \frac{K_a \cdot K_t}{s(J_m s + B_m)} = \frac{40}{s(15.9183 \cdot s + 65.5164)} \quad (5.30)$$

where  $K_t$  is torque constant and  $K_a$  is the driver's constant. Furthermore, the corresponding coprime factors are given as below

$$\begin{aligned} M_n &= \frac{s^2 + 4.241s}{s^2 + 130s + 4200} & N_n &= \frac{2.513}{s^2 + 130s + 4200} \\ X_r &= \frac{s^2 + 2626s + 1.878 \times 10^6}{s^2 + 2500s + 1.560 \times 10^6} & Y_r &= \frac{8.172 \times 10^7 s + 2.608 \times 10^9}{s^2 + 2500s + 1.560 \times 10^6} \end{aligned} \quad (5.31)$$

Table 5.1 Physical parameters of AC servomotor of experiment

Parameter	Value	Unit
Inertial, $J_m$	15.9183	$Kg \cdot m^2$
Viscous, $B_m$	67.5164	$N \cdot m \cdot sec/rad$
Electronic system gain constant, $K_a \cdot K_t$	40	$Nt/Volt$
Encoder Resolution	8000	$counter/rev$

Since the servomotor system is a minimum phase system, the parameter  $Q(s)$  is designed as  $Q(s) = J \cdot N_n^{-1} \cdot Y_r^{-1}(s)$  to suppress input disturbances, i.e. cogging force and Coulomb friction force, and a low-pass filter with bandwidth of  $508 rad/s$  and an output feedback controller  $K(s)$  are given as

$$J(s) = \frac{10^9}{(s + 1000)^3} \quad (5.32)$$

$$K(s) = \frac{8.172 \times 10^7 (s + 31.91)}{(s^2 + 2626s + 1.878 \times 10^6)} \quad (5.33)$$

The position command is given as an S curve and motor position arrives at 4000 counts (half revolution) at 5sec. The tracking responses and tracking errors are plotted in Figs. 5.35(a)-(b). From these figures, the tracking error without DFCDOB compensation is influenced by not only cogging force but also measurement noise and the error of compensated one only influenced by measurement noise and constant tracking error.



Tracking errors from 1sec to 4sec (constant rotating speed) and each frequency analysis are shown in Fig. 5.36(a)-(d). The uncompensated tracking error is about 40-60 counts and the cogging force makes the tracking error approximate sinusoid wave and the compensated one is about 10 counts. From the frequency analysis plot in Fig. 5.36(c), there exists a peak around 1.2Hz. Comparing the one using DCFDOB at the same scale of Y-axis in Fig. 5.36(d), one finds that the influence of compensated one almost invisible.

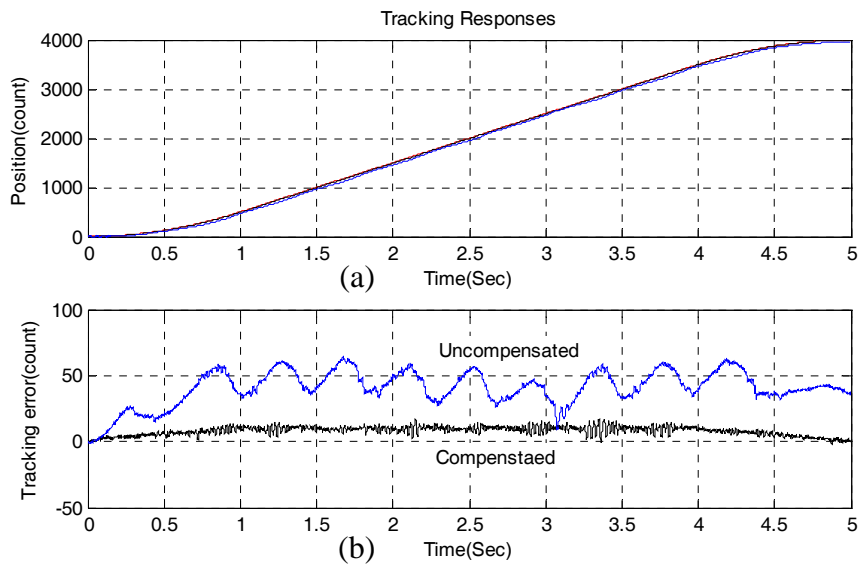


Fig. 5.35 (a)Tracking responses of 4000 counts position command

(b) Tracking errors of 4000 counts position command

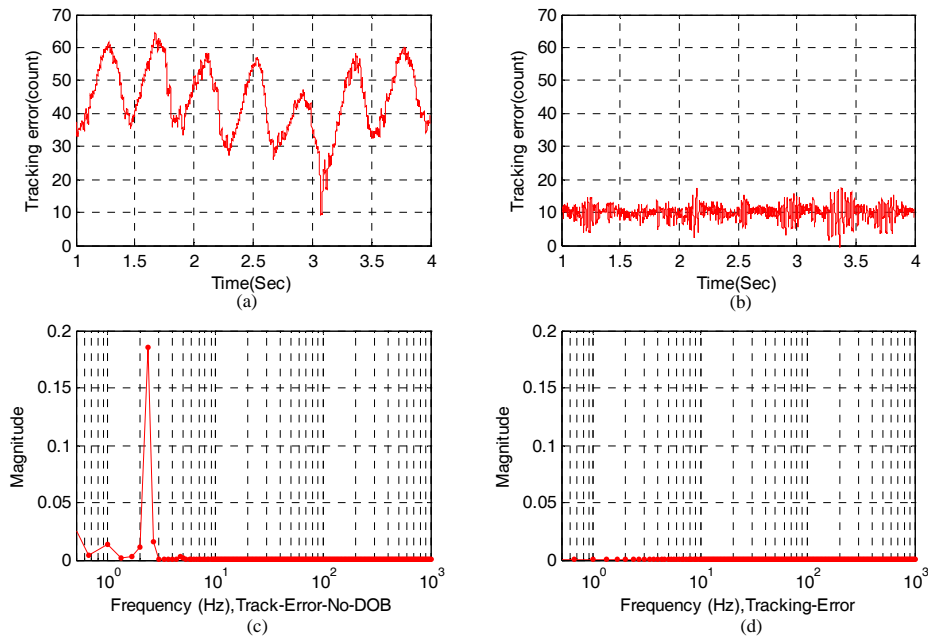


Fig. 5.36 (a) Tracking errors without DCFDOB from 1 sec to 4 sec

(b) Tracking errors with DCFDOB from 1 sec to 4 sec

(c) Frequency analysis of Fig. 5.36(a)

(d) Frequency analysis of Fig. 5.36(b)

Figures 5.37(a)-(b) and 5.38(a)-(b) show the extra-low rotating speed experiment results which rotating at  $0.01\text{ rev/sec}$  and  $0.005\text{ rev/sec}$  and the position arrives 400 ( $18^\circ$ ) and 200 ( $9^\circ$ ) counts at 5sec, respectively. The tracking response which without disturbance compensator has large tracking error and the friction also influences the positioning accuracy seriously. The root-mean-square values of compensated tracking error is about 1.8691 counts ( $0.0837^\circ$ ) and 1.2709 counts ( $0.0572^\circ$ ), respectively.

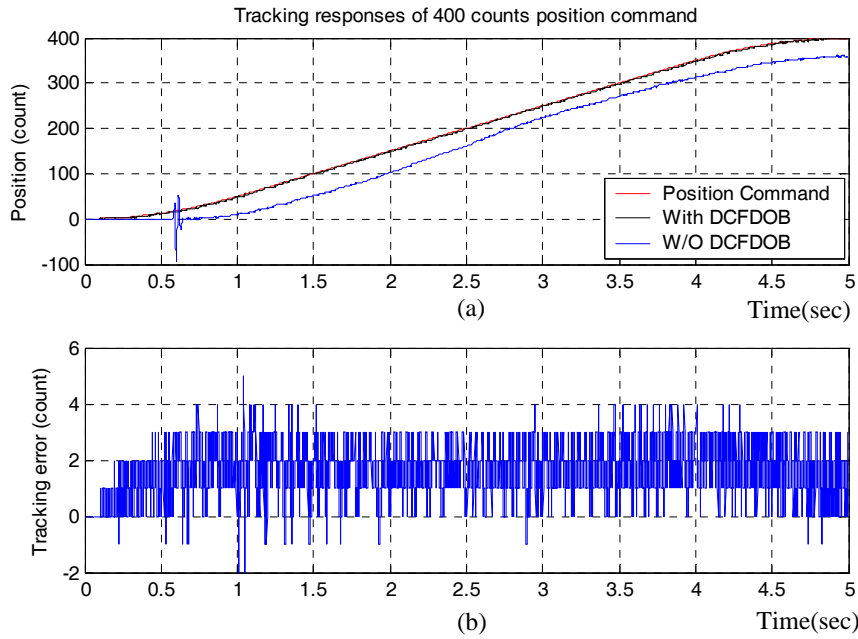


Fig. 5.37 (a)Tracking responses of 400 counts ( $18^\circ$ ) position command

(b)Tracking error of 400 counts ( $18^\circ$ ) position command with DCFDOB

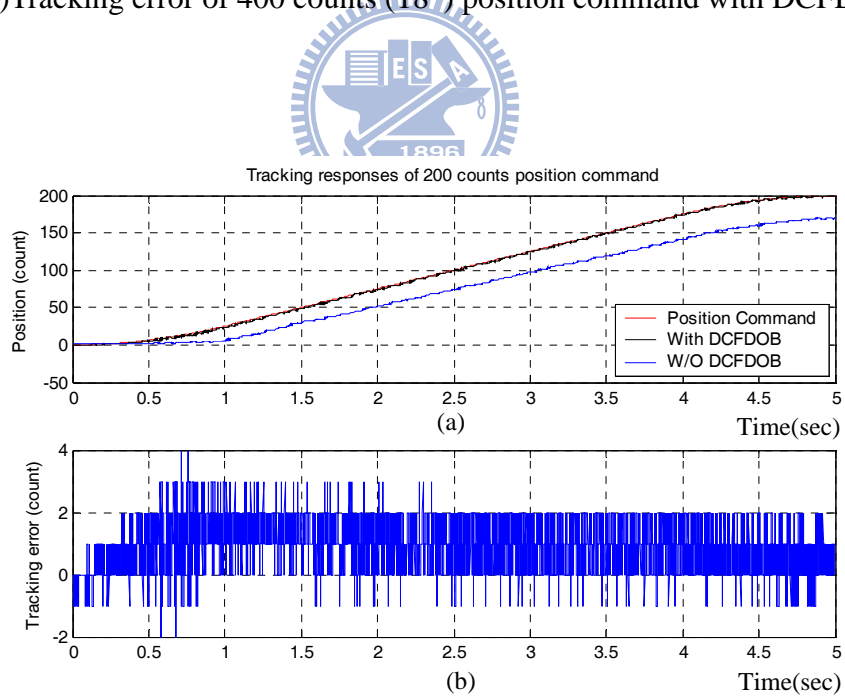


Fig. 5.38 (a)Tracking responses of 200 counts ( $9^\circ$ ) position command

(b)Tracking error of 200 counts ( $9^\circ$ ) position command with DCFDOB

## CONCLUSION AND FUTURE WORK

This dissertation provided a new Doubly Coprime Factorization Disturbance Observer structure that motivated from *Bezout Identity* and doubly coprime factorization. After introducing the DCFDOB structure, one analyzed the properties of this structure and presented how the parameter  $Q(s)$  be designed. Moreover, this dissertation also discussed the waterbed effect, model matching method and system robust stability as well as input and output disturbances for generality. When the plant is non-square, the non-square type will restrict the capability of disturbance elimination and we knew that to eliminate the input disturbance completely, the output channel numbers must greater / equal than input channel numbers and duality. Finally, four numerical examples are presented to demonstrate the design methods. One also studied Vidyasagar's structure and combined it with our DCFDOB to form a 2DOF system. The feedback system which made by Vidyasagar's structure provides the tracking property while the DCFDOB provides the disturbance attenuation; furthermore, this novel structure attains to internal stability. After that, one looked into the plant uncertainty and system robustness. One of the advantages of the DCFDOB is that the actual plant will be forced to the nominal plant while the disturbance is rejected. After discussing the robust properties of the DCFDOB, one discussed how the robust DCFDOB to be designed to have robust stability under a given plant uncertainty bound. Besides, to

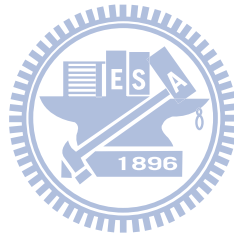
have the robust performance, the robust DCFDOB is obtained by  $H_\infty$ - loop shaping design method and all closed – loop objectives bounds are guaranteed. In the final chapter, from the numerical examples, one knew that the design of DCFDOB is more flexible than the traditional one, and the DCFDOB eliminates both input and output disturbances simultaneously in SISO and square MIMO system. This is one of the main contributions of the DCFDOB structure; furthermore, one can also keep down the influence of plant uncertainties to push the actual plant to nominal plant and design an outer loop controller for more accurate and simple tracking control. There are still remaining many interesting topics that can be researched in the future, such as

1. The optimum Q parameter for non-square plants. For a specific non-square type, a corresponding index, for example, the cost function of tracking error can be found to design the optimum Q parameter.
2. Disturbance rejection in non-square, non-minimum phase plant cases. As mentioned in chapter 3, the non-square, non-minimum phase plant was formed as a 4-block Nehari problem. It is a complex problem and can be looked into in the future.
3. The advanced research such as system robustness for DCFDOB-VS and the design method for  $H(s)$  parameter. In this dissertation, we only used a simple method to obtain the  $H(s)$  parameter in minimum phase plants.

However, it cannot be utilized in non-minimum phase and non-square system.

The way for designing a better  $H(s)$  parameter is an interesting topic.

4. Extend the DCFDOB to the system with time delay. [43] researched the predictive disturbance observer based control for a time delay system. In that dissertation, the author decomposed the non-minimum phase into two parts, the minimum phase part and the non-minimum phase one, to attain to system stability and realization. This concept is similar to the one of coprime factorization and some references, [44]-[46], can be referred for this topic.



## REFERENCE

- [1] K. Ohnishi, "A new servo method in mechatronics," *Transaction on Japan Society of electronic Engineering* 1987; **107**(D):83—86.
- [2] H. S. Lee and M. Tomizuka, "Robust motion controller design for high-accuracy positioning systems," *IEEE Transaction on Industrial Electronics* 1996; **43**(1):48—55.
- [3] S. Komada, N. Machii and T. Hori, "Control of redundant manipulators considering order of disturbance observer," *IEEE Transaction on Industrial Electronics* 2000; **47**(2):413—420.
- [4] M. T. White, M. Tomizuka and C. Smith, "Improved track following in magnetic disk drives using a disturbance observer," *IEEE/ASME Transaction on Mechanics* 2000; **5**(1):3—11.
- [5] R. H. Horng, H. L. Chou and A. C. Lee, "Rejection of limit cycles induced from disturbance observers in motion control," *IEEE Transaction on Industrial Electronics* 2006; **53**(6):1770—1780.
- [6] S. H. Choi, J. S. Ko, I. D. Kim, J. S. Park and S. C. Hong, "Precise position control using a PMSM with a disturbance observer containing a system parameter compensator," *IEE Proceedings-Electric power Applications* 2005; **152**(6):1573—1577.

- [7] K. B. Lee, "Disturbance observer that uses radial basis function networks for the low speed control of a servo motor," *IEE Proceedings-Electric power Applications* 2005; **152**(2):118—124.
- [8] M. Danesh, F. Sheikholeslam and M. Keshmiri, "An adaptive manipulator controller based on force and parameter estimation," *IEICE Transaction on Fundamentals of Electronics Communications and computer Sciences* 2006, **E89A**(10):2803—2811.
- [9] Y. Y. Huang, R. H. Horng, Y. T. Shih and A. C. Lee, "Dual-position-controller design for the linear-motor-driven motion system," *Journal of System Design and Dynamics* 2007; **1**(2):270—282.
- [10] S. Katsura, Y. Matsumoto and K. Ohnishi, "Modeling of force sensing and validation of disturbance observer for force control," *IEEE Transaction on Industrial Electronics* 2007; **54**(1):530—538.
- [11] T. Umeno, T. Kaneko and Y. Hori, "Robust Servo system design with two degrees of freedom and its application to novel motion control of robot manipulators," *IEEE Transaction on Industrial Electronics* 1993; **40**(5):473—485.
- [12] M. Vidyasagar, *Control System Synthesis: A Factorization Approach*, MIT Press, 1994.



- [13] J. H. Shin, K. Fujiune, T. Suzuki, S. Okuma and K. Yamada, "Positioning control of direct drive robot with two-degree-of-freedom compensator," *IEEE International Conference on Robotics and Automation*, Nagoya, Japan, May 21-27, 1995; 3137—3142.
- [14] K. Yamada, S. Komada, M. Ishida and T. Hori, "Characteristics of servo system using high order disturbance observer," *IEEE Conference on Decision and Control-Proceedings*, Kobe, Japan, Dec. 11-13, 1996; 3252—3257.
- [15] Y. Choi, W. K. Chung and Y. Youm, "Disturbance observer in  $H_\infty$  frameworks," *Proceedings of the 1996 IEEE IECON-22<sup>nd</sup> International Conference on Industrial Electronics, Control, and Instrumentation*, Taipei, Taiwan, Aug. 05-10 1996; 1394—1400.
- [16] K. Yamada, S. Komada, M. Ishida and T. Hori, "Robust control of robot manipulators by MIMO disturbance observer," *Proceedings of the 24<sup>th</sup> Annual conference of the IEEE Industrial Electronics Society*, Aachen, Germany, Aug. 31-Sep. 04, 1998; 1451—1456.
- [17] S. Komada, N. Machii, and T. Hori, "Control of redundant manipulators considering order of disturbance observer," *IEEE Transaction on Industrial Electronics* 2000; **47**(2):413—420.
- [18] M. T. White, M. Tomizuka, and C. Smith, "Improved Track Following in

- Magnetic Disk Drives Using a Disturbance Observer,” *IEEE/ASM Transactions on Mechatronics* 2000; **5**(1):3—11.
- [19] K. Ohishi, H. Kudo, K. Arai and H. Tokumaru, “Robust high speed tracking servo system for optical disk system,” *6<sup>th</sup> International Workshop on Advanced Motion Control, Proceedings*, Nagoya, Japan, Mar. 30-Apr. 01, 2000; 92—97.
- [20] K. J. Yang, Y. J. Choi, W. K. Chung, “On the tracking performance improvement of optical disk drive servo systems using error-based disturbance observer,” *IEEE Transactions on Industrial electronics* 2005; **52**(1):270—279.
- [21] Y. J. Choi, K. J. Yang, W. K. Chung, H. R. Kim, and I. H. Suh, “On the robustness and performance of disturbance observers for second-order systems,” *IEEE Transactions on Automatic control* 2003; **48**(2):315—320.
- [22] X. Chen, G. Zhai and T. Fukuda, “An approximate inverse system for non-minimum phase systems and its application to disturbance observer,” *System & control letters* 2004; **52**(3-4):193—207.
- [23] W. C. Yang and M. Tomizuka, “Disturbance rejection through an external model for non-minimum phase systems,” *Journal of Dynamic Systems Measurement and Control-Transactions of the ASME* 1994; **116**(1):39—44.
- [24] J. Chang, “Applying discrete-time proportional integral observers for state and disturbance estimations,” *IEEE Transaction on automatic Control* 2006;

51(5):814—818.

- [25] M. Yang and Y. Shiu, “Theory and application of a combined feedback-feedforward control and disturbance observer in linear motor drive wire-EDM machines,” *International Journal of Machine Tools and Manufacture* 2008; **48**:388—401.
- [26] H. Shim, N. H. Jo and Y. I. Son, “A new disturbance observer for non-minimum phase linear systems,” *Proceedings of the American Control conference*, Seattle, Washington, USA, June 11-13, 2008; 3385—3389.
- [27] C. N. Nett, C. A. Jacobson and M. J. Balas, “A connection between state-space and doubly coprime fractional representations,” *IEEE Transaction on Automatic Control* 1984; **29**(9):831—832.
- [28] F. W. Fairman: *Linear control theory: The state space approach*, New York, USA, John Wiley & Sons, 1998.
- [29] F. B. Yeh, C. D. Yang, *Post Modern Control Theory and Design*, Chinese Edition. Taipei: Eurasia Book Company, 1992
- [30] Z. Nehari, “On bounded bilinear forms,” *The Annals of Mathematics* 1957; **65**(1):153—162.
- [31] V. M. Adamjan, D. Z. Arov, and M. G. Krein, “Infinite block hankel matrices and related extension problems,” *Transactions of the American Mathematical*

*Society* 1978; **111**: 133—156.

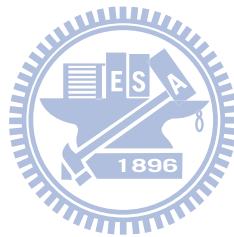
- [32] J. S. Freudenberg and D. P. Looze, “Right half plane poles and zeros and design tradeoffs in feedback systems,” *IEEE Transactions on Automatic Control* 1985; **30**(6): 555—565.
- [33] Y. Y. Huang and A. C. Lee, “Generalization of all stabilizing compensators for finite-dimensional linear systems,” *Journal of the Franklin Institute-engineering and Applied Mathematics* 2007; **344**(8): 1075—1090.
- [34] M. Vidyasagar, *Control System Synthesis*. Cambridge, MA: MIT Press, 1985.
- [35] M. Vidyasagar and N. Viswanadham, “Stabilization of linear and non-linear dynamical-system using an observer-controller configuration,” *Systems & Control Letters* 1981; **1**(2):87—91.
- [36] K. Zhou and J. C. Doyle, *Essential of Robust Control*, Upper Saddle River, New Jersey: Prentice-Hall, 1998.
- [37] F. B. Yeh and C. D. Yang, “Singular value decomposition of an infinite block-hankel matrix and its applications,” *Numerical Functional Analysis and Optimization* 1987; **9**(7—8): 881—916.
- [38] C. D. Yang and F. B. Yeh, “One-step extension approach to optimal Hankel-norm approximation and  $H_\infty$  optimization problem,” *IEEE Transactions on Automatic Control* 1993; **38**(5): 674—688.

- [39] J. C. Doyle, K. Glover, P. P. Khargonekar and B. A. Francis, “State-space solutions to standard  $H_2$  and  $H_\infty$  control problems,” *IEEE Transactions on Automatic Control* 1989; **34**(8):831—847.
- [40] K. Glover, D. J. N. Limebeer, J. C. Doyle, E. M. Kasenally and M. G. Safonov, “A characterization of all solutions to the 4-block general disturbance problem,” *SIAM Journal on Control and Optimization* 1991; **29**(2): 283—324.
- [41] K. Glover and D. C. McFarlane, “Robust stabilization of normalized coprime factor plant description with  $H_\infty$ - bounded uncertainty.” *IEEE Transactions on Automatic Control* 1989; **34**(8): 821—830.
- [42] D. C. McFarlane and K. Glover, Robust Controller Design Using Normalized Coprime Factor Plant Descriptions, **138**, Lecture Notes in Control and Information Sciences, New York, Springer-Verlag, 1990.
- [43] 林俞誠，「基於預測干擾觀測器之控制方法於時間延遲系統」，碩士論文，國立交通大學機械研究所，中華民國九十八年七月
- [44] J. R. Partington and K. Glover, “Robust Stability of Delay System by Approximation of Coprime Factors.” *System & Control Letters* 1990; **14**(4): 325—331.
- [45] J. R. Partington and G. K. Sankaran, “Algebraic Construction of Normalized Coprime Factors for Delay Systems.” *Mathematics of Control Signal and*

*Systems* 2002; **15**(1): 1—12.

[46] I. Skrjanc, “Coprime-Factorized Model Predictive Control for Unstable Processes With Delay.” *Journal of Intelligent & Robotic Systems* 2007; **49**(3): 237—251.

[47] D. G. Zill and M. R. Cullen, *Advanced Engineering Mathematics*, Second Edition. Massachusetts: Jones and Bartlett Publishers, 2000.



## APPENDIX A

The corresponding coprime factorizations of example 2 of part 2 are given as follows.

$$\left[ \begin{array}{c|c} M_n & -Y_l \\ \hline N_n & X_l \end{array} \right] = \left[ \begin{array}{c|c|c} A+BF & B & -L \\ \hline F & I & 0 \\ \hline C+DF & D & I \end{array} \right], \left[ \begin{array}{c|c} X_r & Y_r \\ \hline -\tilde{N}_n & \tilde{M}_n \end{array} \right] = \left[ \begin{array}{c|c|c} A+LC & -(B+LD) & L \\ \hline F & I & 0 \\ \hline C & -D & I \end{array} \right] \quad (\text{A.1})$$

where

$$A = \begin{bmatrix} -0.5384 & -1.8968 & 0 & 0 & 0 & 0 \\ 1.8968 & -4.4616 & 0 & 0 & 0 & 0 \\ 0 & 0 & -3 & 0 & 0 & 0 \\ 0 & 0 & 0 & -4 & 0 & 0 \\ 0 & 0 & 0 & 0 & -0.8329 & -2.9205 \\ 0 & 0 & 0 & 0 & 2.9205 & -4.1671 \end{bmatrix}, B = \begin{bmatrix} -1.076 & 0 \\ 1.469 & 0 \\ 1 & 0 \\ 0 & 1 \\ 0 & 1.4088 \\ 0 & -1.7276 \end{bmatrix}$$

$$C = \begin{bmatrix} 1.076 & 1.469 & 0 & 1 & 0 & 0 \\ 0 & 0 & 1 & 0 & -1.4088 & -1.7276 \end{bmatrix}, D = \begin{bmatrix} 0 & 0 \\ 0 & 0 \end{bmatrix} \quad (\text{A.2})$$

and

$$F = \begin{bmatrix} 1.3340 & -0.2195 & -0.1958 & 0.2445 & 0.4269 & 0.2392 \\ -0.1101 & -0.2170 & 0.6329 & -0.1290 & -2.0199 & 0.2657 \end{bmatrix} \quad (\text{A.3})$$

$$L = \begin{bmatrix} -0.7599 & -0.1862 & 0.1738 & -0.0913 & -0.1821 & 0.1580 \\ 0.1208 & -0.1394 & -0.1012 & 0.2323 & 1.0727 & 0.2446 \end{bmatrix}^T \quad (\text{A.4})$$

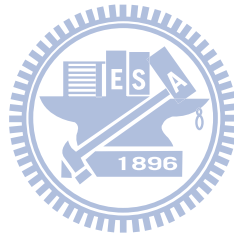
and the central solution  $\hat{Q}_o$  of Nehari problem can be obtained.

$$\hat{Q}_o = \left[ \begin{array}{c|c} A_{\hat{Q}_o} & B_{\hat{Q}_o} \\ \hline C_{\hat{Q}_o} & D_{\hat{Q}_o} \end{array} \right]$$

$$= \left[ \begin{array}{cccccc|cc} -28.4535 & 16.0849 & 17.6764 & -6.0052 & 0.1167 & -0.3226 & -4.2114 & -0.8456 \\ 9.2074 & -21.4223 & 3.4811 & -2.4010 & -5.7570 & -2.1393 & -0.0501 & -0.5216 \\ 8.1318 & 30.1309 & -2.1641 & -8.4116 & -8.6214 & 6.2997 & -6.5877 & -4.4685 \\ 21.8680 & 56.3393 & 48.1235 & -31.1878 & -30.0341 & 11.4388 & -17.3901 & -10.6469 \\ 24.8242 & 46.9474 & 36.3134 & -26.8365 & -27.4543 & 10.4417 & -12.8833 & -9.6086 \\ \hline 0 & 0 & 0 & 0 & 0 & -0.05 & 0.0382 & -1.7015 \\ \hline -0.0580 & -0.2156 & 0.0069 & -1.5131 & 0.6904 & 0.5816 & 0 & 0 \\ \hline 0.1898 & 0.3597 & -0.3138 & -0.7476 & -0.1882 & -1.5051 & 0 & 0 \end{array} \right]$$

(A.5)

Then the parameter  $Q(s)$  can be obtained according to Eq. (3.18).





## APPENDIX B

The corresponding coprime factorizations of nominal plant of example 1 of part 3 are given as follows.

$$P_n = \begin{bmatrix} \frac{1}{s+5} & \frac{2}{s+6} \\ \frac{4}{s+7} & \frac{3}{s+8} \\ \frac{2}{s+5} & \frac{5}{s+4} \end{bmatrix}_{3 \times 2} = N_{n,3 \times 2} \cdot M_{n,2 \times 2}^{-1}$$

$$M_{n,2 \times 2} = \begin{bmatrix} -5.7174 & -1.0721 & -1.0146 & 0 & 0 & 0 & 1 & 0 \\ -1.4348 & -9.1442 & -2.0291 & 0 & 0 & 0 & 2 & 0 \\ -1.0146 & -1.5162 & -6.4348 & 0 & 0 & 0 & 1.4142 & 0 \\ 0 & 0 & 0 & -7.0732 & -1.0438 & -2.3541 & 0 & 1.4142 \\ 0 & 0 & 0 & -1.3144 & -9.2783 & -2.8832 & 0 & 1.7321 \\ 0 & 0 & 0 & -1.6969 & -1.6503 & -7.7222 & 0 & 2.2361 \\ \hline 0.71741 & 1.0721 & 1.0146 & 0 & 0 & 0 & -1 & 0 \\ 0 & 0 & 0 & 0.75888 & 0.73805 & 1.6646 & 0 & -1 \end{bmatrix}$$

$$N_{n,3 \times 2} = \begin{bmatrix} -5.7174 & -1.0721 & -1.0146 & 0 & 0 & 0 & 1 & 0 \\ -1.4348 & -9.1442 & -2.0291 & 0 & 0 & 0 & 2 & 0 \\ -1.0146 & -1.5162 & -6.4348 & 0 & 0 & 0 & 1.4142 & 0 \\ 0 & 0 & 0 & -7.0732 & -1.0438 & -2.3541 & 0 & 1.4142 \\ 0 & 0 & 0 & -1.3144 & -9.2783 & -2.8832 & 0 & 1.7321 \\ 0 & 0 & 0 & -1.6969 & -1.6503 & -7.7222 & 0 & 2.2361 \\ \hline 1 & 0 & 0 & 1.4142 & 0 & 0 & 0 & 0 \\ 0 & 2 & 0 & 0 & 1.7321 & 0 & 0 & 0 \\ 0 & 0 & 1.4142 & 0 & 0 & 2.2361 & 0 & 0 \end{bmatrix}$$

(B.1)

$$X_{r,2 \times 2} = \left[ \begin{array}{cccccc|cc} -5.8266 & 0 & 0 & -1.169 & 0 & 0 & 1 & 0 \\ 0 & -9.2638 & 0 & 0 & -1.9605 & 0 & 2 & 0 \\ 0 & 0 & -6.2852 & 0 & 0 & -2.0321 & 1.4142 & 0 \\ -0.98894 & 0 & 0 & -7.3986 & 0 & 0 & 0 & 1.4142 \\ 0 & -1.7389 & 0 & 0 & -9.506 & 0 & 0 & 1.7321 \\ 0 & 0 & -2.4342 & 0 & 0 & -7.8488 & 0 & 2.2361 \\ \hline 0.71741 & 1.0721 & 1.0146 & 0 & 0 & 0 & 0 & 0 \\ 0 & 0 & 0 & 0.75888 & 0.73805 & 1.6646 & 0 & 0 \end{array} \right]$$

(B.2)

$$Y_{r,2 \times 3} = \left[ \begin{array}{cccccc|ccc} -5.8266 & 0 & 0 & -1.169 & 0 & 0 & 0.82658 & 0 & 0 \\ 0 & -9.2638 & 0 & 0 & -1.9605 & 0 & 0 & 1.1319 & 0 \\ 0 & 0 & -6.2852 & 0 & 0 & -2.0321 & 0 & 0 & 0.90878 \\ -0.98894 & 0 & 0 & -7.3986 & 0 & 0 & 0.98894 & 0 & 0 \\ 0 & -1.7389 & 0 & 0 & -9.506 & 0 & 0 & 0.86947 & 0 \\ 0 & 0 & -2.4342 & 0 & 0 & -7.8488 & 0 & 0 & 1.7212 \\ \hline 0.71741 & 1.0721 & 1.0146 & 0 & 0 & 0 & 0 & 0 & 0 \\ 0 & 0 & 0 & 0.75888 & 0.73805 & 1.6646 & 0 & 0 & 0 \end{array} \right]$$

(B.3)

$$\tilde{N}_{n,3 \times 2} = \left[ \begin{array}{cccccc|cc} -5.8266 & 0 & 0 & -1.169 & 0 & 0 & 1 & 0 \\ 0 & -9.2638 & 0 & 0 & -1.9605 & 0 & 2 & 0 \\ 0 & 0 & -6.2852 & 0 & 0 & -2.0321 & 1.4142 & 0 \\ -0.98894 & 0 & 0 & -7.3986 & 0 & 0 & 0 & 1.4142 \\ 0 & -1.7389 & 0 & 0 & -9.506 & 0 & 0 & 1.7321 \\ 0 & 0 & -2.4342 & 0 & 0 & -7.8488 & 0 & 2.2361 \\ \hline 1 & 0 & 0 & 1.4142 & 0 & 0 & 0 & 0 \\ 0 & 2 & 0 & 0 & 1.7321 & 0 & 0 & 0 \\ 0 & 0 & 1.4142 & 0 & 0 & 2.2361 & 0 & 0 \end{array} \right]$$

(B.4)

$$Y_{l,2 \times 3} = \left[ \begin{array}{cccccc|ccc} -5.7174 & -1.0721 & -1.0146 & 0 & 0 & 0 & -0.8266 & 0 & 0 \\ -1.4348 & -9.1442 & -2.0291 & 0 & 0 & 0 & 0 & -1.1319 & 0 \\ -1.0146 & -1.5162 & -6.4348 & 0 & 0 & 0 & 0 & 0 & -0.0988 \\ 0 & 0 & 0 & -7.0732 & -1.0438 & -2.3541 & -0.9889 & 0 & 0 \\ 0 & 0 & 0 & -1.3144 & -9.2783 & -2.8832 & 0 & -0.86947 & 0 \\ 0 & 0 & 0 & -1.6969 & -1.6503 & -7.7222 & 0 & 0 & -1.7212 \\ \hline -0.71741 & -1.0721 & -1.0146 & 0 & 0 & 0 & 0 & 0 & 0 \\ 0 & 0 & 0 & -0.7588 & -0.7381 & -1.6646 & 0 & 0 & 0 \end{array} \right]$$

(B.5)

$$Q_{2 \times 2} \cdot Y_{l,2 \times 3} \cdot \tilde{N}_{n,3 \times 2} = \begin{bmatrix} J_{11} & 0 \\ 0 & J_{22} \end{bmatrix}, \text{ where } J_{2 \times 2}(s) \text{ is given as:}$$

$$J_{2 \times 2}(s) = \begin{bmatrix} \frac{100}{s^2 + 20s + 100} & 0 \\ 0 & \frac{100}{s^2 + 20s + 100} \end{bmatrix}$$

(B.6)

and the reduced order parameter is solved as follows.

$$Q_{2 \times 2}(s) = \begin{bmatrix} Q_{11} & Q_{12} \\ Q_{21} & Q_{22} \end{bmatrix}$$

$$Q_{11}(s) = \frac{40.2987(s + 12.33)(s + 4.546)}{(s + 11.9)(s + 5.155)}$$

$$Q_{12}(s) = -\frac{21.4218(s + 13)(s + 4.768)}{(s + 12.18)(s + 5.864)}$$

$$Q_{21}(s) = -\frac{20.5391(s + 15.24)(s + 3.935)}{(s + 15.14)(s + 5.644)}$$

$$Q_{22}(s) = \frac{16.5512(s + 12.99)(s + 4.345)}{(s + 12.24)(s + 6.213)}$$

(B.7)

## APPENDIX C

The corresponding normalized coprime factors of nominal plant of part 4 example are given as follows.

$$\begin{aligned}
 P_n &= \begin{bmatrix} \frac{1}{s+5} & \frac{2}{s+6} \\ \frac{5}{s+7} & \frac{3}{s+8} \end{bmatrix} = N_n M_n^{-1} \\
 M_n &= \left[ \begin{array}{cccc|cc} -5.0754 & -0.69009 & -0.09888 & -0.50343 & 1 & 0 \\ -0.16852 & -8.5431 & -0.2211 & -1.1257 & 2.2361 & 0 \\ -0.23351 & -0.53549 & -6.3048 & -0.39299 & 0 & 1.4142 \\ -0.28599 & -0.65584 & -0.37327 & -8.4813 & 0 & 1.732 \\ \hline -0.075364 & -0.69009 & -0.09888 & -0.50343 & 1 & 0 \\ -0.16512 & -0.37865 & -0.21551 & -0.27789 & 0 & 1 \end{array} \right] \\
 N_n &= \left[ \begin{array}{cccc|cc} -5.0754 & -0.69009 & -0.09888 & -0.50343 & 0 & 4 \\ -0.16852 & -8.5431 & -0.2211 & -1.1257 & 0 & 0 \\ -0.23351 & -0.53549 & -6.3048 & -0.39299 & 1.4142 & 0 \\ -0.28599 & -0.65584 & -0.37327 & -8.4813 & 1.7321 & 0 \\ \hline 1 & 0 & 1.4142 & 0 & 0 & 0 \\ 0 & 2.2361 & 0 & 1.7321 & 0 & 0 \end{array} \right] \tag{C.1}
 \end{aligned}$$

and the solutions of GCARE and GFARE are

$$\begin{aligned}
 X_\infty &= \begin{bmatrix} 0.096706 & -0.0095441 & 0.12465 & -0.006448 \\ -0.0095441 & 0.31289 & -0.011526 & 0.22802 \\ 0.12465 & -0.011526 & 0.16198 & -0.0078333 \\ -0.006448 & 0.22802 & -0.0078333 & 0.16683 \end{bmatrix}, \\
 Y_\infty &= \begin{bmatrix} 0.086946 & 0.16504 & -0.0095599 & -0.0088287 \\ 0.16504 & 0.32141 & -0.015823 & -0.014967 \\ -0.0095599 & -0.015823 & 0.15754 & 0.1665 \\ -0.0088287 & -0.014967 & 0.1665 & 0.17948 \end{bmatrix}. \tag{C.2}
 \end{aligned}$$

The control gain matrix,  $F$ , and observer gain matrix,  $L$ , are shown as follows.

$$\begin{aligned}
F &= \begin{bmatrix} -0.075364 & -0.69009 & -0.09888 & -0.50343 \\ -0.16512 & -0.37865 & -0.21551 & -0.27789 \end{bmatrix} \\
L &= \begin{bmatrix} -0.073427 & -0.35376 \\ -0.14267 & -0.69277 \\ -0.21324 & -0.253 \\ -0.22664 & -0.2774 \end{bmatrix}
\end{aligned} \tag{C.3}$$

and the  $Q(s)$  filter is

$$\begin{aligned}
Q &= \begin{bmatrix} Q_{11} & Q_{12} \\ Q_{21} & Q_{22} \end{bmatrix} \\
Q_{11}(s) &= \frac{6247.5s^6 + 1.115 \times 10^6 s^5 + 4.342 \times 10^7 s^4 + 4.882 \times 10^8 s^3 + 2.1536 \times 10^9 s^2 + 3.393 \times 10^9 s + 1.132 \times 10^9}{s^6 + 1032.7s^5 + 5.659 \times 10^4 s^4 + 9.494 \times 10^6 s^3 + 5.209 \times 10^6 s^2 + 5.063 \times 10^6 s + 1.087 \times 10^6} \\
Q_{12}(s) &= \frac{-2486.5s^6 - 1.340 \times 10^6 s^5 - 5.849 \times 10^7 s^4 - 6.659 \times 10^8 s^3 - 2.931 \times 10^9 s^2 - 4.634 \times 10^9 s + 1.551 \times 10^9}{s^6 + 1032.8s^5 + 5.62 \times 10^4 s^4 + 9.547 \times 10^6 s^3 + 5.264 \times 10^6 s^2 + 5.117 \times 10^6 s + 1.097 \times 10^6} \\
Q_{21}(s) &= \frac{2483.1s^6 - 1.133 \times 10^6 s^5 - 5.573 \times 10^7 s^4 - 6.678 \times 10^8 s^3 - 3.062 \times 10^9 s^2 - 5.018 \times 10^9 s - 1.694 \times 10^9}{s^6 + 1032.1s^5 + 5.605 \times 10^4 s^4 + 9.244 \times 10^6 s^3 + 4.929 \times 10^6 s^2 + 4.808 \times 10^6 s + 1.037 \times 10^6} \\
Q_{22}(s) &= \frac{1010s^6 + 1.868 \times 10^6 s^5 + 8.468 \times 10^7 s^4 + 9.865 \times 10^8 s^3 + 4.420 \times 10^9 s^2 + 7.094 \times 10^9 s + 2.373 \times 10^9}{s^6 + 1032.2s^5 + 5.615 \times 10^4 s^4 + 9.295 \times 10^6 s^3 + 4.990 \times 10^6 s^2 + 4.860 \times 10^6 s + 1.047 \times 10^6}
\end{aligned} \tag{C.4}$$